Technical University of Munich
TUM School of Medicine and Health

Validation of Exportin-1 (XPO1) and Mitogen-Activated Protein Kinase Kinase 2 (MAP2K2) as Molecular Drug Targets in Amyotrophic Lateral Sclerosis

Mojan Parvaz

Complete reprint of the dissertation approved by the TUM School of Medicine and Health

of the Technical University of Munich for the award of the

Doktor der Naturwissenschaften (Dr. rer. nat)

Chair: Prof. Dr. Thomas Misgeld

Examiners:

1. Prof. Dr. Paul Lingor
2. Prof. Dr. Wolfgang Wurst

The dissertation was submitted to the Technical University of Munich on 27.12.2023

and accepted by the TUM School of Medicine and Health on 10.04.2024.

Abstract

Background: Amyotrophic lateral sclerosis (ALS) is a rapidly progressive neurodegenerative disorder and effective therapeutic options are lacking. Profiling ALS pathomechanisms could assist with the development of new treatment avenues. Therefore, this study aimed to validate molecular candidates with potential implications in ALS pathology which were derived from multiomic profiling studies conducted in the context of the MAXOMOD consortium (*Multiomic analysis of axono-synaptic degeneration in motoneuron disease*). Based on differential expression results and functional enrichment analyses, Exportin 1 (XPO1) and mitogen-activated protein kinase kinase 2 (MAP2K2, MEK2) were selected to be validated *in vitro*. XPO1 is a major regulator of nuclear RNA export and MAP2K2 has an important role in various cell functions, including neuronal differentiation and survival.

Methods: Multiomic analysis of human postmortem prefrontal cortex (PFC) and PFC from transgenic ALS mouse models revealed multiple deregulated molecular targets and pathways underlying the degeneration of ALS-affected brains. To validate selected molecular targets, we established primary cortical neuron cultures from P0 C57/Bl6 mice. To assess the role of the targets on neuronal survival we used *in vitro* toxin models mimicking known disease mechanisms in ALS, such as glutamate excitotoxicity and arsenite-induced stress granule formation. Basal expression of the targets (XPO1 and MAPK2K2), toxicity and functional effects of the inhibitors (selinexor and trametinib) were investigated by Western blot. Neuroprotective effects of target inhibition were investigated in toxin models by immunocytochemistry (cleaved caspase-3) and analysis of neurite outgrowth using image J.

Results: We modulated the expression of XPO1 and MAP2K2 with FDA-approved pharmacological small molecule inhibitors (selinexor and trametinib). Our results demonstrated that 72 h treatment with 20 nM and 200 nM trametinib, completely restored highly phosphorylated ERK1/2 protein which is a direct target of MAP2K2 ($n=3$; $P < 0.05$) and significantly reduced cell death and increased average neurite length in glutamate-intoxicated cells ($n=4$; $P < 0.0001$). 1 nM and 10 nM selinexor on the other hand, significantly reduced cell death in both stress-induced cultures ($n=4$; $P < 0.05$) but didn't affect neurite outgrowth.

Conclusion: Our findings suggest that XPO1 as well as MAP2K2 could be auspicious drug targets to be further validated for the treatment of ALS.

Table of Contents

1 Introduction

1.1 Amyotrophic lateral sclerosis (ALS)

Amyotrophic lateral sclerosis, initially described by Charcot in the 19th century (Rowland 2001), is a rapidly progressive neurodegenerative disorder that results in muscle weakness, disability, and ultimately, death. The median survival for ALS patients ranges from 3-5 years after the first symptoms due to motor dysfunctions, in particular by respiratory failure. Historically, ALS was identified as a distinct clinical syndrome separate from other motor neuron diseases (MNDs) like primary lateral sclerosis, primary muscular atrophy, and progressive bulbar palsy. The distinction was based on the location of the initial symptoms and the extent of involvement of anterior horn cells or corticomotor neurons. However, it has become increasingly clear that ALS exhibits clinical and pathophysiological diversity (M. R. Turner and Swash 2015) with evident overlaps with frontotemporal dementia (FTD) (M. R. Turner et al. 2013). Multiple genetic variations can produce similar clinical phenotypes, and conversely, a single variant may be associated with pure ALS, ALS with FTD (ALS-FTD), or pure FTD. These conditions exist on a spectrum with distinct clinicopathological features, possibly stemming from different causes, but ultimately converge on a common pathway leading to degeneration of both upper and lower motor neurons. The poor prognosis and insufficient therapeutic options for ALS demand a better characterization of neuropathological changes happening in the course of the disease.

1.1.1 Epidemiology and pathophysiology of ALS

The epidemiology of ALS reveals several important aspects of this neurodegenerative disorder and is essential for identifying potential risk factors and improving early diagnosis. ALS is a relatively rare disease, with an estimated annual incidence ranging from 2 to 3 cases per 100,000 individuals worldwide (Worms 2001). It affects both genders, with a slightly higher incidence observed in men. The onset of ALS typically occurs between the ages of 40 and 70, although cases can occur at younger ages, even in adolescence (Camacho-Soto et al. 2022). Geographically, there are variations in ALS prevalence, with higher rates reported in certain regions like North Europe (1.89 cases per 100,000 person-years) compared to East Asia (0.83 cases per 100,000 person-years) and South Asia (0.73 cases per 100,000 person-years). In contrast, more consistent rates were found in Europe, North America, and New Zealand, with a pooled ALS standardized incidence of 1.81 cases per 100,000 person-years for those areas (Marin et al. 2017). The exact etiology of ALS remains largely unknown, although a small

proportion of cases are associated with genetic mutations. Familial forms make up 5 to 10 percent of cases. The majority (90-95%) of ALS cases are considered sporadic, lacking a clear family history. Genetic susceptibility in sporadic ALS appears to be influenced by variations in multiple genes and loci (Leblond et al. 2014). Among these, some are associated with known or suspected familial ALS, such as pathogenic variants in superoxide dismutase 1(*SOD1*), TAR DNA-binding protein 43 (*TDP-43*), chromosome 9 open reading frame 72 (*C9ORF72*), fused in sarcoma (*FUS*), angiogenin (*ANG*), optineurin (*OPTN*), senataxin (*SETX*), and sequestosome 1 (*SQSTM1*) genes, while others are not typically linked to familial ALS, including variants in TANK-binding kinase 1(*TBK1*) (Cirulli et al. 2015), ataxin-2 (*ATXN2*) (Lattante et al. 2012), chromosome 21 open reading frame 2 (*C21ORF2*) (van Rheenen et al. 2016), NIMA related kinase 1 (*NEK1*) (Kenna et al. 2016). A comprehensive 2017 meta-analysis of 111 studies revealed distinct variations in the frequencies of genetic variants in the most common ALS-related genes (*C9ORF72*, *SOD1*, *TDP-43*, and *FUS*) between European and Asian populations with sporadic ALS (Zou et al. 2017). In European populations, *C9ORF72* repeat expansions were the most prevalent (5.1 percent), followed by *SOD1* variants (1.2 %), *TDP-43* variants (0.8 %), and *FUS* variants (0.3 %). In Asian populations, *SOD1* variants were the most common (1.5 %), followed by *FUS* variants (0.9 %), *C9ORF72* repeat expansions (0.3 %), and *TDP-43* variants (0.2 %). An earlier study also found around 28 percent of sporadic ALS cases harboring rare or novel coding variants in known ALS genes, possibly pathogenic but not definitively proven, with approximately 4 percent showing variants in more than one ALS gene. These genes may play a role as Mendelian genes in familial ALS or act as low-penetrance susceptibility factors in sporadic ALS, indicating the complex genetic factors contributing to both forms of the disease warranting further investigation (Cady et al. 2015).

ALS is distinguished by the degeneration and death of motor neurons, accompanied by gliosis (T Philips and Rothstein 2014). Additionally, the spinal cord undergoes atrophy, with thinning of the ventral roots and loss of large myelinated fibers in motor nerves. The affected muscles display denervation atrophy (Saberi et al. 2015). In ALS, neuropathological observations reveal frequent intracellular inclusions in degenerating neurons and glia. These inclusions include phosphorylated and nonphosphorylated neurofilaments found predominantly in spinal motor neurons, potentially associated with immunoreactive SOD1 or nitric oxide (Ince et al. 1998). Ubiquitinated inclusions, distinct from those in other neurodegenerative disorders, are observed in ALS, particularly in the frontal and temporal lobes of cortical neurons in ALS-FTD cases. TDP-43 accumulation and inclusion formation are common in sporadic ALS, FTD with

ubiquitin-positive/tau-negative inclusions, and overlapping ALS with FTD (Geser et al. 2009). Additionally, FUS-positive immunoreactive inclusions are detected in both sporadic and familial ALS (Deng et al. 2010).

1.1.2 Pathogenic pathways linked to ALS

The exact cause of ALS remains unidentified. Numerous potential mechanisms have been suggested, encompassing abnormal RNA processing, protein quality control disorders, excitotoxicity, cytoskeletal abnormalities, mitochondrial dysfunction, viral infections, apoptosis, abnormalities in growth factors, inflammatory responses, and other factors (Peters, Ghasemi, and Brown 2015). The development of ALS is believed to be influenced by a combination of genetic and environmental factors, which set off various biochemical cascades (Bozzoni et al. 2016). The intricate interplay of these factors contributes to the complex pathogenesis of ALS. Increasing evidence highlights the idea that altered RNA processing and the aggregation of abnormal proteins play a crucial role in the development of ALS. Several genes encoding RNA binding proteins, including TDP-43 and FUS, have been linked to both ALS and related neurodegenerative disorders (Ito and Suzuki 2011), (Verma and Tandan 2013). These proteins possess prion-like domains that exhibit an inherent tendency to self-aggregate (Polymenidou and Cleveland 2011). Under normal circumstances, they assist in assembling RNA into stress granules, which are temporary structures involved in regulating protein synthesis as part of the cellular stress response (Wolozin 2012). However, variants in the prion-like domains of these proteins may lead to excessive incorporation into stress granules (SGs) that resist degradation, or promote self-aggregation of abnormal RNA binding proteins (like TDP-43), ultimately resulting in the formation of cytoplasmic inclusions and neurodegenerative diseases.

C9ORF72 expansions are the most common genetic cause of familial ALS and are also detected in some sporadic ALS cases. The hexanucleotide repeat sequence (GGGGCC) in the *C9ORF72* gene can form G-quadruplex structures, and its expansion may trigger pathologic molecular alterations (Haeusler et al. 2014). These alterations involve the formation of RNA/DNA hybrids (R-loops), production of defective RNA transcripts, and decreased production of full-length RNA transcripts. These defective RNA transcripts can mislocalize essential proteins in the nucleolus, leading to reduced cell viability. The expansion also interacts with Ran GTPase activating protein 1, potentially disrupting nucleocytoplasmic transport by clogging nuclear membrane pores (Ke Zhang et al. 2015). Additionally, repeat-associated non-ATG translation (RAN translation) within the expanded repeat sequence can generate toxic dipeptide repeat

proteins that interfere with RNA processing (Mori et al. 2013). Another possible mechanism is the reduced expression of C9ORF72 protein levels, leading to disease by a loss-of-function mechanism (Ciura et al. 2013).

SOD1-mediated toxicity in ALS involves variants in the *SOD1* gene, leading to a toxic gain or loss-of-function mechanism (Reaume et al. 1996). While SOD1 primarily acts as an antioxidant, pathogenic variants can increase pro-oxidant pathways, leading to oxidative injury and the generation of reactive oxygen species (Gurney 1997), (Harraz et al. 2008). Additionally, abnormal SOD1 may induce protein aggregates potentially toxic to motor neurons, although this aggregation might be a secondary manifestation rather than a primary cause of ALS (Durham et al. 1997). Abnormal SOD1 protein levels increase in the later stages of the disease, but even low levels of SOD1 aggregates may be sufficient to mediate toxicity (Karch et al. 2009).

In ALS, inflammatory responses play a significant role in disease progression and neuronal death. Studies have demonstrated the involvement of inflammatory processes, including activation of microglia and astrocytes and infiltration of natural killer cells, peripheral T cells, and monocytes into the central nervous system (CNS) (Thomas Philips and Robberecht 2011), (Beers et al. 2008), (Butovsky et al. 2012). Particularly, microglia, as immune-modulating cells in the CNS, have been extensively studied in the context of ALS. Once activated, microglia release various factors, such as nitric oxide, oxygen radicals, cytokines, and glutamate, which may contribute to the cascade leading to motor neuron cell death (O'Rourke et al. 2016).

While the exact cause of motor neuron degeneration remains elusive, recent years have seen increased attention on potential factors like excitotoxicity and impaired stress granules in the context of ALS pathophysiology. As my study aims to replicate these two established disease pathways in ALS, these mechanisms will be further elaborated upon in the next chapters.

1.1.3 Glutamate excitotoxicity in ALS

Substantial evidence for the excitotoxicity hypothesis in ALS pathology has been documented recently, although further mechanistic studies would be needed to comprehensively determine the role of excitotoxic insults in ALS. The hypothesis suggests that abnormally high levels of the excitatory neurotransmitter glutamate may trigger a series of events leading to the death of motor neurons in ALS **(Figure 1)**. This excessive activation of glutamate receptors can result in an influx of calcium into cells, setting off a cascade of processes that cause cellular damage,

including lipid peroxidation, nucleic acid damage, and disruption of mitochondrial function (Dong, Wang, and Qin 2009),(Satarker et al. 2022).

Elevated glutamate levels have been found in the cerebrospinal fluid of patients with sporadic ALS (Rothstein et al. 1990), and defects in glutamate transport have been observed in both patients with sporadic ALS and in the transgenic SOD1 mouse model of ALS (Lin et al. 1998). These defects involve transmembrane glutamate transporters found on neurons and glial cells, which are responsible for rapidly inactivating glutamate after its release.

A hypothesis proposes that specific nonfunctional, truncated forms of the primary excitatory amino acid transporter 2 (EAAT2) on astrocytes may be particularly prevalent in ALS tissues. However, some of these truncated forms have also been found in normal tissue, and there is evidence that a splice-variant of this protein (EAAT2b) may actually be upregulated in ALS, particularly in neurons, potentially indicating a compensatory response to elevated extracellular glutamate (Maragakis, Dykes-Hoberg, and Rothstein 2004)**.**

Glutamate receptor dysfunction is another potential mechanism contributing to excitotoxicity. Various postsynaptic glutamate receptors, including N-methyl-D-aspartate (NMDA), α-amino-3-hydroxy-5-methyl-4-isoxazolepropionic acid (AMPA), kainate, and G-protein-coupled receptors, could be involved in this process. For example, defective mRNA editing of glutamate AMPA receptors has been discovered in spinal motor neurons of ALS patients, which has been linked to increased calcium permeability through this receptor subtype, potentially leading to neuronal death (Kawahara et al. 2004)**.**

One significant piece of evidence supporting the role of glutamate excitotoxicity in ALS is the beneficial effect of the anti-glutaminergic drug Riluzole, which has been shown to improve survival in ALS patients (Miller, Mitchell, and Moore 2012).

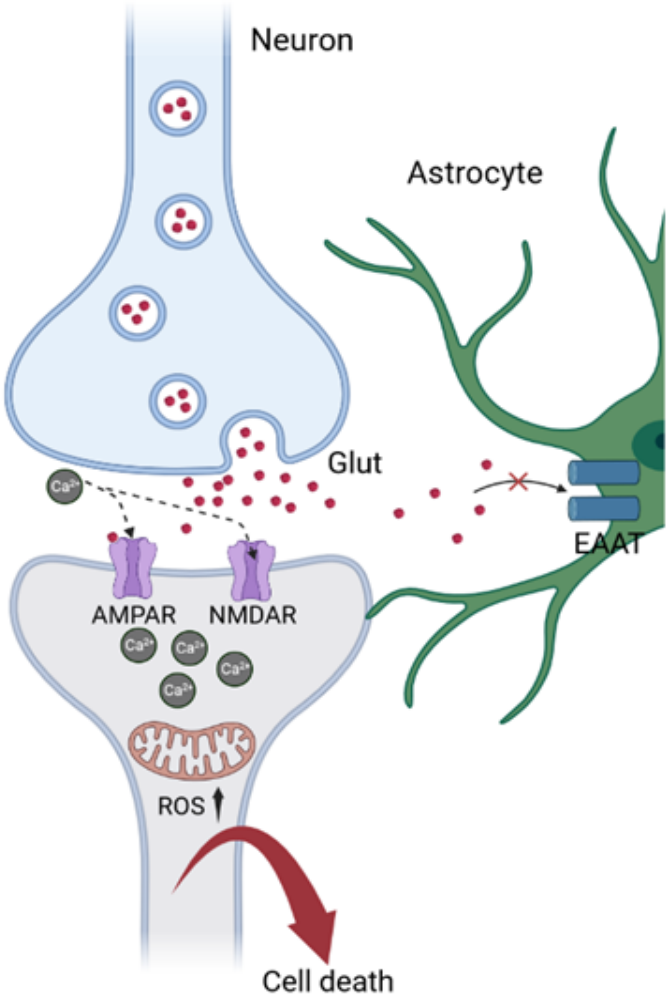

Figure 1: Schematic representation of glutamate excitotoxicity pathology in ALS. Upon neurotransmission, glutamate (red dots) is released into the synaptic cleft, initiating the activation of post-synaptic glutamate receptors such as AMPAR and NMDAR. In situations of excitotoxicity, an elevated release of glutamate occurs, coupled with a diminished ability for glutamate clearance by EAAT2. This imbalance triggers an excessive stimulation of glutamate receptors, resulting in the influx of calcium ions. Consequently, a complex sequence of events is set into motion, involving the increasing reactive oxygen species, mitochondrial dysfunction and altered metabolism and results in in cell death pathways, including apoptosis or necrosis (Figure generated with Biorender.com).

1.1.4 Stress granules and ALS

The involvement of the RNA metabolism machinery's response to stress has been strongly implicated in the pathology of neurodegeneration, with particular emphasis on its role in ALS. Stress granules are dynamic, non-membrane-bound structures whose primary function is to promote cell survival by condensing translationally stalled mRNAs, ribosomal components, translation initiation factors, and RNA-binding proteins (RBPs) that form in response to cellular

stress and play a role in mRNA metabolism (Campos-Melo et al. 2021). Dysregulation of stress granule dynamics, such as aberrant aggregation or impaired clearance, may contribute to the accumulation of toxic proteins and RNA, leading to motor neuron degeneration in ALS. A few of the well-known genetic causes of ALS including *TDP-43*, *FUS*, and *C9ORF72* are associated with SGs dysregulation which is linked to several cellular phenotypes in ALS. These dynamic structures are believed to seed the pathological aggregations of TDP43 and FUS. Moreover, SGs play a role in contributing to mitochondrial dysfunction, inflammasome activation, and nucleo-cytoplasmic transport in the context of ALS. Figure 2 lists the genes associated with each of these pathological processes **(Figure 2)** (Dudman and Qi 2020).

Aberrant SG assembly and disassembly have been associated with various neurodegenerative disorders, including ALS. In ALS patient samples, cytoplasmic inclusions often contain RBPs such as TDP-43 and FUS that colocalize with SG markers (Dudman and Qi 2020). Most of our insights into the potential involvement of nucleocytoplasmic transport defects in ALS have been derived from studies focusing on the four most frequent genetic causes of fALS (mutations in the genes *C9ORF72*, *SOD1*, *TDP-43*, and *FUS*) (Vanneste and Van Den Bosch 2021). The morphology and composition of SGs differ depending on the cell type and the specific stressor that induces them. It has been shown that cortical neurons took approximately twice as long as astrocytes to develop and disassemble the SGs (Khalfallah et al. 2018).

The presence of SGs directly hinders the formation of the NLR family pyrin domain containing 3 (NLRP3) inflammasome by competitively sequestering DEAD-Box Helicase 3 X-Linked (DDX3X). Consequently, free DDX3X promotes cell survival when sequestered within SGs, whereas its binding to the NLRP3 inflammasome complex triggers pyroptosis (Samir et al. 2019).

Mitochondrial stress can induce the formation of SGs (Carrì et al. 2015). It is known that mitochondrial dysfunction and fragmentation are common features observed in various neurodegenerative disease models. Mutations in genes associated with the autophagy/mitophagy pathway, such as *OPTN*, are known to contribute to neurodegenerative diseases, including ALS. OPTN, which is implicated in ALS and Parkinson's disease, plays a role in facilitating mitophagy by binding the autophagosome receptor, microtubule-associated protein 1A/1B-light chain 3 (LC3). The ALS-linked mutation OPTNE478G in the ubiquitin-binding domain of *OPTN* reduces its autophagic ability (Monahan, Shewmaker, and Pandey 2016). The dysregulation of TDP-43 has been linked to mitochondrial stress and the formation

of SGs. Notably, when TDP-43 is overexpressed in motor neuron-like NSC-34 cells, it increases the production of reactive oxygen species (ROS) and oxidative damage (T. Chen et al. 2018).

The functional connections between integrated stress response (ISR) activation and nucleo-cytosol trafficking, particularly focusing on the nuclear localization of spliceosomal U-rich small nuclear ribonucleoproteins (UsnRNPs) – the core components of the spliceosome have been investigated. It was discovered that ISR activation leads to significant changes in nuclear gems and Cajal bodies, which are involved in UsnRNP maturation and storage (Fischer, Englbrecht, and Chari 2011). This effect is dependent on the cytoplasmic assembly of SGs and interferes with the nuclear import of UsnRNPs mediated by the snurportin-1/importin-β1 system. Importantly, manipulating the nucleo-cytosol trafficking of UsnRNPs through SGs or importin-β1 influences alternative splicing in response to stress. (Rossi et al. 2020).

Several studies have linked SG components to ALS pathology. These findings suggest that investigating SG pathology could be a promising avenue for future research in the field of ALS and highlight promising therapeutic strategies targeting SG components in ALS.

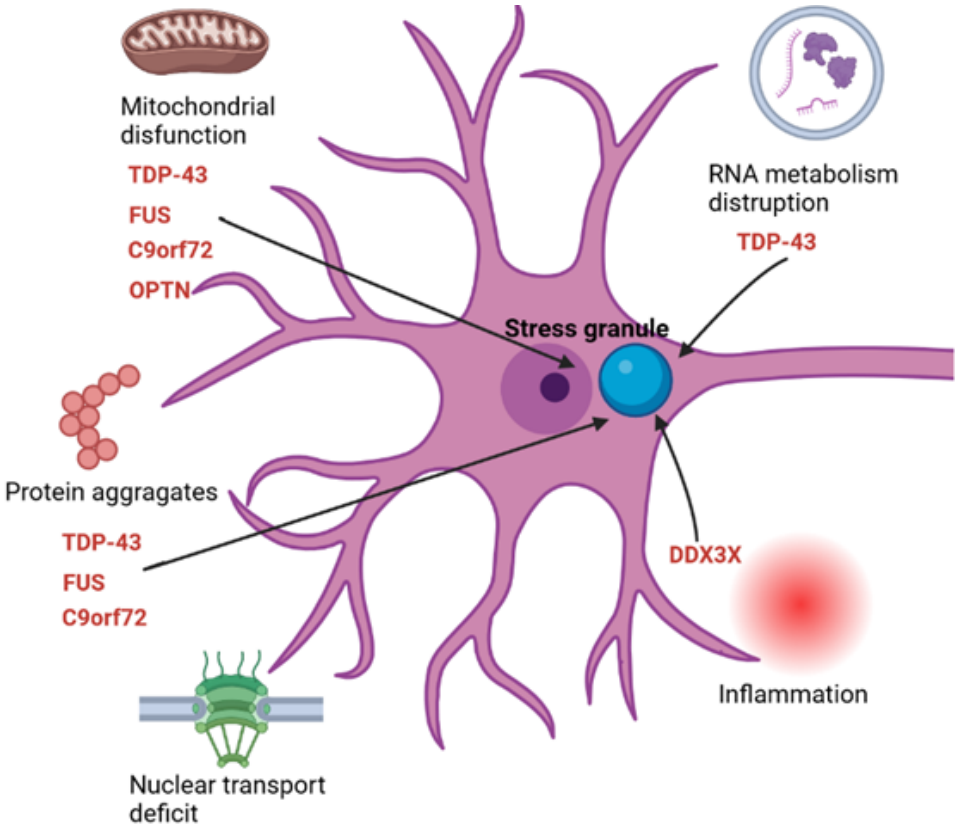

Figure 2: Schematic representation of stress granules dysregulation involved in ALS pathology. SGs dysregulation associated with multiple cellular phenotypes in ALS. Genes involved in each pathological process are listed. SGs are hypothesized to act as a seeding

mechanism for the pathological aggregation of proteins such as TDP-43, FUS and C9ORF72. SGs are implicated in influencing mitochondrial dysfunction, triggering inflammasome activation, and impacting nucleo-cytoplasmic transport within ALS pathomechanisms (Figure generated with Biorender.com).

1.1.5 ALS diagnosis and therapeutic options

Currently, the diagnosis of ALS relies solely on clinical criteria, which involve identifying first and second motoneuron abnormalities in various parts of the body, which can be supported by electrophysiological findings. However, in most industrialized countries, this process takes approximately 12 months from the onset of initial symptoms to reach a definitive ALS diagnosis (Hardiman, van den Berg, and Kiernan 2011).

Various molecular biomarkers, including neurofilaments (Nf) in cerebrospinal fluid (CSF) and serum (Lu et al. 2015), soluble p75ECR in urine (Shepheard et al. 2017) and chromogranin A in saliva (Obayashi et al. 2008) have been suggested as potential aids in the diagnosis of ALS. However, none of these biomarkers have yet demonstrated sufficient clinical effectiveness. Therefore, there is a need to improve the timing and accuracy of diagnosis and identify a reliable disease progression marker for use in disease-modification trials.

Currently, the available therapeutic options for ALS are limited. Glutamate antagonist Riluzole is one of the approved drugs. Studies have demonstrated that Riluzole can extend survival and decelerate functional decline in ALS patients (Miller, Mitchell, and Moore 2012). The United States Food and Drug Administration (FDA) approved the use of Riluzole in 1995. Riluzole is believed to employ at least three distinct mechanisms to mitigate glutamate-induced excitotoxicity: it inhibits the release of glutamic acid, blocks NMDA receptor-mediated responses in a noncompetitive manner, and directly affects the voltage-dependent sodium channel (Kennel et al. 2000). Nevertheless, the precise mechanism through which it operates in ALS remains unclear (Riviere et al. 1998).

Edaravone, which is an antioxidant, is licensed as a disease-modifying drug in certain countries, although its impact on disease progression and survival is limited, but it has shown to slow functional deterioration in ALS patients. Edaravone functions as a free-radical scavenger, targeting oxidative stress, which is believed to be involved in the development of ALS (Writing Group and Edaravone (MCI-186) ALS 19 Study Group 2017),(Hardiman and Van Den Berg 2017). Recently, U.S. FDA approved AMX0035 as the third medication for slowing ALS progression. It is a combination of sodium phenylbutyrate (PB) and taurursodiol (TUDCA, TURSO). Clinical trials from 2020 showed that it could significantly slow functional decline

and extend the lives of ALS patients and improve their ability to perform daily activities (Fels et al. 2022). Tofersen is an antisense oligonucleotide and received FDA approval in the United States on April 25, 2023 for treating ALS in adults with a mutation in the *SOD1* gene. Tofersen functions by binding to the *SOD1* mRNA, leading to its degradation and a decrease in the synthesis of SOD1 protein, which shows a gain of function in *SOD1*-fALS. In preclinical investigations, the sustained intraventricular delivery of tofersen demonstrated a reduction in both SOD1 protein and mRNA levels in the brain and spinal cord (Smith et al. 2006) (Blair 2023). Long-term effects of tofersen are not known yet.

Nevertheless, the therapeutic effects of these drugs remain highly limited. As a result, there is an urgent need for identifying and validating new therapeutic targets that can lead to more effective treatments for ALS.

1.1.6 Lack of comprehensive profiling in ALS and the power of omics studies

A better understanding of early disease mechanisms holds the potential to aid in the discovery of diagnostic and prognostic biomarkers, as well as novel and potentially more effective therapeutic drug targets. While analyzing affected nervous system tissue directly remains the main standard for understanding neuropathology, obtaining patient material is only possible post-mortem and in restricted quantities. This limitation poses a risk of primarily describing disease end-stages, thereby concealing crucial mechanisms that occur during earlier phases and may present more promising avenues for drug targeting. In recent years, there has been a notable surge in publications focusing on -omics techniques such as genomics, epigenomics, transcriptomics, miRNA, proteomics and metabolomics concerning ALS which is nicely summarized in a review by Caballero-Hernandez et al (Caballero-Hernandez et al. 2016). As a result, several studies have provided significant new insights into the pathogenesis of the disease. With advancements in structural genomics, we now know of over 20 genes that undergo mutations, leading to familial forms of ALS (Bettencourt and Houlden 2015).

Through the use of microarray technology to analyze RNA expression patterns in postmortem human ALS tissue, researchers have discovered notable changes in various functional clusters. Among these clusters are apoptosis and survival, as well as cytoskeleton remodeling and axonal transport (Aronica et al. 2015). Notably, in line with the crucial involvement of TDP-43, other studies have corroborated the presence of abnormal exon splicing in ALS patients. These findings have shown a remarkable enrichment of genes related to the regulation of cell-matrix adhesion and extracellular matrix biology in motoneurons (Rabin et al. 2010). Using deep

sequencing analysis, significant alterations in gene expression were discovered in inflammation-related genes within the monocytes of ALS patients (Zhao et al. 2017). Furthermore, the miRNAome of ALS patients has been extensively examined in various tissues, such as blood, CSF and spinal cord tissue (De Felice et al. 2014). Intriguingly, evidence indicates that miRNA changes can be detected many years prior to the onset of the disease, even in individuals who are asymptomatic mutation carriers (Freischmidt et al. 2014).

Recent studies aimed to explore synaptic dysfunction as a central factor in ALS by analyzing the synaptic proteome in the ALS and control brains. Using advanced proteomics techniques, the researchers identified over 6000 proteins in the isolated synaptoneurosomes. They discovered more than 30 ALS-associated proteins, including TDP-43, FUS, SOD1, and C9ORF72, as well as nearly 500 proteins with altered expression levels specific to ALS (Laszlo et al. 2022). Numerous proteomic studies have explored human cerebrospinal fluid (CSF) in search of reliable biomarkers for ALS (Barschke et al. 2017) (Ranganathan et al. 2005) (Collins et al. 2015). Neurofilaments have already shown to be promising as disease markers and recently, chitinases have emerged as novel targets for detection. Chitotriosidase (CHIT1), chitinase-3-like protein 1 (CHI3L1), and chitinase-3-like protein 2 (CHI3L2) levels in the CSF of ALS patients have been investigated, and all three chitinases, were found to correlate with disease progression rate (Costa et al. 2021). Another study highlighted proteins such as Nucleotide-binding oligomerization domain-containing protein 2 (NOD2) and osteopontin (SPP1), demonstrating differential expression in the CSF and motor cortex transcriptome of ALS patients (de Luna et al. 2022). However, it's important to note that not all of these candidate markers have shown reproducibility to date. Phospho-proteomic analyses are relatively scarce in animal studies and are not feasible using human post-mortem tissue due to the loss of signal. However, an examination of the axoplasmic compartment in SOD1.G93A mice indicated a decrease in phosphorylated tropomyosin receptor kinase (p-TRK) and an increase in phosphorylation of Jun N-terminal kinase (p-JNK), suggesting potential dysregulation of retrograde axonal transport (Perlson et al. 2009). On the other hand, there has been a growing number of metabolomic analyses in ALS. Similar to proteomic studies, no single metabolomic marker characterizing the disease has been identified so far, which is likely attributed to the disorder's heterogeneity (Blasco et al. 2016). However Recent studies have delved into the progression of ALS and the associated metabolic changes in patients at different disease stages. Using magnetoencephalography (MEG), these studies showcased global brain hyperconnectivity in both early and advanced ALS stages and identified metabolites linked to energy deficits, neurotoxic compounds, and neurotransmitter production as characteristic of

advanced ALS (Marino et al. 2022). Furthermore, another study conducted untargeted metabolomics analysis on plasma from two independent ALS cohorts and healthy controls, revealing recurrently dysregulated metabolic pathways, with a notable emphasis on lipid sub-pathways, thus indicating their significance in ALS pathomechanisms and potential as therapeutic targets (Goutman et al. 2022).

In most of these previous studies, investigations of ALS brain tissue and biofluids have mainly focused on individual molecular subsets, indicating the complexity and heterogeneity of ALS as a disease. However, recent transcriptomic analysis has made progress in identifying potential distinct ALS populations. These populations have been stratified into different subclusters based on gene set enrichment analyses, highlighting oxidative stress, retrotransposon activation and glial dysfunction (Eshima et al. 2023). More recently, the field has seen advancements through studies utilizing multi-omics analysis on induced pluripotent stem cells (iPSC) derived from ALS patients. Catanese et al analyzed transcriptional, epigenetic and mutational aspects on hiPSC-derived motor neurons with mutations in *C9ORF72*, *TDP-43*, *SOD1*, and *FUS*, along with datasets from patients' biopsies. A common signature was identified, indicating increased stress and synaptic abnormalities. Epigenetic alterations were linked to abnormal transcriptional signatures, and machine learning revealed correlations between gene sets in blood and spinal cord transcriptomes, providing tissue-independent insights into ALS marker genes (Catanese et al. 2023).

Approaches in identifying new ALS biomarkers, focusing on various multi-omics biotechnology platforms like miRNomics, proteomics and metabolomics, in circulating biofluids, which have contributed to a deeper and more comprehensive understanding of the molecular mechanisms underlying ALS are summarized in a recent review (Mitropoulos et al. 2018). Despite numerous studies that explore ALS pathogenesis, there is a notable absence of publications that simultaneously employ multiple -omics methods on both human samples and animal models of the disease in a standardized manner.

While numerous studies have focused on analyzing the motor cortex in ALS, it is believed that this region mainly represents the advanced stages of the disease due to its severe involvement (Aronica et al. 2015). On the other hand, the PFC typically shows intermediate TDP-43 pathology at the time of death (Brettschneider et al. 2013), suggesting that studying this area could provide valuable insights into earlier disease-related changes in post-mortem tissue. Our recent study in the context of the MAXOMOD project, investigated early ALS pathogenesis using an integrative multi-omics approach in the PFC of ALS patients and four mouse models of the disease. The comprehensive analysis of transcriptomes, (phospho-)proteomes, and

miRNAomes showed sex-specific changes and identified specific human ALS-subclusters, driven by immune response, extracellular matrix, mitochondrial respiration, and RNA metabolism, based on transcriptome data. These molecular signatures were also observed in corresponding mouse models. Additionally, the mitogen-activated protein kinase (MAPK) pathway as well as exportin 1 (XPO1) emerged as early disease-relevant targets through individual and integrative multi-omics analysis. These findings highlighted both candidates as promising therapeutic targets for ALS patients (Caldi Gomes et al. 2023).

1.2 Exportin 1 as an important nuclear export factor

The nuclear envelope plays a vital role in creating a compartmentalized intracellular environment essential for DNA replication, RNA synthesis, and ribosome production. This regulation extends to cellular processes like apoptosis and proliferation. Nucleocytoplasmic trafficking of various molecules, including RNAs, ribosomes, transcription regulators, and cell cycle modulators, is meticulously controlled by the nuclear pore complex and transport receptor molecules, such as the karyopherin-β family proteins (J. G. Turner, Dawson, and Sullivan 2012). Each karyopherin-β protein recognizes a distinct set of cargo proteins or RNAs and facilitates their nucleocytoplasmic import or export by recognizing nuclear localization signals. Chromosome maintenance protein 1 (CRM1) or XPO1, one of the seven exportins, stands out as the only transporter responsible for transporting over 230 proteins (Ishizawa et al. 2015). XPO1 serves as a nuclear exporter protein, possessing a pocket that allows nuclear proteins to bind. Inside the nucleus, XPO1 binds to the nuclear export signal (NES) on its target proteins and also to RAN in its active GTP-bound form (RAN-GTP). This complex is then docked to the nuclear pore complex (NPC) and transported through the nuclear membrane into the cytoplasm. When RAN-GTP is hydrolyzed to RAN-GDP, the complex disassembles, and the cargoes are released in the cytoplasm (Figure 3A). The direction of XPO1-mediated export is determined by the concentration gradient of RAN-GTP, which is primarily localized within the nucleus (Azizian and Li 2020), (Darui Xu, Grishin, and Chook 2012).

Maintaining cellular homeostasis relies on proper nuclear-cytoplasmic partitioning of large molecules, a process often dysregulated in cancer. In various human cancers, XPO1 is frequently overexpressed and/or mutated, contributing to its oncogenic driver function, making it an attractive therapeutic target for cancer treatment. This has led to development of various XPO1 inhibitors and them being tested in many clinical trials involving selective inhibitors of nuclear export (SINE) compounds (Azizian and Li 2020).

Emerging evidence suggests that nucleocytoplasmic transport dysfunction is a shared pathway contributing to neurodegeneration and the age-related vulnerability to neurodegenerative diseases. Defective nuclear import of TDP-43 may be one such mechanism, and a study found that karyopherin-beta1 and cellular apoptosis susceptibility protein play roles in regulating TDP-43's nuclear transport (Khalil et al. 2022). Reduced expression of cellular apoptosis susceptibility protein was observed in post-mortem brain and spinal cord samples from patients with TDP-43 positive frontotemporal lobar degeneration and ALS (Nishimura et al. 2010). Impaired nuclear import due to hexanucleotide repeat expansion (HRE) expression is observed also in the fly model and *C9ORF72* ALS patient-derived neurons (Ke Zhang et al. 2015).

ALS is also characterized by the exclusion of the RNA-binding protein TDP-43 from the cell nucleus and its accumulation in the cytoplasm. The potential of SINE compounds, targeting XPO1, to prevent neurodegeneration in ALS/FTD models has been investigated. SINE compounds showed modest improvement in cellular survival and motor symptoms in an *in vivo* rat ALS model. Interestingly, the study found that multiple pathways are involved in regulating TDP-43 nuclear export, suggesting that targeting several overlapping mechanisms could be more effective in preventing cytoplasmic TDP-43 accumulation in ALS/FTD (Archbold et al. 2018).

In 2019, the FDA approved KPT-330 (Selinexor), the first-in-class XPO1 inhibitor, as a fifth-line treatment for multiple myeloma (Commissioner 2020)(https://www.fda.gov/news-events/press-announcements/fda-approves-new-treatment-refractory-multiple-myeloma).
Selinexor binds to and inhibits XPO1, leading to the accumulation of XPO1 targets, including tumor suppressors, in the nucleus of cancer cells (Figure 3B). This results in increased transcription of tumor suppressor genes and affects various tumor suppressor proteins (Gandhi et al. 2018). While XPO1 inhibition has shown promising results in rescuing TDP-43-induced cell death and improving locomotor deficits in ALS models, recent studies suggest that the protective effects of XPO1 SINEs may be independent of TDP-43 localization (Ederle et al. 2018). Additionally, XPO1 inhibition has demonstrated beneficial effects in other ALS-related models, suggesting potential therapeutic benefits beyond TDP-43 pathology, possibly through the stimulation of autophagy (Silvestrini et al. 2018),(Wobst et al. 2020).

Despite all these studies on the involvement of nucleo-cytoplasmic transport in ALS pathology, there is still no clear evidence of its functional neuroprotective effect. However, this does not diminish the potential significance of targeting this process for ALS therapy, especially in exploring other etiological aspects of ALS.

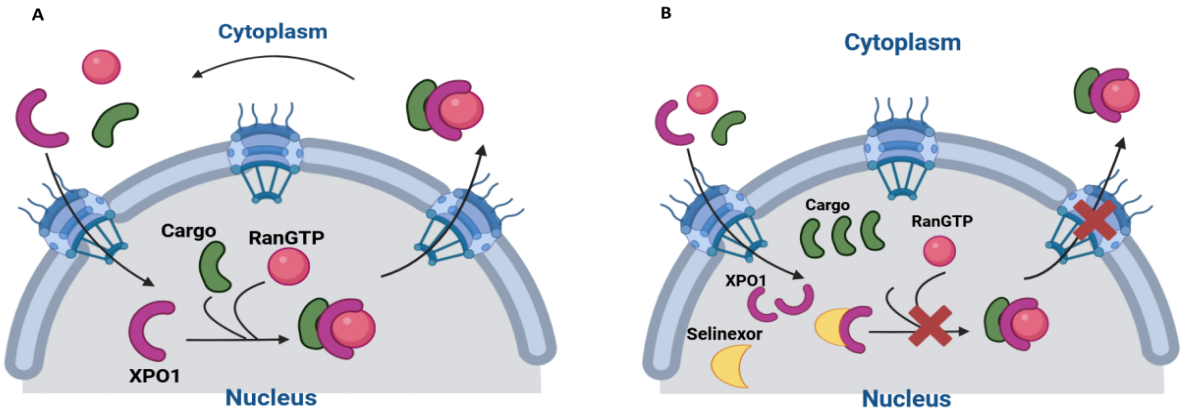

Figure 3: Schematic representation of XPO1 and selinexor mechanism of action. (A) XPO1 facilitates the transport of various cargo molecules from the nucleus to the cytoplasm. It recognizes and binds to the cargo molecules, forming a XPO1-Cargo-RanGTP complex and then translocated through the nuclear pore to reach the cytoplasm, where the cargo is released. This mechanism ensures the proper distribution of molecules between the nucleus and cytoplasm. **(B)** selinexor binds to XPO1 and prevents the formation of the complex and disrupts the normal nuclear export process, resulting in accumulation of XPO1 targets in the nucleus (Figure generated by BioRender.com).

1.3 Mitogen-activated protein kinase kinase 2 (MEK2)

MAPK families play crucial roles in various cellular processes, such as proliferation, differentiation, development, transformation, and apoptosis. There are three well-characterized MAPK families in mammalian cells: extracellular signal-regulated kinase (ERK), Jun kinase (JNK/SAPK), and p38 MAPK. These MAPKs regulate cell cycle machinery and other proteins related to cell proliferation. In mammalian cells, there are at least 14 MAPKKKs, 7 MAPKKs, and 12 MAPKs that participate in protein kinase cascades to transmit extracellular signals and trigger cellular responses (Widmann et al. 1999), (W. Zhang and Liu 2002).

Stimulation of tyrosine kinase receptors (RTKs) initiates a multistep process leading to the activation of MAPKs. This process involves various components, including protein kinases known as MAPKK (such as MEK1 and MEK2). Ultimately, MEKs phosphorylate p44 MAPK and p42 MAPK, also known as ERK1 and ERK2, respectively, increasing their enzymatic activity. The activated ERKs then translocate to the nucleus, where they transactivate transcription factors, influencing gene expression to promote growth, differentiation, or mitosis (W. Zhang and Liu 2002). The p42/p44 mitogen-activated protein kinase cascade plays a crucial role in cellular signaling. Combined deletion of *MEK1/2* in development or adulthood resulted

in a loss of ERK1/2 phosphorylation, leading to reduced cell proliferation, increased apoptosis, skin barrier defects, and eventually, death. Furthermore, combined *MEK1/2* loss also halted the hyperproliferation induced by RAF (Scholl et al. 2007).

MEK2 is a crucial component of the RAS-RAF-MEK-ERK pathway, a chain of proteins responsible for transmitting signals from cell surface receptors to the cell's nucleus and DNA. This signaling cascade involves a series of activation and phosphorylation steps. When a ligand activates a cell surface receptor, and calcium influx occurs, kinases like phosphoinositide 3-kinases (PI3K) trigger the activation of RAS. RAS, in turn, phosphorylates RAF, p-RAF then activates MEK by phosphorylating its activation loop, requiring phosphorylation at two specific sites. This, in turn, leads to the phosphorylation of ERK. The entire pathway is essential for cell proliferation and survival (Yoon and Seger 2006). Physiologically, the activation of ERK is subject to negative feedback regulation at multiple levels, both upstream and downstream of MEK. This feedback regulation is achieved through the induction of protein expression, such as dual specificity phosphatases (DUSPs), and direct phosphorylation and inhibition of proteins like RAF (Pratilas et al. 2009). When RTK is activated, resulting in higher levels of p-ERK, it inhibits MEK phosphorylation (Figure 4A).

The RAS-dependent RAF/MEK/ERK1/2 signaling pathway plays a crucial role in regulating cell proliferation and survival. However, abnormal activation of this pathway, either due to receptor tyrosine kinase abnormalities or genetic mutations in *RAS* or *RAF* genes, is frequently observed in human cancers (Song et al. 2023), (Bang et al. 1998), (Fang and Richardson 2005). As a result, components of this pathway have become promising targets for the development of targeted cancer therapies and foundational research has led to the clinical development of small molecule inhibitors targeting the ERK1/2 pathway (Frémin and Meloche 2010). Recent research findings indicate the crucial role of ERK1/2 signaling in neuronal development. Involvement of the ERK1/2 signaling activation in the development of several ALS-related neuropathological dysfunctions such as glial overactivation (M. Chen et al. 2019), neuroinflammation (Kang Zhang et al. 2019) and mitochondrial dysfunction (Nowak et al. 2006) has been summarized in a recent review article (Sahu, Upadhayay, and Mehan 2021). These findings are suggesting that ERK1/2 might significantly contribute to the development of neurodegenerative diseases such as ALS and the use of ERK1/2 inhibitors could show promising benefits in reducing the likelihood of various neurological disorders. Furthermore, another study revealed that under stress conditions, cytosolic aggregates containing ERK1/2 were observed in neurons and other spinal cord cells, and abnormal phosphorylated ERK1/2

aggregates were also found in motor neurons with abnormal TDP-43 aggregates, indicating the involvement of ERK1/2 in ALS pathogenesis (Ayala et al. 2011).

Trametinib is a highly selective and reversible allosteric inhibitor that specifically targets the activity of MEK1 and MEK2 enzymes (Yamaguchi et al. 2011). Acting as an ATP non-competitive inhibitor, it binds to the activation loop, which requires phosphorylation at two specific sites for maximum activation of MEK. By inhibiting the RAF-dependent phosphorylation of MEK1 at S217, trametinib disrupts the dual phosphorylation process of MEK (S217 and S221), essential for its activation (Figure 4B) (Gilmartin et al. 2011a).

Very recently an unpublished study focused on MEK1/2 inhibition by trametinib and demonstrated some promising effects in the context of ALS treatment. The use of trametinib led to improvements in survival rates, grip strength, motor function and protecting spinal cord from degeneration of SOD1 G93A mice with overactivated ERK1/2 signaling. These positive outcomes were attributed to the enhancement of lysosomal maturation and autophagic flux facilitated by trametinib, which in turn resulted in a reduction of mutant SOD1 aggregation (Motor Neuron Disease: Therapeutics (P293.01). Currently, trametinib is undergoing clinical trials (Phase I/IIa) for the specific indication of ALS in Korea, showcasing its potential as a repurposed drug candidate in this context (NCT04326283). These findings highlight the encouraging prospects of MEK inhibition using trametinib as a promising candidate for tackling ALS and improving the quality of life for affected individuals.

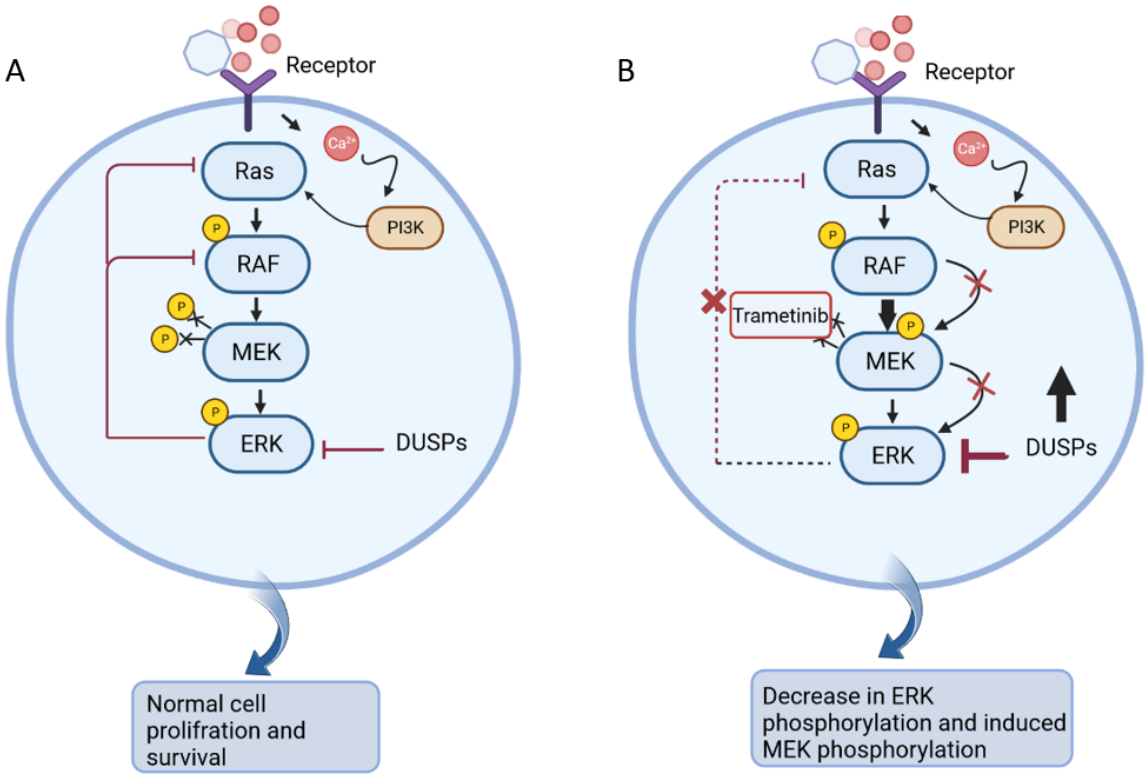

Figure 4: Schematic representation of the RAS-RAF-MEK-ERK signaling pathway and trametinib mechanism of action. (A) A chain of proteins in the cell communicates a signal from a receptor on the surface of the cell to the DNA in the nucleus through the cascade of activation and phosphorylation steps. Ligand receptor activation leads to an influx of calcium and activation of RAS through the phosphorylation by PI3K. Phosphorylation of RAF follows. P-RAF then activates MEK by phosphorylating its activation loop in two sites. This process results in phosphorylation of ERK which is necessary for cell proliferation and survival. Physiological activation of ERK is negatively feedback-regulated both downstream and upstream of MEK and is mediated by expression of DUSPs and by direct phosphorylation and inhibition of proteins like RAF. **(B)** Trametinib binds to the activation loop of MEK and disrupts the RAF- dependent phosphorylation of MEK which results in lower P-MEK expression and P-ERK. Pharmacologic inhibition of MEK by trametinib rapidly abrogates this feedback and induces phosphorylation of MEK (Figure created with BioRender.com).

1.4 Objectives of the doctoral thesis

Axono-synaptic degeneration and alterations in cytoskeleton dynamics occur early in ALS development. Due to the prominent role of RNA metabolism in ALS pathogenesis, a study of disease mechanisms restricted to the proteome is insufficient and calls for an integrative multi-omic analysis spanning all the way from the genotype to epigenetic (miRNA) and

transcriptomic analyses, the metabolome and (phospho-)proteome investigations. Improving the understanding of disease mechanisms will result in the identification of better molecular biomarkers for diagnosis, assessment of disease progression and treatment effects as well as more targeted disease-modifying therapeutic approaches. The focus of this doctoral thesis is to validate molecular candidates with potential implication in ALS pathology which were derived from multiomic profiling of human PFC and PFC from transgenic mouse models of ALS conducted in the context of the MAXOMOD consortium. Using pharmacological inhibitors, two molecular targets were validated in stress induced mouse primary cortical cultures. The approach taken in this work aimed to simulate cellular stresses and toxicities that are known to play an important role in ALS pathogenesis by exposing the cells to high concentrations of chemicals. Targets were validated, using FDA-approved inhibitors. Drug target engagement and the toxicity were tested for different concentrations prior to the experiments. To assess whether the compounds can mitigate the effects of cellular stress, the drugs were added at varying concentrations prior to stress induction. In order to quantify the neuroprotective effects of the target's inhibition, cell death and neurite outgrowth were investigated with immunocytochemistry. A schematic overview of the project steps is demonstrated below (Fig 5). It was hypothesized that the inhibition of the dysregulated proteins could rescue cell apoptosis and induce neurite regeneration.

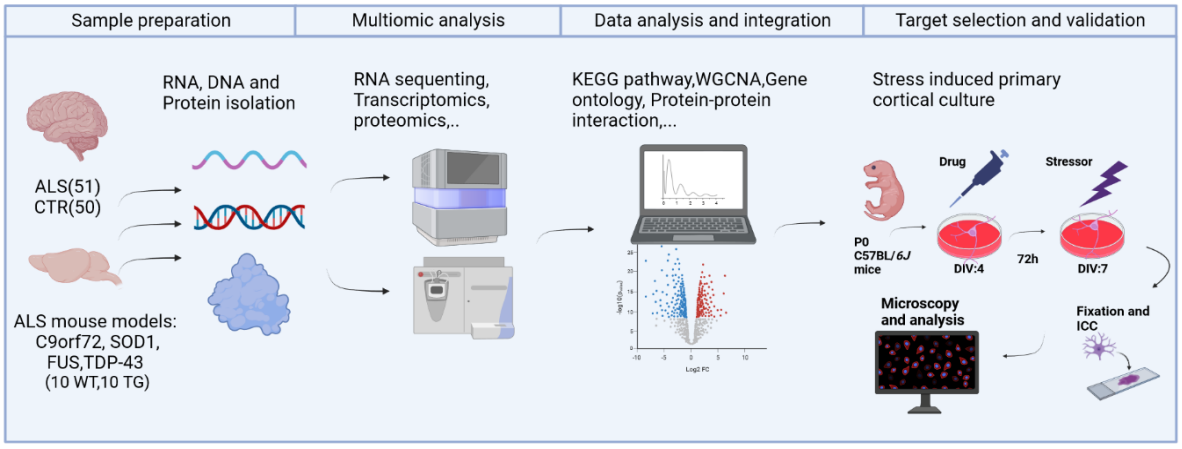

Figure 5: Schematic representation of the project: Protein and RNA were extracted from brain tissues of 51 ALS patients and 50 control subjects, along with four transgenic ALS mouse models and their respective wild-type controls (total n=10 brains per condition). Subsequently, multiple-omics analyses were performed, followed by comprehensive data integration and analysis. Potential molecular targets were selected. To validate the targets, stress-induced primary cortical cell cultures were employed. Pharmacological inhibitors were used to modulate

the expression of the targets. The neuroprotective effects by target inhibition were assessed by quantifying neurite outgrowth and cell death after immunocytochemistry and subsequent imaging (Figure generated with BioRender.com).

2 Material and methods

2.1 Material

2.1.1 Postmortem human prefrontal cortex tissue samples

Human prefrontal cortex samples (Brodmann area 6) used in the MAXOMOD project were provided by four different brain banks: the Netherlands Brain Bank, King's College London Brain Bank (London Neurodegenerative Diseases Brain Bank), Parkinson ‘s UK Brain Bank, Oxford Brain Bank. In total, 51 ALS and 50 control (CTR) samples (without signs of neurodegeneration) were included. Frozen tissues were shipped on dry ice to the Department of Neurology at the Klinikum rechts der Isar of the Technical University of Munich and stored at -80 °C. Ethical approval for the use of human tissue was obtained from the Ethics Commission (EC) of the University Medical Center Göttingen (2/8/18 AN) and the EC of the Technical University Munich (145/19 S-SR). A further characterization of the patients demographics and clinical parameters is provided elsewhere (Caldi Gomes et al. 2023).

2.1.2 Mouse prefrontal cortex samples

Multi-omic studies were conducted using four transgenic mouse models that encompassed the most common genes associated with ALS. All procedures related to animal care and experimentation in this research adhered to the relevant animal welfare regulations and received approval from the respective regulatory bodies at the participating research institutions. The mice were kept in standard cages within a pathogen-free facility, following a 12-hour light-dark cycle, and provided with unrestricted access to food and water. B6;129S6-Gt (ROSA)26Sortm1(TARDBP*M337V/Ypet) Tlbt/J mice (Gordon et al. 2019)(TDP-43-mice) were provided by the laboratory of Prof. Pasterkamp, Department of Translational Neuroscience of the University Medical Center Utrecht. This model was generated by inserting an 80 kb genomic fragment carrying the human *TARDBP* locus (including a patient-derived M337V mutation). TDP-43 transgenic and control wild-type animals were sacrificed at the age of 26 weeks (presymptomatic stage) for biomaterial collection. B6SJL-Tg (SOD1*G93A)1Gur/J mice (Gurney et al. 1994) (SOD1-mice) were provided by the laboratory of Dr. Bonetto in Translational Biomarkers, IRCCS-Istituto di Ricerche Farmacologiche “Mario Negri” (IRFMN) Milano. Male mice carrying a high-copy number of the B6 congenic Tg (SOD1G93A)1Gur/J SOD1G93A mutation, obtained from Jackson Laboratory, were crossbred with C57BL/6 female mice to produce two groups of mice: non-transgenic mice and

mutant transgenic mice expressing G93A*SOD1. Both SOD1 transgenic and control mice were euthanized at 14 weeks of age (presymptomatic stage) (LaClair et al. 2020). C9orf72-mice were provided by the laboratory of Prof. Edbauer at the German Center for Neurodegenerative Diseases in Munich. Animals were generated by electroporating plasmids for conditional expression of dipeptide repeat proteins (DPRs) which were produced by inserting GFP-(GA)175 genes (encoded using non-repeating alternate codons) downstream of a floxed stop-cassette in the pEX CAG stop-bpA vector, into murine RMCE embryonic stem cells at the Rosa26 Safe Harbour. Mouse lines GAstop with germ-line transmission were backcrossed to the C57Bl6N background until >98% purity was confirmed using SNP genotyping. C9orf72 transgenic and control animals were euthanized at 4.5 weeks of age, during the early symptomatic stage. Tg (Prnp-FUS) WT3Cshw/J mice, referred to as FUS mice, (Mitchell et al. 2013) were also provided by the Bonetto Lab of Translational Biomarkers, Istituto di Ricerche Farmacologiche Mario Negri IRCCS Milano, and were sacrificed at 4 weeks after birth. In each model, ten transgenic and ten non-transgenic mice were carefully selected and balanced for sex and PFC were dissected as described in methods (Tissue sampling section).

2.1.3 Reagents, buffers and chemicals

Table 1: List of reagents, buffers and chemicals used in experiments.

Reagent	Producer
1-Bromo-3-Chloropropane	Sigma Aldrich (USA)
2.5 % Trypsin 10X	Thermo Fisher Scientific (USA)
2-Propanol	AppliChem, (Germany)
Ammonium chloride	Merck (Germany)
B-27 Plus Supplement (50X)	Thermo Fisher Scientific (USA)
Bovine serum albumin	Sigma Aldrich (USA)
DNAse I	Merck (Germany)
Ethanol absolute	AppliChem, (Germany)
Fetal bovine serum	Sigma Aldrich (USA)
Formaldehyde solution	Sigma Aldrich (USA)
Glyco blue coprecipitant	Invitrogen, (Germany)
Goat Serum (10X)	Sigma Aldrich (USA)
HBSS (10X)	Thermo Fisher Scientific (USA)
Holo-Transferrin	Sigma Aldrich (USA)
L-glutamic acid	Tocris (UK)
MES-SDS Buffer (20X)	Thermo Fisher Scientific (USA)
Mounting medium with DAPI	Abcam (UK)
Mouse purified Laminin	Thermo Fisher Scientific (USA)
Neurobasal Plus Medium	Thermo Fisher Scientific (USA)
Nitric Acid	Sigma Aldrich (USA)
Nuclease-Free Water	Sigma Aldrich (USA)
NuPAGE LDS sample buffer(4X)	Thermo Fisher Scientific (USA)

NuPAGE sample reducing agent (10X)	Thermo Fisher Scientific (USA)
PBS (10X), pH 7,4	Thermo Fisher Scientific (USA)
PBS-T (1%)	Thermo Fisher Scientific (USA)
Penicillin-Streptomycin-Neomycin (PSN) 100X	Thermo Fisher Scientific (USA)
PhosSTOP (Phosphatase Inhibitor	Sigma Aldrich (USA)
Poly-D-Lysine	Merck (Germany)
Poly-L-Ornithine	Merck (Germany)
Ponceau	Sigma Aldrich (USA)
Protease Inhibitor mix	Sigma Aldrich (USA)
RIPA Lysis Buffer	Thermo Fisher Scientific (USA)
Selinexor (KPT-330) Catalog No. A12582	Adooq Bioscience (USA)
Skim milk powder	Sigma Aldrich (USA)
Sodium arsenate dibasic heptahydrate	Sigma Aldrich (USA)
Sodium bicarbonate	Merck (Germany)
Sodium-L-glutamate monohydrate	Merck (Germany)
Tween 20	Sigma Aldrich (USA)
Trametinib (HY-10999)	Medchemexpress (USA)
Triton X-100	AppliChem (Germany)
Trizol	Ambion life technology (USA)

2.1.4 Antibodies

Table 2. List of antibodies.

Antibody	**Producer**
Alexa Fluor™ 488 Goat anti-mouse (# A-11034)	Life technologies GmbH (Germany)
Anti-G3BP antibody [2F3] (ab56574)	Abcam (UK)
Anti-MAP2 polyclonal rabbit (188002)	Synaptic systems (Germany)
Cleaved Caspase-3 (Asp175) Antibody (#9661)	Cell Signaling (USA)
Cy™3 AffiniPure Goat Anti-Rabbit IgG (H+L) (111-165-144)	Jackson ImmunoResearch (USA)
Exportin-1/CRM1(D6V7N) #46249	Cell Signaling (USA)
GAPDH Rabbit mAB (14C10)	Cell Signaling (USA)
GFAP monoclonal antibody #13-0300	Invitrogen (USA)
Lamin B1 Rabbit polyclonal antibody (12987-1-AP)	Proteintech (USA)
MAP2 Antibody mouse (#4542)	Cell Signaling (USA)
MEK2 Antibody #9125	Cell Signaling (USA)
P44/42 MAPK (ERK1/2) antibody #9102	Cell Signaling (USA)
p62/SQSTM1 Antibody (P0067)	Sigma Aldrich (USA)
Phospho-MEK1/2(Ser217/221) #9121	Cell Signaling (USA)
Phospho-p44/42 MAPK(ERK1/2) #9101	Cell Signaling (USA)

2.1.5 Kits and primers

Table 3: List of kits and primer assays

Kit/Primer	Producer
Agilent RNA 6000 Nano kit	Agilent technologies
BCA Pierce Assay Kit	Thermo Fisher Scientific (USA)
miScript SYBR Green PCR Kit	Qiagen (Germany)
Mm_GAPDH_3_SG Quantitect Primer Assay	Qiagen (Germany)
Mm_Map2k2_1_SG Quantitect Primer Assay	Qiagen (Germany)
Mm_XPO1_SG Quantitect Primer Assay	Qiagen (Germany)
Quantitect Reverse transcription kit	Qiagen (Germany)
RNA Clean & Concentrator-5 KIT	Zymo research (USA)
SuperSignal West Pico PLUS Chemiluminescent Substrate	Thermo Fisher Scientific (USA)
ToxiLight Cytotoxicity Kit	Lonza (Switzerland)

2.1.6 Equipment

Table 4. List of equipment.

Equipment	Producer
20-G Quincke spinal needle	Becton Dickinson, USA
Agilent 2100 Bioanalyzer	Agilent (USA)
Cell culture plates	Greiner Bio-one, Germany
Cell scraper	TPP Techno plastic (Switzerland)
Centrifuge 5424 R	Eppendorf (Germany)
CO2 incubator	Binder (Germany)
Eppendorf tubes	Eppendorf (Germany)
FusionSL Chemiluminescence & Fluorescence Imaging Systems	Vilber Lourmat (France)
Herasafe 2030i cell culture hood	Thermo Fisher Scientific (USA)
iBlot2 gel transfer device and transfer stack	Thermo Fisher Scientific (USA)
Master cycler	Eppendorf (Germany)
Multifuge 3SR+ Centrifuge	Thermo Fisher Scientific (USA)
Multirun Incubation shaker	Infors HT (Switzerland)
Nanodrop One	Thermo Fisher Scientific (USA)
NuPAGE™ 4 to 12%, Bis-Tris	Invitrogen (USA)
Pasteur pipette	Corning (USA)
PowerPac Universal power supply	Biorad (Germany)
Quant Studio 3 q-RT-PCR	systemThermo Fisher Scientific (USA)
QuantStudio 5 qPCR	Thermo Fisher Scientific (USA)
Tecan Infinite 200 Microplate Reader	Group AG (Switzerland)
Thermomixer Comfort	Eppendorf (Germany)
U-100 insulin syringes	B Braun omnifix (Germany)
VXR basic Vibrax	IKA (Germany)
Water bath	Memmert (Germany)
Zeiss Observer Z1 Fluorescence Microscope	Carl Zeiss AG (Germany)

2.1.7 Software

Table 5. List of software used for experiments, data analysis and figure design.

Software	Producer
Image J Fiji Version 2.9.0/ SNT ImageJ Plugin Version 4.1.15	National Institutes of Health (USA)
GraphPad Prism 9	GraphPad software (USA)
Inkscape	Sodipodi
Biorender	Biorender (Canada)
QuantStudio Design and Analysis Software v1.5.1	Thermo Fisher Scientific (USA)

2.2 Methods

2.2.1 Tissue sampling

Frozen tissue blocks from human brains were punched with 20-G Quincke spinal needle (Becton Dickinson, Franklin Lakes, NJ, USA) and around 20 mg of tissue were collected into RNAse/DNAse free tubes for each sample. Tissue punches were kept at -80 °C until further use. To prepare the prefrontal cortex regions from fresh mouse brains, animals underwent perfusion with 50 ml of ice-cold PBS prior to microdissection. The head was separated by cutting at the skull's base and removing the skin. The skull was extracted through small incisions, and the prefrontal cortex region from both hemispheres was microdissected. The olfactory bulb and cerebellum were removed by cutting at the cerebellar peduncle, starting from the olfactory bulb and proceeding along the interhemispheric fissure using fine-tipped tweezers. The cortex was then separated from the rest of the brain. Incisions were made in the middle of the cortex to extract the prefrontal cortex (PFC). The freshly prepared PFC samples were collected in nuclease-free tubes and stored at -80 °C until they were used for RNA isolation experiments.

2.2.2 RNA isolation

Total RNA was isolated from human and animal prefrontal cortex samples using Trizol Reagent (Ambion Life Technology, USA). All RNA-related experiments were performed under an RNA-workstation fume hood. Briefly, 500 µl of Trizol Reagent was added to each sample and tissues were homogenized using a plastic homogenizer, followed by the addition of 50 µl of 1-

Bromo-3-Chlor-Propane (Sigma Aldrich, USA). The reaction tubes were mixed by inversion for 10 -15 seconds and incubated at room temperature (RT) for 3 minutes. The lysates were centrifuged at 12.000 x g for 20 minutes / 4 °C, leading to phase separation. The RNA-containing aqueous phase was collected and transferred to a fresh nuclease-free tube. RNA precipitation was performed by adding 250 µl of 2-propanol (AppliChem, Germany) and 2 µl GlycoBlue Co-precipitant (15 mg/ml) (Invitrogen, Germany), followed by mixing and overnight incubation at -20°C. Next, the samples were centrifuged at 12.000 x g for 30 minutes / 4°C, the supernatant was discarded and the RNA pellets were washed three times with 75% ice-cold ethanol (AppliChem, Germany). The pellets were dried for 5 minutes under the fume hood, reconstituted with 15-20 µl of nuclease-free water (Sigma Aldrich, USA) and RNA samples incubated at 55°C for 2 minutes in a thermoshaker in order to completely dissolve the RNA.

After the RNA isolation, a DNAse treatment was performed in order to remove any DNA contamination from the samples using RNA Clean & Concentrator-5 KIT (Zymo Research, USA). For that, 5 µl of 10X DNAse I Incubation buffer (Life Technologies, Carlsbad, CA, United States), 5 µl DNase I (2U/µl) and 0.5 µl -RNase OUT (40U/µl) were added to each sample. Samples volume was filled up to 50 µl by the addition of nuclease-free water, followed by incubation at 37 °C For 20 minutes. Finally, the RNA samples were cleaned and concentrated with the RNA Clean & Concentrator-5 KIT (Zymo Research, Irvine, CA, USA), following the manufacturer's instructions.

2.2.3 Determination of nucleic acid concentration and purity

Directly after RNA isolation, nucleic acid concentration and purity were measured in the NanoDrop One spectrophotometer (ThermoFisher, Waltham, MA, USA). Spectrophotometric quantification in the NanoDrop system required 1 µl of each sample. For RNA samples used in RNA sequencing experiments, RNA integrity was assessed with the Agilent 6000 Nano Chip in the Agilent 2100 Bioanalyzer (Agilent, Santa Clara, CA, USA).

2.2.4 RNA sequencing experiments

mRNA and small RNA sequencing experiments were performed by Prof. Schlapbach's laboratory in the Functional Genomics Center Zurich. All samples were quantified and quality controlled with the Fragment Analyzer, Advanced Analytical Technologies, Inc. 100 ng of each sample was used to generate mRNA libraries according Truseq mRNA Stranded protocol instructions. Ready libraries were again quality-controlled with the Fragment Analyzer.

Libraries were pooled and sequenced on the Illumina Nova Seq-sequencer. For the mRNA sequencing, total RNA libraries were prepared using either the TruSeq Stranded mRNA (Illumina, Inc, California, USA) (Short Read Sequencing), or the SMARTer® Stranded Total RNA-Seq Kit v2 -Pico Input Mammalian (A Takara Bio Company, California, USA) (Short Read Sequencing). Briefly, In the TruSeq protocol, RNA samples (100-1000 ng) underwent poly-A enrichment and reverse transcription into double-stranded cDNA. After fragmentation, end-repair, and adenylation, TruSeq adapters with unique dual indices (UDI) were ligated for multiplexing. PCR was used to enrich fragments with adapters on both ends, resulting in an average size of 260 bp. Libraries were normalized to 10 nM. For the SMARTer® Stranded Total RNA-Seq Kit v2 -Pico Input Mammalian protocol, RNA samples (0.25–10 ng) were reverse-transcribed with random priming and a template switch oligo (TSO). PCR added full-length Illumina adapters, including multiplexing indices. ZapR cleaved ribosomal cDNA, and a second PCR enriched remaining fragments (average size 360 bp). Libraries were normalized to 5 nM. Quality and quantity were validated with a Fragment Analyzer or Tape station. Sequencing was performed on a Novaseq 6000 with single-end 100 bp configuration. For small RNA sequencing with RealSeq-AC miRNA, RNA samples (1 ng - 1 ug) were ligated, circularized, reverse-transcribed, and amplified with sample barcodes. The library had an approximate fragment size of 149 bp, normalized to 10 nM. Quality and quantity were verified, and sequencing was done on a Novaseq 6000 with single-end 100 bp configuration.

Transcriptomics data was processed using the Next Flow Core RNASeq pipeline (version 3.0) and demultiplexed with bcl2fastq. Quality checks were conducted using FastQC. Salmon (tool for quantifying the expression of transcripts using RNA-seq data) was employed for pseudo alignment and quantitation, with indices built from GENCODE annotations (vM26 for mice and v37 for humans). Count matrices from Salmon were used for subsequent analysis. Principal Component Analysis and heatmaps used these count matrices after filtering and normalization via a variance stabilizing transformation, without knowledge of the experimental design. Genes with at least ten counts in 50% of samples within any condition and sex were retained after filtering. Differential expression analysis with DESeq2 was followed by gene set enrichment analysis on Gene Ontology terms using the cluster Profiler R package. Terms with gene counts between 10 and 500 were selected, and p-values were adjusted using the Benjamini-Hochberg correction.

2.2.5 Reverse transcription

For quantitative real-time PCR experiments (q-RT-PCR), complementary DNA (cDNA) synthesis was performed. For miRNA q-RT-PCR validation experiments, 1 µg of RNA from each sample were reverse transcribed using the QuantiTect reverse transcription Kit (Qiagen, Hilden, Germany). All steps were performed on ice. A master-mix was prepared for each RT reaction, as follows: 2 µl gDNA wipeout buffer, 7x, 1µg of the RNA and RNase-free water up to 14 µl followed by incubation for 2 min at 42 °C and putting immediately on ice this step was performed in order to eliminate the genomic DNA in the samples. The master mix for the reverse transcription step was prepared (Table 7). Following the addition of the master mix to the samples, the reaction tubes were incubated for 15 minutes at 42 °C in the Master cycler nexus gradient PCR thermocycler (Eppendorf, Hamburg, Germany), followed by incubation at 95 °C for 3 minutes to inactivate the reverse transcriptase. cDNA samples were diluted 1:2 in nuclease-free water and stored at -20 °C until q-RT-PCR experiments. To determine the total gene expression levels of selected targets, q-RT-PCR reactions were conducted in the QuantStudio 3 system (ThermoFisher, Waltham, MA, USA) using GAPDH as a housekeeping control. MicroAmp Optical 96-Well Reaction Plates (Applied Biosystems, Foster City, CA, USA) were prepared at room temperature and the reaction plates were tightly sealed with a heat-sealing adhesive film before placement inside the cycler. Reaction volumes were calculated as described in the tables below.

Table 7. Reverse-transcription reaction components.

Component	**Volume/reaction**
Quantiscript reverse transcriptase	1 µl
Quantiscript RT buffer, 5X	4 µl
RT primer mix	1 µl
Template RNA	14 µl
Total reaction volume	**20 µl**

2.2.6 Quantitative Real-Time Polymerase Chain Reaction (q-RT-PCR)

To determine gene expression levels of targets in toxicity models, q-RT-PCR reactions were conducted in the QuantStudio 3 system (ThermoFisher, Waltham, MA, USA). For q-RT-PCR experiments, the QuantiTect SYBR Green PCR Kit (Qiagen, Hilden, Germany) was used, and gene expression was normalized to the housekeeping control GAPDH. MicroAmp Optical 96-Well Reaction Plates (Applied Biosystems, Foster City, CA, USA) were prepared at room

temperature and the reaction plates were tightly sealed with a heat-sealing adhesive film before placement inside the cycler. Reaction volumes were calculated as described in table 8. PCR initial activation step starts with 15 min at 95 °C followed by 3-step cycling denaturation 15 s, 94 °C, annealing, 33 s, 55 °C, extension 30 s, 70 °C and 40 cycles. The relative expression levels of miRNA and mRNA species were calculated by the ΔΔCt method (delta-delta-Ct). Ct values for each sample were compared to the average of ΔCt of the respective control group.

Table 8. QuantiTect q-RT-PCR reactions master mix.

Component	**Volume/reaction**
SYBR green	7.5 µl
Primer	1.5 µl
RNAse free water	4 µl
cDNA	2 µl
Total reaction volume	**15 µl**

2.2.7 Proteomics analysis of mouse and human PFC tissue samples

Proteomics analysis was performed by the Dr. Carapito's Lab in BioOrganic Mass Spectrometry Laboratory, Institut Pluridisciplinaire Hubert Curien, University of Strasbourg. Briefly, prepared tissues were homogenized with a biomasher using 350 µl MeOH: H2O (4:1). Protein pellets were reconstituted in 200 µl Laemmli buffer (10% SDS, 1 M Tris pH 6.8, and glycerol) and then centrifuged at 16.600 x g at 4 °C for five minutes. The protein concentration was determined following the manufacturer's instructions using a DC assay (Bio-Rad, Hercules, CA, USA). Subsequently, each sample containing 100 µg of protein lysate was heated at 95 °C for five minutes, loaded onto a 5% acrylamide SDS–PAGE stacking gel, and subjected to overnight digestion at 37 °C using modified porcine trypsin (Mass Spectrometry Grade, Promega, Madison, WI, USA) at an enzyme–protein ratio of 1:80 after prior reduction and alkylation of the gel bands. The resulting peptides were extracted using 60% acetonitrile (ACN) followed by 100% ACN, and they were resuspended in a solution containing 30 µl of H2O, 2% ACN, and 0.1% fluoroacetic acid. To serve as internal quality controls (QCs), iRT peptides (Biognosys, Schlieren, Switzerland) were added to each sample. NanoLC–MS/MS experiments were carried out utilizing a nanoAcquity UltraPerformance LC (UPLC) system (Waters in Milford, MA, USA), which was coupled to a Q-Exactive Plus Mass Spectrometer (Thermo Fisher Scientific, USA). For the analysis, samples containing 800 ng of protein were loaded

onto a precolumn, and peptides were separated through the use of an ACQUITY UPLC BEH130 C18 column employing a gradient. The mass spectrometry system operated in a data-dependent acquisition (DDA) mode, which alternated between MS and MS/MS modes, selecting the ten most abundant precursor ions for further isolation. Periodic injections of quality control samples were conducted. Raw data processing was carried out using MaxQuant version 1.6.14, and the Andromeda search engine was used to identify peaks based on a protein sequence database. To ensure data accuracy, false discovery control measures were implemented, and protein intensities were extracted for subsequent statistical analysis. The MaxQuant protein vs. sample table was utilized for downstream analyses. After filtering out proteins with low abundance (detected in less than 50% of samples across different conditions and sexes) and imputing missing values, log2-transformed intensities were utilized for principal component analysis, heat map generation, and differential abundance analysis. Linear modeling was performed using the limma package, and p-values were adjusted using the Benjamini–Hochberg correction.

2.2.8 Primary cortical culture from mice

Cortical neuronal cell cultures were prepared from C57Bl/6J mouse pup postnatal day 0 or 1(P0-P1). The protocol for generating the primary neuronal cell cultures was in accordance with local and international guidelines on the ethical use of animals. Animal care followed official governmental guidelines and all efforts were made to minimize the number of animals used and their suffering. Pups were decapitated and the brains were collected in dissection media containing 10X Hanks balanced salt solution (HBSS) (Thermo Fisher Scientific, USA) and sodium bicarbonate (Merck, Germany). The cortex was dissected, the meninges were removed and small pieces of the cortex were collected in a reaction tube. Tissues were trypsinized at 37 °C in a water bath for 13 min and was treated with 200 µl of DNAse I (10 mg/ml) (Merck, Germany). Tissues were triturated in fetal bovine serum with a fire polished pasteur pipette until tissue pieces were disintegrated and then it was centrifuged for 4 min at 800 g. Cell pellet was suspended and maintained in neurobasal medium (Thermo Fisher Scientific, USA) supplemented with B27 (Thermo Fisher Scientific, USA) and antibiotics (0.06µg/mL penicillin and 0.1µg/mL streptomycin). The cells were seeded at a density of 300.000 cells per well in 24-well plates, respectively. Before cell seeding, coverslips were acid-washed overnight and rinsed many times with water. Coverslips were then sterilized with ethanol overnight and UV lighted for at least 30 min after being placed in the 24-well plate. The plates were then coated with poly-L-ornithine (0.05 mg/mL) (Merck, Germany) overnight and Laminin (1:1000) (Thermo

Fisher Scientific, USA) for 2 h in the incubator before use. The cells were cultured at 37 ℃ in a humidified atmosphere containing 5% CO2 for 7 days prior to experimentation. Medium was exchanged every 3 days.

2.2.9 Toxicity induction in primary cortical culture from mice

Glutamate-induced excitotoxicity in mouse primary cortical culture was induced by treating the cells at day *in vitro* 7 (DIV7) with glutamate. L-glutamic acid (Tocris, UK) was dissolved in 50 mM sodium hydroxide (NaOH), and a stock solution of 50 mM was prepared prior to use. An appropriate concentration of glutamate was prepared in maintenance media (neurobasal medium supplemented with B27 and antibiotics). Cells were exposed to 5 mM glutamate by exchanging 1:3 of the media. After 6 h of incubation, glutamate was washed out thoroughly and the cells were fixed for immunocytochemistry or lysed for protein extraction.

Sodium arsenite (Sigma Aldrich, USA) was prepared first at the 0.05 M concentration stock by dissolving the powder in distilled water. An appropriate concentration of sodium arsenite was prepared in maintenance media (neurobasal medium supplemented with B27 and antibiotics). Cells were exposed to 10 mM sodium arsenite by exchanging 1:3 of the media. After 3 h of incubation, cells were fixed for immunocytochemistry or lysed for protein extraction.

2.2.10 Protein extraction from cell culture, determining protein concentrations and Western blotting

For protein extraction, cells were washed once with 1X PBS. RIPA lysis buffer (Thermo Fisher Scientific, USA) containing protease inhibitor cocktail (Sigma Aldrich, USA) 1:25 and phosphatase inhibitor (Sigma Aldrich, USA) 1:20 was added and the plate was incubated on ice for 5 min. Cells were scratched with a cell scraper on ice and transferred in Eppendorf tubes and homogenized by passing through the U-100 insulin syringes a few times. protein concentration was determined using Thermo Scientific™Pierce™ BCA Protein Assay Kit (Thermo Fisher Scientific, USA) following the manufacturer's instructions. 1 µl of a protein sample was used in the assay. The prepared colorimetric reactions were read in the ELISA plate reader (Group AG, Switzerland). 20 mg of the samples were loaded in the gel. NuPAGE LDS-sample buffer 1:4 (Thermo Fisher Scientific, USA) and sample reducing buffer (Thermo Fisher Scientific, USA) 1:10 was added to lysed protein before loading in the gels and incubated shaking at 75 ℃ for 13 min followed by centrifugation at 12000 g at 4 ℃ for 2 min. Proteins were separated by gel electrophoresis using 200 volts. Proteins were transferred to a nitrocellulose membrane using the iBlot2 gel transfer device and transfer stack (Thermo Fisher

Scientific, USA). Membranes were blocked for 30 minutes at room temperature with 5% nonfat milk (Sigma Aldrich, USA) or 4% bovine serum albumin (Sigma Aldrich, USA) in 0.05% tween-PBS followed by incubation with primary antibodies (diluted in blocking buffer) overnight at 4 °C under rotation. After washing 4 times with PBST (5 min each time) the membranes were incubated with highly-sensitive HRP-labeled secondary antibodies (1:10,000 diluted in blocking buffer) at room temperature for 1 h followed by intensive washing with PBST. Blots were incubated with ECL reagent using SuperSignal West Pico PLUS chemiluminescent substrate kit (Thermo Scientific, USA) for 5 min following the manufacturer's instructions. Protein bands were visualized on a BioRad Molecular Imager ChemiDoc™ (Vilber lourmat, France) and quantified with Image J Software.

2.2.11 Subcellular fractionation of primary cortical neuron lysates

Cultured mice cortical neurons were lysed using the subcellular fractionation buffer (Table 9). Cells were scraped immediately and transferred to Eppendorf tubes. Lysate was homogenized by passing it through a needle 10 times and incubated on ice for 20 min. Lysate was centrifuged at 1000 G for 5 min. The supernatant (first fraction S1) was collected. The pellet was washed by adding a fractionation buffer and dispersing the pellet by pipette and passing through the needle 10 times. After centrifugation at 1000 g for 10 min, supernatant (second fraction S1) was collected and added to the first S1 and pellet (nuclear pellet P1) was resuspended in 74 µl of the fractionation buffer with 10% glycerol and 0.1% SDS and passed through needle again for homogenization.

Table 9. Fractionation Buffer (50 ml 1x solution).

HEPES (pH 7.4) 1M	1ml
KCI	0.0373 g
$MgCl_2$	75 µl from 1 M
EDTA	100 µl from 0.5 M
EGTA	100 µl from 0.5 M
150 mM Sucrose	4.28 g
1 mM DTT (1M)*	10 µl (Per 10 ml)
PI Cocktail (III)*	50 µl (Per 10 ml)

***Added just before use**

2.2.12 Toxilight toxicity assay

For detecting the toxicity range of different concentrations of the inhibitors (selinexor and trametinib), the ToxiLight cytotoxicity assay kit (Lonza, Switzerland) was used. On DIV4 of the primary neuronal cell culture, one third of the media was exchanged with the fresh media mixed with the required concentrations of the inhibitors. Toxilight assay was performed on timepoints 24 h, 48 h and 72 h after adding the inhibitors. The typical sensitivity of the assay is < 10 cells/well. The assay can also be used on samples of culture media taken from experimental wells so, media was directly taken from the 24 wells culture plate and diluted to be scaled down to the detection range of the kit. ToxiLight 100% lysis reagent, adenylate kinase (AK) assay buffer was brought to room temperature and the kit instructions were followed. 10 ml of assay buffer were added into the bottle containing the AK detection reagent (AKDR). After 10 minutes, 100 µl of AKDR and 20 µl of the diluted cells was transferred into a new 96-well plate (2x wells for each condition). RIPA was added to one of the wells and the lysed cells were used as positive control. After 15 min of incubation, the plate was centrifuged for 1 min at 800 rpm. The plate was placed into the TECAN luminometer and a 1-second read was taken of each well using a preconfigured protocol TECAN i-control software.

2.2.13 Immunocytochemistry and microscopy

Cells were cultured on coverslips following the described methods and were immunostained at DIV7 neuronal culture according to standard techniques. Cells were fixed with 4% paraformaldehyde (Sigma Aldrich, USA) in PBS at room temperature for 10 minutes. For quenching the free aldehyde groups, cells were treated with 50 mM ammonium chloride (Merck, Germany) for 15 min and then washed with PBS 2X (5 min each). Permeabilization of the cell membrane was done by applying PBS with 0.25% Triton X-100 (AppliChem, Germany) for 10 min at RT. Nonspecific binding sites were blocked by applying 10% goat serum in PBS for at least 20 min. Required concentrations of primary antibodies were prepared in blocking solution to a final volume of 180 µl per 18-mm coverslip and cells were incubated for 90 min at 37 °C shaking. The following primary antibodies were used: mouse anti-MAP2 (1:500) (Cell Signaling, USA), rabbit anti-cleaved caspase 3 (1:250) (Cell Signaling, USA), mouse anti-G3BP1 (1:500) (Cell Signaling, USA), rat anti-GFAP (1:500) (Invitrogen, USA), rabbit anti-MAP2 (1:500) (Synaptic systems, Germany), rabbit anti-XPO1 (1:500) (Cell Signaling, USA), rabbit anti-p62 (1:500) (Sigma Aldrich, USA). Cells were washed 3 times for 5 min with PBS before applying the secondary antibodies. Secondary antibodies Alexa Fluor™ 488 Goat anti-mouse (Life technologies GmbH, Germany) or Cy™3 AffiniPure Goat Anti-

Rabbit IgG (Jackson ImmunoResearch, USA) were applied to cells (1:250), and incubated for 30 min followed by repeating the washing steps. For double staining, a second primary antibody was added and the same steps were repeated. Coverslips were mounted on slides using a mounting medium with DAPI (Abcam, UK). Images were acquired with a 63x oil objective on a Zeiss inverted fluorescence microscope (Zeiss, Oberkochen, Germany) and analyzed by Image J software. Fifteen random images from each coverslip were analyzed for cell death by counting the number of cleaved caspase-3 positive cells. Average Neurite length were measured using the simple neurite tracing (SNT) plugin in Image j software.

2.2.14 Bioinformatics analyses

Small RNA and RNA sequencing data processing and mapping, mass spectrometry analysis data processing and mapping, differential expression and sample correlation analyses, gene ontology and pathway enrichment analyses and weighted gene co-expression network analysis (WGCNA) were performed by the University Medical Center Hamburg-Eppendorf, Institute of Medical Systems Biology, Hamburg, Germany, in collaboration. Detailed methods and tools that were used are provided elsewhere (Caldi Gomes et al. 2023) Statistical analysis of validation experiments was done using GraphPad Prism 9. Ordinary one-way Analysis of variance (ANOVA) was used to determine the significant differences between more than two conditions for WB data, q-RT-PCR relative expression data and for ICC quantification data. Unpaired t-tests were conducted to assess significant differences in mean values between two conditions (stressed and non-stressed cells) in toxicity models establishment experiments. Identifying outliers were performed using Grubbs test (Alpha = 0.1). Data are given as mean ± standard error of the mean (SEM). Differences were considered significant when $p < 0.05$.

3 Results

3.1 Identification of novel pharmacological targets based on multi-omic data integration

Because of the incomplete understanding of ALS disease mechanisms, particularly in early stages of the disease, the MAXOMOD project aimed at characterizing the molecular changes in ALS-affected brains to identify molecular determinants and novel mechanisms of motoneuron degeneration. In the scope of the E-Rare-2018-funded multinational research consortium this project conducted a multi-omic profiling of ALS-affected brains. In collaboration with different research groups in Europe we analyzed well-characterized human postmortem tissue from the prefrontal cortex (region BA6) of sporadic ALS patients (n=51) and age-adjusted control subjects (n=50) from four European brain banks. RNA and protein were isolated from brain tissue and samples were subjected to genotyping, transcriptomic, proteomic and micro-RNAomic analysis, followed by data integration. In addition, we compared these findings with four transgenic mouse models of ALS bearing mutations in the four most common ALS-causative genes: *SOD1, C9ORF72, TARDBP* and *FUS*. The results of this study revealed multiple differentially expressed genes and proteins as well as deregulated molecular pathways in ALS-affected brains. It also identified transcriptome-based human ALS-subclusters that are driven by specific cellular processes such as immune response, extracellular matrix, mitochondrial respiration, and RNA metabolism. Interestingly the molecular signatures of human subclusters are reflected in specific mouse models. Hierarchical clustering for enriched pathways revealed four distinct molecular subgroups: C1-C4. In summary, this study shows that molecular subclusters and sex-specific differences drive the heterogeneity in the PFC of ALS patients (Caldi Gomes et al. 2023). In general, this study provides valuable insights into the molecular changes occurring in ALS-affected brains and contributes to the identification of potential targets for further research and the development of therapeutic strategies.

A major goal of the MAXOMOD project was the identification of novel molecular targets as early denominators of ALS pathogenesis that could be addressed by drug candidates. The selection of potential pharmacological targets was achieved by performing weighted gene co-expression network analysis (WGCNA) based upon deregulated transcripts- and proteins from PFC samples of ALS- and CTRL samples and the four mouse models. While we observed transcriptional and cell composition differences between mouse models and human ALS clusters, we found consistent changes in MAPK signaling in TDP43-, SOD1-, and C9orf72-

models as well as in human ALS samples. Moreover, analysis of subclusters shows that the classical MAPK pathway was deregulated in 3 of these subclusters. Deregulation of MAPK pathways is a common theme in both human ALS and mouse transcriptomes.

MEK2 is an important component of this pathway and intimately related to neuronal differentiation, microtubule assembly also neuronal survival, and it was deregulated for proteomics in the C9orf72 (males and females) and SOD1 (females) model. It was also identified as one of the most deregulated pathways in WGCNA analyses for these models. WGCNA transcriptomic enrichment results for C9orf72: Pathway Description=MAPK signaling pathway; pvalue= 7.30E-05; padj= 0.019865724; Gene Count= 18; Gene Ratio=18/196. For SOD1: Pathway Description=MAPK signaling pathway; pvalue= 3.83E-06; padj= 0.000409475; Gene Count= 48; Gene Ratio= 48/747. Functional enrichment showed a strong representation of the MAPK signaling pathway particularly in the human samples, but also in almost all other transgenic mouse models of ALS (Fig. 6) (Caldi Gomes et al. 2023).

Differential expression analysis in SOD1 animals showed XPO1 as the most differentially expressed protein in both sexes (padj=0.052) as well as showing corresponding increased gene expression levels in the same model. This protein is a major regulator of nuclear RNA export. XPO1 deregulation was also observed in TDP-43 females, FUS-males and the C9orf72 animals. Functional enrichment analysis also highlighted nucleocytoplasmic transport in human samples and different mouse models (Fig. 7) (Caldi Gomes et al. 2023). This deregulation observed on multiple molecular levels in different analyzed models suggested an important role of XPO1 for the disease-mechanism of ALS. Although multiple molecular pathways identified in our analysis would merit therapeutic validation, we decided to choose MEK2 and XPO1 as our molecular drug targets.

The identification of XPO1 and MEK2 as molecular targets resulted in the selection of two pharmacological substances, selinexor (inhibitor of XPO1) and trametinib (inhibitor of MEK2) subsequently, that are known to modulate these targets. Selinexor is an FDA-approved selective inhibitor of nuclear transport (SINE) compounds. It binds to XPO1 and inhibits the nuclear export of proteins. Trametinib, is also an FDA-approved compound currently used in cancer treatment due to its antitumor properties, inhibiting cell proliferation and tumor growth. It is a reversible, allosteric inhibitor of MEK1 and MEK2.

I have been involved in the preparation of all human and animal samples for omics analysis (e.g. RNA and protein isolation) for this project, and have also contributed to the process of selecting the validation targets. However, the main tasks I conducted in for this doctoral dissertation was related to the experimental validation of the selected targets *in vitro*. In the next

chapters, the validation of these pharmacological drug candidates in stress-induced cell culture models mimicking different aspects of ALS pathology will be discussed. Positive results in the validation will advocate the translation of these pharmacological drug targets to clinical phase II trials in ALS patients.

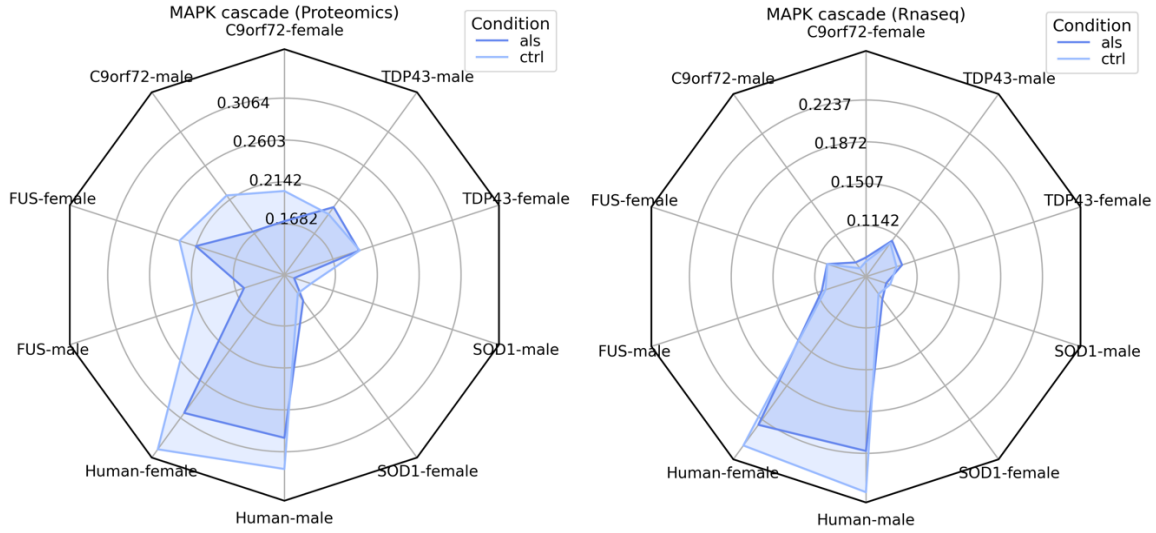

Figure 6: Radar plots showing the functional enrichment for the MAPK signaling pathway, the pathway involving MEK2 function, in proteomics (left) and RNAseq (right) in the human samples and four other transgenic mouse models of ALS (Caldi Gomes et al. 2023).

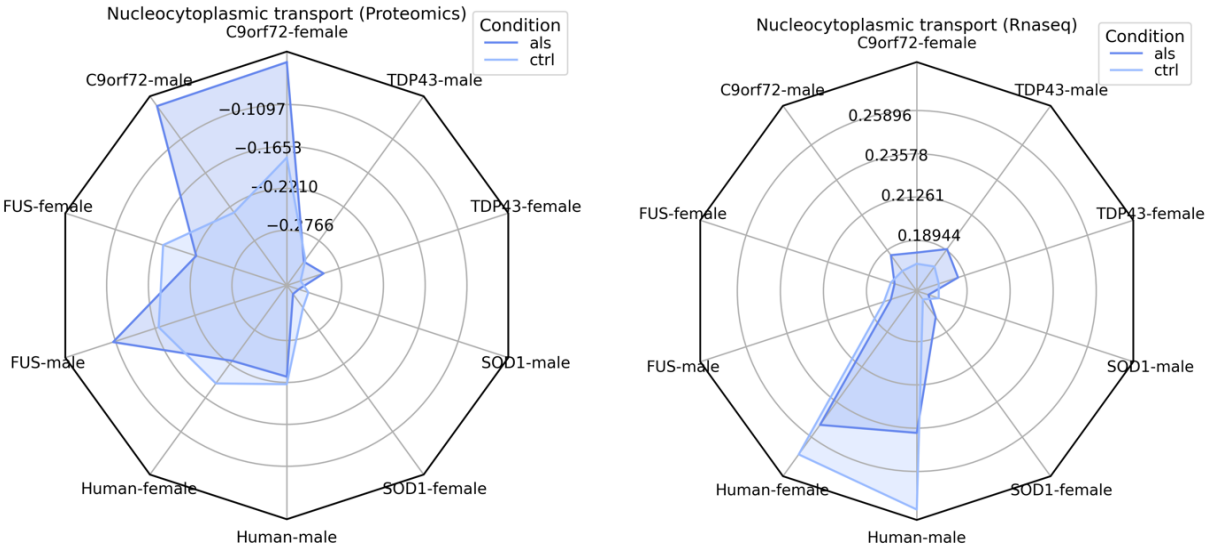

Figure 7: Radar plots showing the functional enrichment for nucleocytoplasmic transport, the pathway involving XPO1 function, in proteomics (left) and RNAseq (right) in the human samples and four other transgenic mouse models of ALS (Caldi Gomes et al. 2023).

3.2 Establishment and characterization of cortical primary cell cultures

To validate the selected molecular targets, we established primary cortical cell cultures from P0-1 B57/Bl6 mice brains. Cells were cultured for 7 days *in vitro* to reach the desired level of maturity and develop a sufficiently connected neurite network. Given that ALS pathology affects not only neurons but also glial cells, such as astrocytes, we decided to establish a mixed culture. In doing so, we avoided inhibiting glial proliferation by treating the culture with Ara-C or other compounds, aiming to create a more relevant and relatable model for the study of ALS (Pehar et al. 2017). Cultures were fixed at DIV7 and immunocytochemistry (ICC) was performed. Cells were stained for neuronal markers (MAP2) and astrocytes markers (GFAP) and DAPI. Fluorescence microscopy was done using 20x objective and random images were captured **(Figure 8A)**. The number of neurons and astrocytes were counted for three independent cultures. Surviving cells contained 48.17% cortical neurons, 15.77% astrocytes and 36.06% other glial cells (e.g. microglia, oligodendrocytes, oligodendrocyte progenitor cells). Cultures have not been stained for other glial markers **(Figure 8B, C)**.

In order to assess the influence of the targets on neuronal survival, we induced toxicity in neurons, by treating the cells on DIV7 with chemical compounds that simulate some of the known disease mechanisms in ALS, such as glutamate excitotoxicity (3.3.1) and stress granule formation (3.3.4).

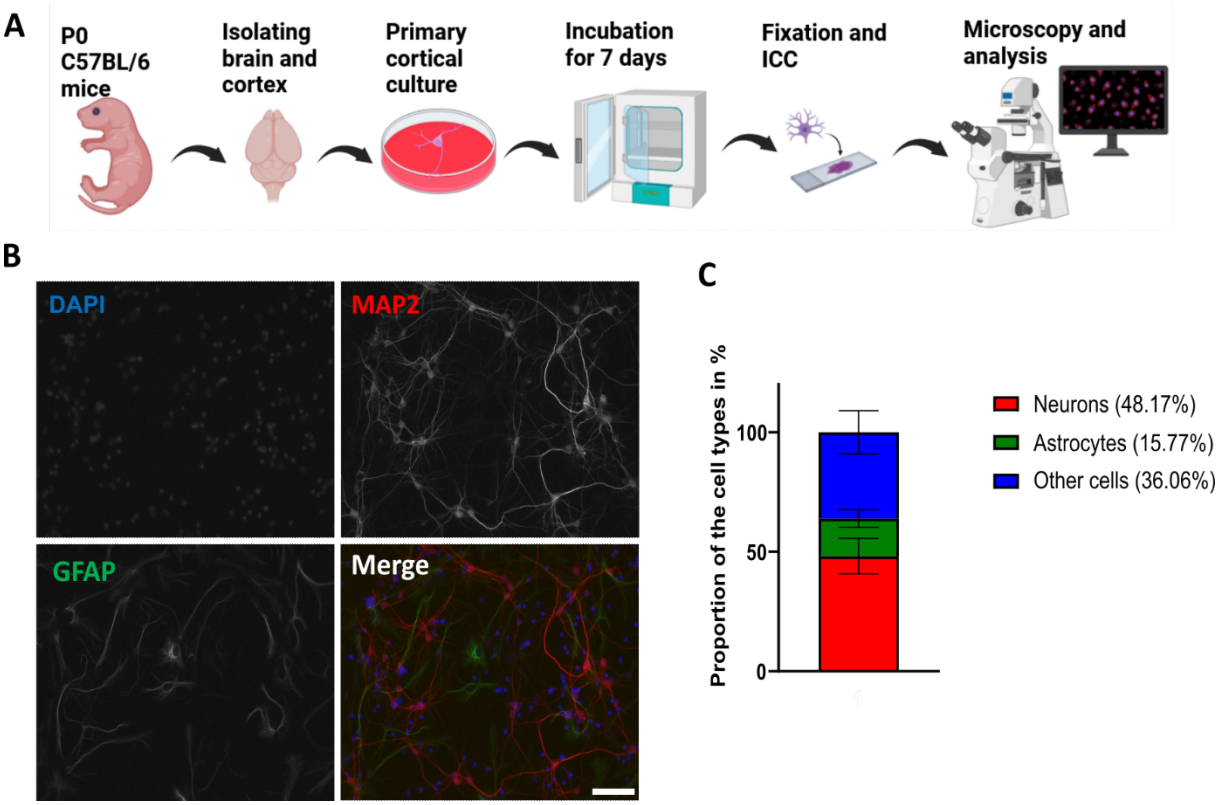

Figure 8: Experimental design and characterization of the primary cortical culture. (A) Schematic representation of the experimental steps. **(B)** Characterization of the culture through immunocytochemistry. Cell nuclei stained with DAPI represents an estimation of the total number of cells (blue). MAP2 was used as a neuronal marker (red) and GFAP shows astrocytes (green). **(C)** Stacked bar plot demonstrates the proportion of the cell types present in three independent cultures.

3.2.1 Glutamate excitotoxicity induces cell death and reduces neurite outgrowth in primary cortical cultures

An excess amount of glutamate and glutamatergic activity causing excitotoxicity has been recognized to contribute to motor neuron cell death occurring in ALS. In order to simulate this effect, primary cortical cells were cultured for 7 days as described and treated with different concentrations of glutamate (1 mM, 5 mM, and 10 mM) for 3 h (data not shown) and 6 h as suggested in previous studies (Y. Zhang and Bhavnani 2005). Cells were fixed and stained for MAP2 and the apoptosis marker cleaved caspase 3. Random fluorescence microscopy was performed using a 63x oil objective. Image analysis was performed by counting cleaved caspase 3 positive cells and measuring average neurite length using the neurite tracing plugin in Image J. Significant cell death up to 50 % was observed after treatment with 5 mM glutamate for 6 h **(Figure 9A, B)**. 5 mM glutamate significantly increased apoptosis compared to vehicle-treated cultures (cleaved caspase 3 relative signal intensity: 2.1 ± 0.1 vs. 0.98 ± 0.06; P <0.0001;

unpaired t-test; n = 7; **Figure 9A, C**). Glutamate-treated cells also showed significant reduction in neurite length in comparison to vehicle-treated cells (0.6 µm ± 0.05 vs. 0.97 µm ± 0.06; P <0.0001; unpaired t-test; n = 7; **Figure 9A, D**).

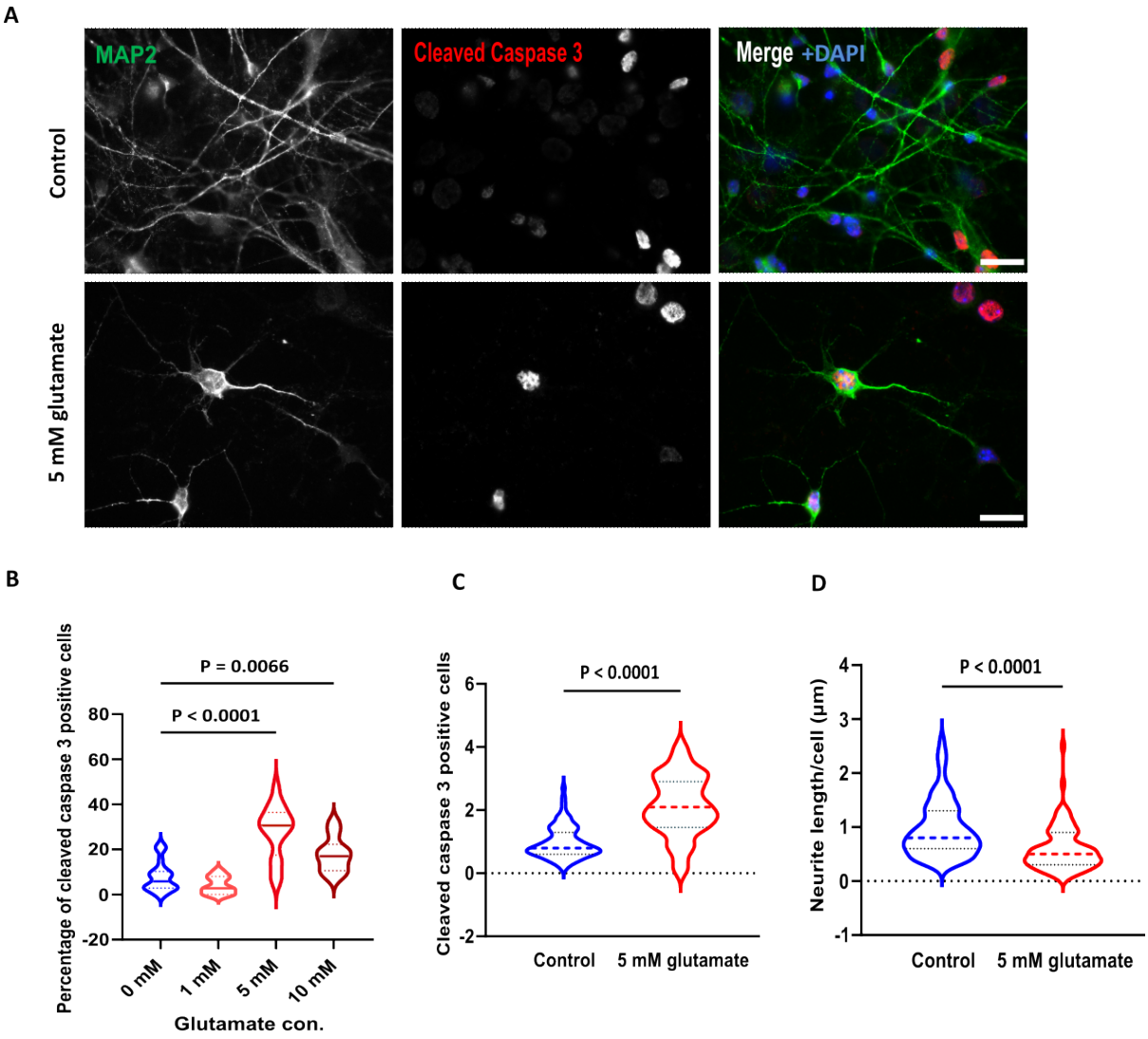

Figure 9: Effects of glutamate excitotoxicity on primary cortical cultures. (A) Representative images for the effects of glutamate treatment on primary cortical cultures assessed by ICC. The neuronal marker MAP2 is represented in green and the apoptosis marker cleaved caspase 3 is represented in red (merge images). **(B)** Percentage of cleaved caspase-positive cells after treatment with different concentrations of glutamate. **(C-D)** Effect of 5 mM glutamate on cell death **(C)** and on average neurite length **(D).** Individual values for treated and control conditions were normalized to the average of the controls within each individual experiment. Scale bar: 20 µm for all the images. Data are represented as mean ± SEM for five independent cultures and were tested by one-way ANOVA and unpaired t-test.

3.2.1.1 Glutamate excitotoxicity effects on XPO1

In order to investigate the effects of glutamate toxicity on XPO1 gene and protein expression, Western blot and q-RT-PCR were performed. Cells were cultured for 7 days to reach maturity and were treated either with 5 mM glutamate or vehicle for 6 h and RNA and protein were isolated. Total XPO1 gene expression was not significantly altered in glutamate-treated cells compared to vehicle-treated cells ($\Delta\Delta Ct = 0.99 \pm 0.09$ vs. 1.04 ± 0.09; $P = 0.6894$; unpaired t-test; $n = 4$; **Figure 10A**). However, our results from 5 different cultures showed a significant increase in XPO1 total protein expression after treatment with glutamate in comparison to vehicle-treated cells (XPO1/Lamin B1 band ratio = 1.060 ± 0.04 vs. 2.52 ± 0.12; $P < 0.0001$; unpaired t-test; n = 5; **Figure 10B, C**). In order to quantify the effects of glutamate excitotoxicity on XPO1 nuclear localization, cells were treated with 5 mM glutamate for 6 h and MAP2- and XPO1-positive cells were quantified by ICC. Image analysis revealed a significant increase in XPO1 signal intensity in the nucleus of cells in the toxicity-induced condition compared to vehicle-treated cultures (XPO1 relative signal intensity $=1.41 \pm 0.09$ vs. 0.99 ± 0.05; $P = 0.0008$; unpaired t-test; $n = 4$; **Figure 10D, E**). This suggests that glutamate excitotoxicity results in XPO1 nuclear accumulation.

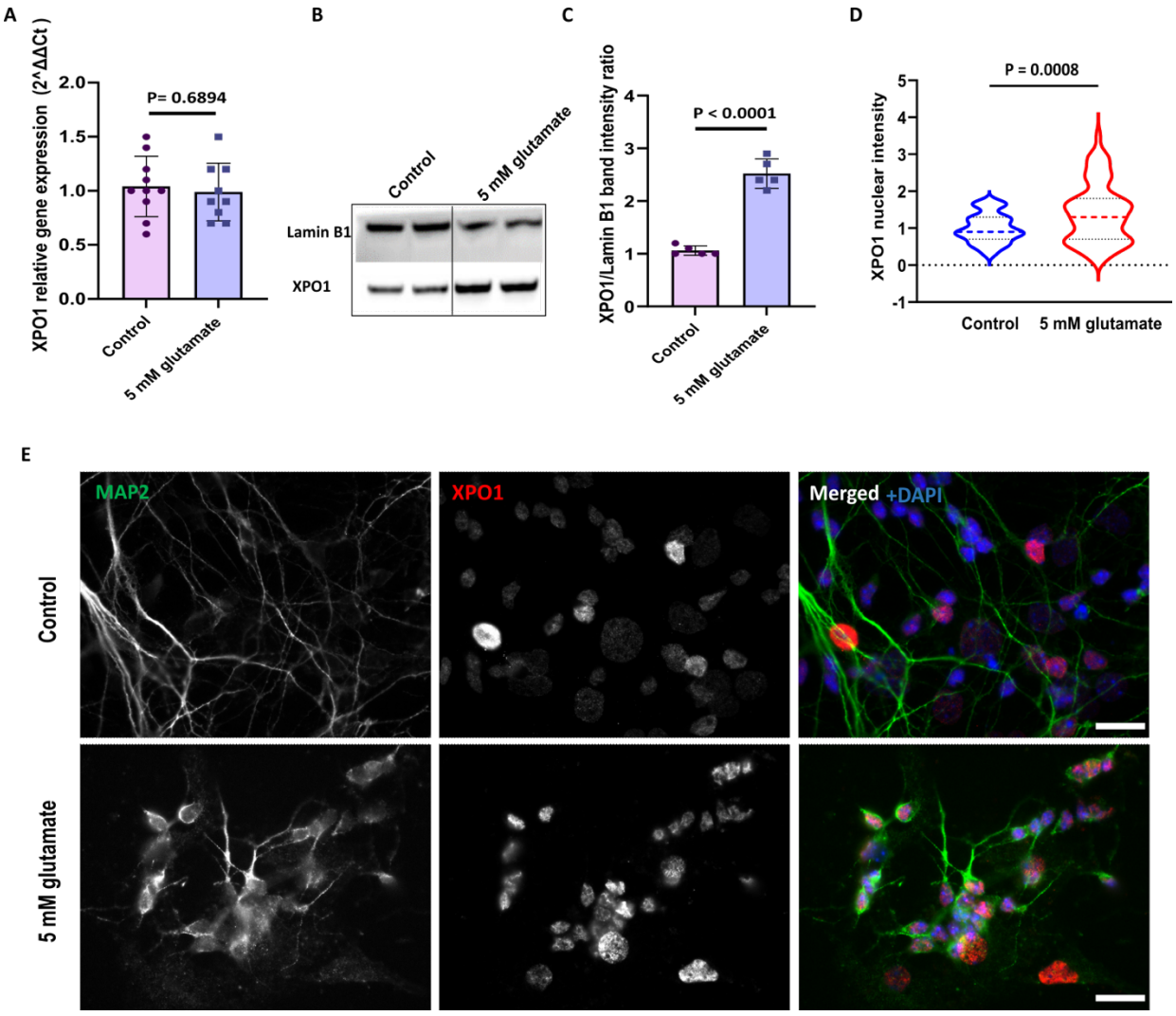

Figure 10: Effects of glutamate excitotoxicity on XPO1 gene and protein expression. (A-E) Glutamate excitotoxicity effects on XPO1 total gene expression **(A)**, on XPO1 total protein expression **(B, C)** and on XPO1 nuclear localization **(D, E)**. Scale bar: 20 µm for all images. Data are represented as single data points (in bar plots) and mean ± SEM of four independent cultures and were tested by unpaired t-test.

3.2.1.2 Glutamate excitotoxicity effects on MAP2K2 (MEK2)

To determine whether glutamate excitotoxicity impacts the expression of MEK2, we conducted an analysis of both total gene and protein expression levels of MEK2. The effects of glutamate toxicity on MEK2 gene and protein expression were investigated also by q-RT-PCR and Western blot. After treating the cells with glutamate for 6 h, total gene and protein level was measured. Results from 5 different cultures showed a significant reduction in the overall gene expression of MEK2 in glutamate-treated cultures compared to vehicle-treated cultures (ΔΔCt = 0.76 ± 0.06 vs. 1.02 ± 0.07; P = 0.0144; unpaired t-test; n = 5; **Figure 11A**). WB results

revealed a minor, albeit statistically insignificant, decrease in MEK2 protein expression in stress-induced cells in comparison to non-stressed cells (MEK2/Lamin B1 band ratio = 0.67 ± 0.18 vs.1.0 ± 0.11; P = 0.1350; unpaired t-test; n = 5; **Figure 11B, C**). Next, since MEK2 is a direct regulator of ERK1/2 phosphorylation in the MAPK pathway, we investigated the effect of excitotoxicity on phosphorylation of ERK1/2 by Western blot for p-ERK1/2. Our results showed a significant increase in p-ERK1/2 in glutamate-treated cells compared to vehicle-treated cells (p-ERK1/2/ERK1/2 band ratio: 2.67 ± 0.23 vs. 1.13 ± 0.07; P = 0.0032; unpaired t-test; n = 4; **Figure 11B, D**). These findings suggest that excitotoxicity induces ERK1/2 phosphorylation and results in activation of the cascade.

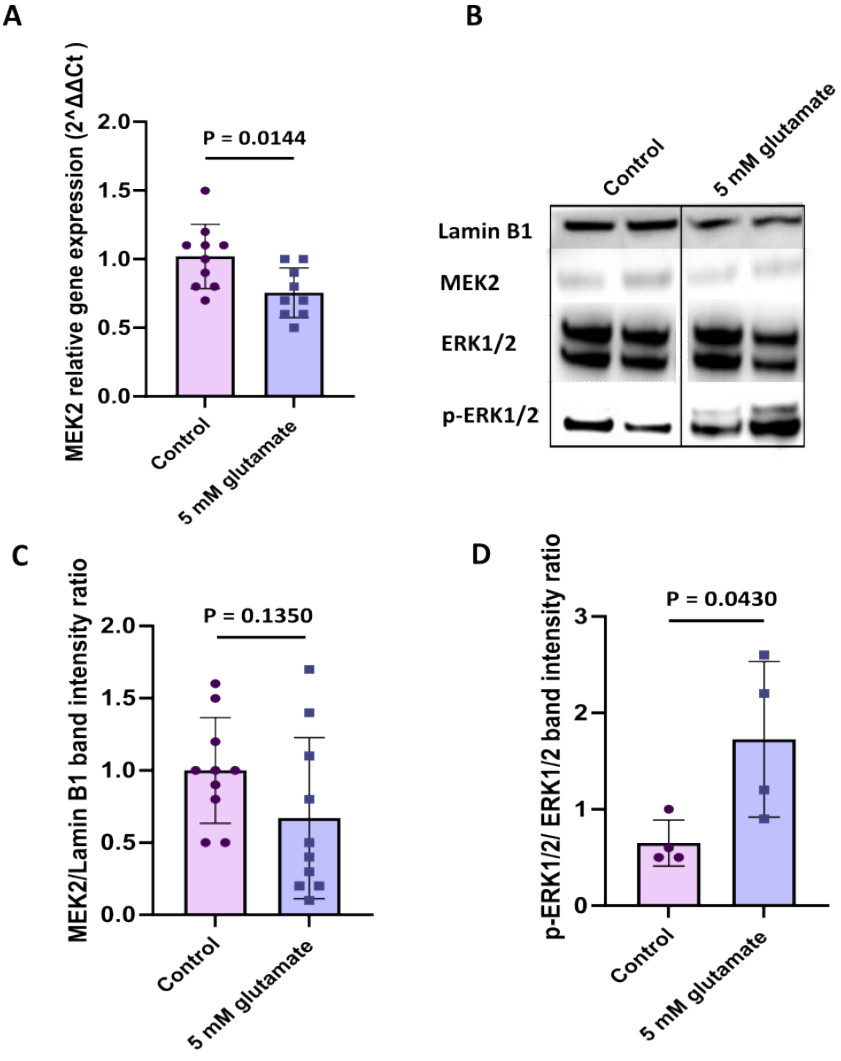

Figure 11: Effects of glutamate excitotoxicity on MEK2 and p-ERK1/2 expression. (A) Bar graph is showing the effect of 5 mM glutamate on MEK2 total gene expression quantified by q-RT-PCR. **(B-D)** Effect of glutamate excitotoxicity on MEK2 total protein level **(B, C)** and on ERK1/2 phosphorylation **(B, D)**. Data are represented as single data points and mean ± SEM of at least four independent cultures and were tested by unpaired t-test.

3.2.2 Sodium arsenite treatment induces stress granule formation, cell death and reduces neurite average length

In order to induce stress granules, cells were treated with different concentrations of sodium arsenite (SA) for different time periods: 0.5 mM, 1 mM, 10 mM for 30 min, 1 h, and 3 h. Cells were fixed and stained for MAP2 and stress granule marker GTPase-activating protein-binding protein 1 (G3BP1). This enzyme is a member of the heterogeneous nuclear RNA-binding proteins and is also an element of the RAS signal transduction pathway. After microscopical image acquisition, SGs were quantified by calculating the total G3BP1 fluorescence signal and then dividing it by the total cell count. Notably, cortical neurons exhibited a higher level of resistance to SG formation compared to astrocytes. Mature stress granule formation was observed after 3 h treatment with 10 mM SA. The SA treatment led to a substantial increase in the G3BP1 signal intensity when compared to vehicle- treated cultures (G3BP1 relative signal intensity = 3.01 ± 0.2 vs. 1.01 ± 0.12; P <0.0001; unpaired t-test; n = 5; **Figure 12A-C**). Additionally, the SA treatment significantly increased cell death when compared to vehicle-treated cells (cleaved caspase 3 relative signal intensity = 1.46 ± 0.12 vs. 0.99 ± 0.07; P = 0.0017; unpaired t-test; n = 5; **Figure 12E, D**). Furthermore, SA-treated cells showed significant reduction in average neurite length compared to vehicle-treated cultures (0.75 µm ± 0.08 vs. 1.0 µm ± 0.05; P = 0.0126; unpaired t-test; n = 5; **Figure 12F, D**).

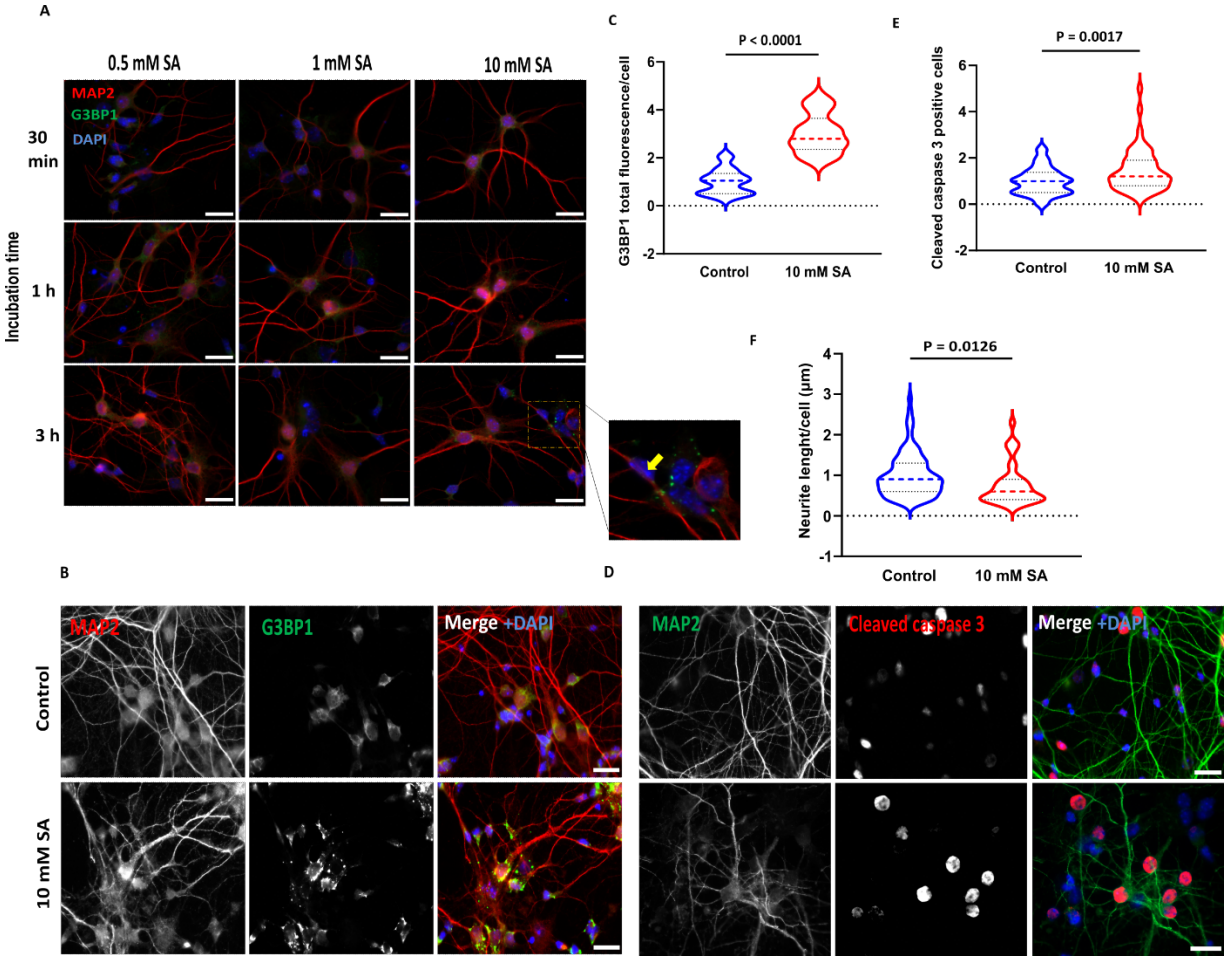

Figure 12: Effects of stress granule induction on cell death and neurite length in primary cortical cultures. (A) Exemplary images of cortical cultures treated with SA in different concentrations and different incubation times. SGs are visualized by ICC using G3BP1 antibody (green signal, yellow arrow in magnified inset). **(B, C)** SGs quantification by ICC and measuring G3BP1 fluorescence intensity. **(D-F)** Effect of SGs induction by 10 mM SA on cell death **(D, E)** and on average neurite length **(D, F)**. Scale bar: 20 µm for all the images. Data are represented as mean ± SEM of five independent cultures and were tested by unpaired t-test.

3.2.2.1 Expression and nuclear localization of XPO1 in the stress granule model

In order to evaluate the XPO1 gene and protein expression, cells were subjected to a 3-hour treatment with 10 mM SA, followed by q-RT-PCR and Western blot. A significant increase in total XPO1 gene expression was observed under SA-treated cultures in comparison to vehicle-treated cultures ($\Delta\Delta Ct = 6.59 \pm 2.02$ vs. 1.04 ± 0.11; $P = 0.0160$; unpaired t-test; $n = 5$; **Figure 13A**). However, Western blot results indicated no significant difference in protein expression between the SA-treated and vehicle-treated cells (XPO1/Lamin B1 band ratio = 1.1 ± 0.17 vs. 1.01 ± 0.15; $P = 0.6989$; unpaired t-test; $n = 5$; **Figure 13B, C**). To assess whether the induction

of stress granules influenced the nuclear localization of XPO1, cells were treated with SA, double-stained for MAP2 and XPO1. The fluorescence intensity of XPO1 in the nucleus indicated no substantial alterations in XPO1 signal intensity within the nucleus of cells treated with SA compared to vehicle-treated cells (XPO1 relative signal intensity = 1.01 ± 0.05 vs. 1.0 ± 0.07; P = 0.9801; n = 5; **Figure 13D, E**). Our findings suggest that SGs induction leads to an elevation in XPO1 total gene expression, while it does not appear to influence XPO1 protein expression or its retention within the nucleus.

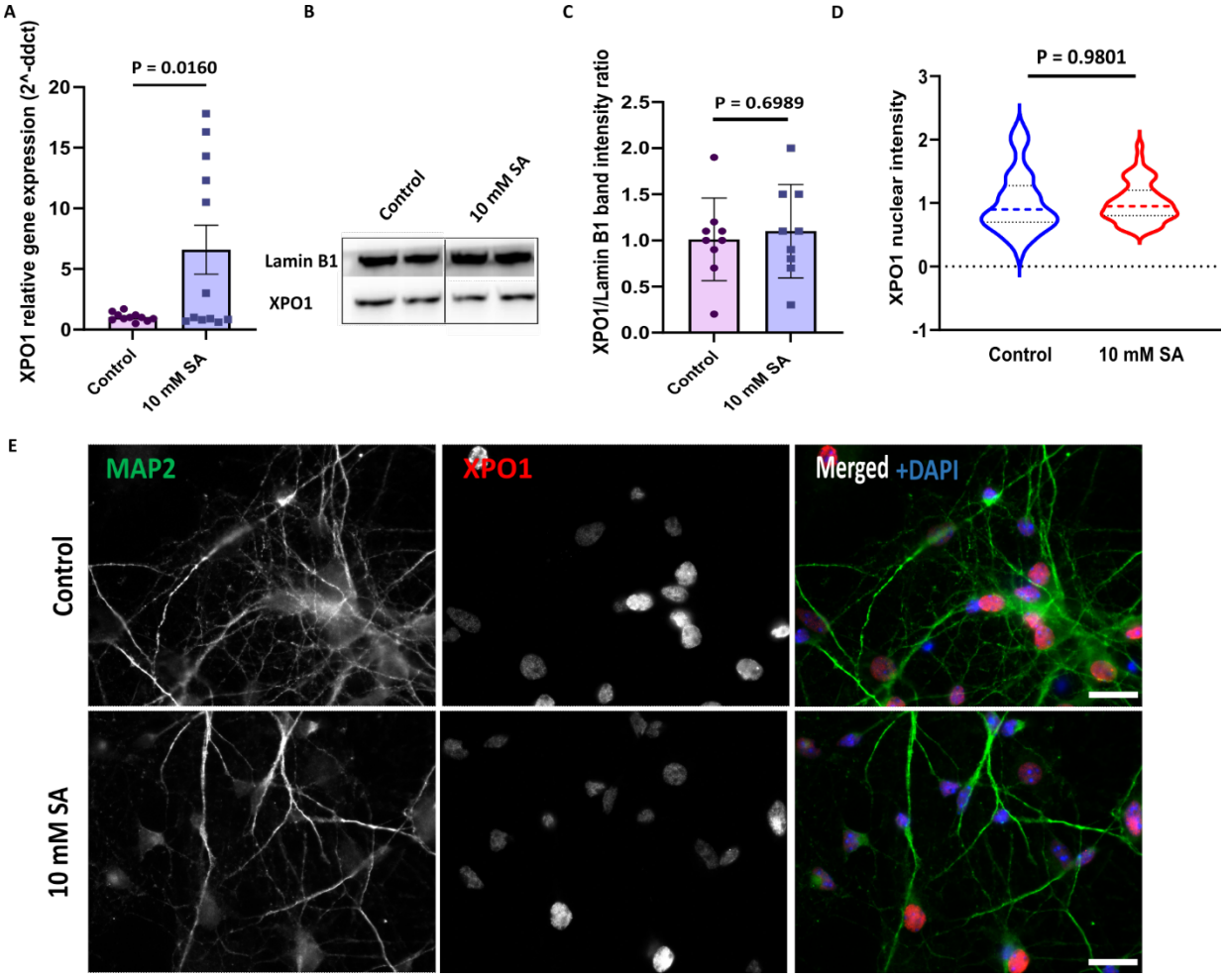

Figure 13: Expression and nuclear localization of XPO1 after stress granule induction (A-E) Effects of SA treatment on XPO1 relative gene expression **(A)**, total protein expression **(B, C)**, and its nuclear localization **(D, E)**. Scale bar: 20 µm for all the images. Data are represented as single data points (in bar plots) and mean ± SEM of five independent cultures and were tested by unpaired t-test.

3.2.2.2 Stress granule formation effects on MEK2

The effects of stress granule induction on MEK2 gene and protein expression were investigated by q-RT-PCR and WB after 3 h treatment with 10 mM SA. Our results from 5 different cultures showed no significant alteration in MEK2 total gene expression in SA-treated cultures compared to vehicle-treated cultures ($\Delta\Delta Ct = 1.46 \pm 0.5$ vs. 1.19 ± 0.24; $P = 0.6302$; unpaired t-test; $n = 5$; **Figure 14A**). WB analysis also showed no significant changes in MEK2 protein expression after SA treatment in comparison to vehicle-treated cells (MEK2/Lamin B1 band ratio = 0.9 ± 0.15 vs. 1.0 ± 0.1; $P = 0.5803$; unpaired t-test; $n = 5$; **Figure 14B, D**). We investigated the phosphorylation of ERK1/2 as the main target of MEK2 in the MAPK pathway, by WB. Our results showed a significant increase in phospho-ERK1/2 protein expression in SA-treated cells compared to vehicle-treated cells (p-ERK1/2/ ERK1/2 band ratio = 2.53 ± 0.52 vs. 1.07 ± 0.07; $P = 0.0188$; unpaired t-test; $n = 3$; **Figure 14C, D**). Overall, our results indicate that SGs formation does not have a discernible impact on MEK2 gene or protein expression. However, it does seem to activate the MAPK pathway through the induction of ERK1/2 phosphorylation.

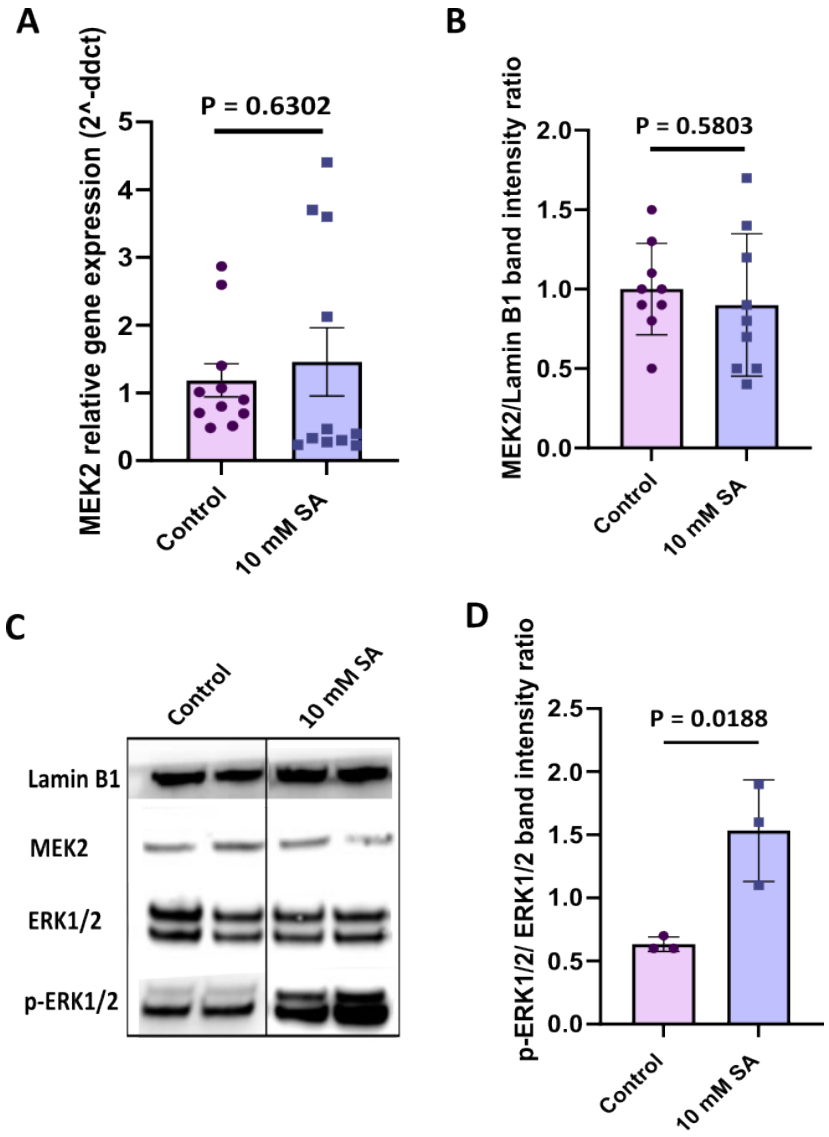

Figure 14: Stress granule induction effects on MEK2 gene and protein expression. (A-D) SA treatment effect on MEK2 relative gene expression quantified by q-PCR **(A)**, MEK2 total protein expression quantified by WB **(B, D)**, and on ERK1/2 phosphorylation **(C, D)**. Data are represented as single data points and mean ± SEM of three of five different cultures and were tested by unpaired t-test.

3.3 Toxicity of selinexor and trametinib *in vitro*

Assessment of toxic drug concentrations was conducted with the toxilight assay (Lonza, Switzerland), which employs bioluminescence to measure the release of adenylate kinase (AK) from cells undergoing toxicity-induced apoptosis. Higher values of luminometer light output, relative light units (RLUs) are indicative of higher toxicity in cells. The selected test concentrations were determined based on previously reported IC50 values for these drugs. Selinexor (KPT-330) has an IC50 range of 34-203 nM (Etchin et al. 2013) and we tested

concentrations of 1 nM, 10 nM, 100 nM, 1 µM. For trametinib, an IC50 of approximately 2 nM has been reported (Gilmartin et al. 2011b), and we evaluated concentrations of 2 nM, 20 nM, and 200 nM, as well as 2 µM. As a positive control for the toxilight assay, cells were used which were lysed by applying RIPA buffer. Cells were exposed to various drug concentrations at DIV4. Toxicity was monitored at 24 h, 48 h, and 72 h **(Figure 15A-C)**. As anticipated, the highest concentration of selinexor (1 µM) exhibited noticeable toxicity at 48 h compared to vehicle-treated cells (RLUs = 1327 ± 95.54 vs. 831.5 ± 26.94; P = <0.0001; ANOVA; n = 3; **Figure 15B**) as well as at 72 h (RLUs = 1381 ± 61.21 vs. 979.2 ± 36.13; P = <0.0001; ANOVA; n = 3; **Figure 15C**). Additionally, 100 nM selinexor treatment induced higher toxicity compared to vehicle-treated cultures at 72 h (RLUs = 1149 ± 15.35 vs. 979.2 ± 36.13; P = 0.0196; ANOVA; n = 3; **Figure 15C**). For validation experiments, 1 nM, 10 nM, and 100 nM concentrations were selected. In the case of trametinib, a significant increase in toxicity was only observed in the culture media of cells treated with 2 µM for 72 h in comparison to vehicle-treated cells (RLUs = 1206 ± 91.13 vs. 931.3 ± 48.44; P = 0.0445; ANOVA; n = 3; **Figure 15F**). Thus, for the subsequent experiments, concentrations of 2 nM, 20 nM, and 200 nM for trametinib were chosen.

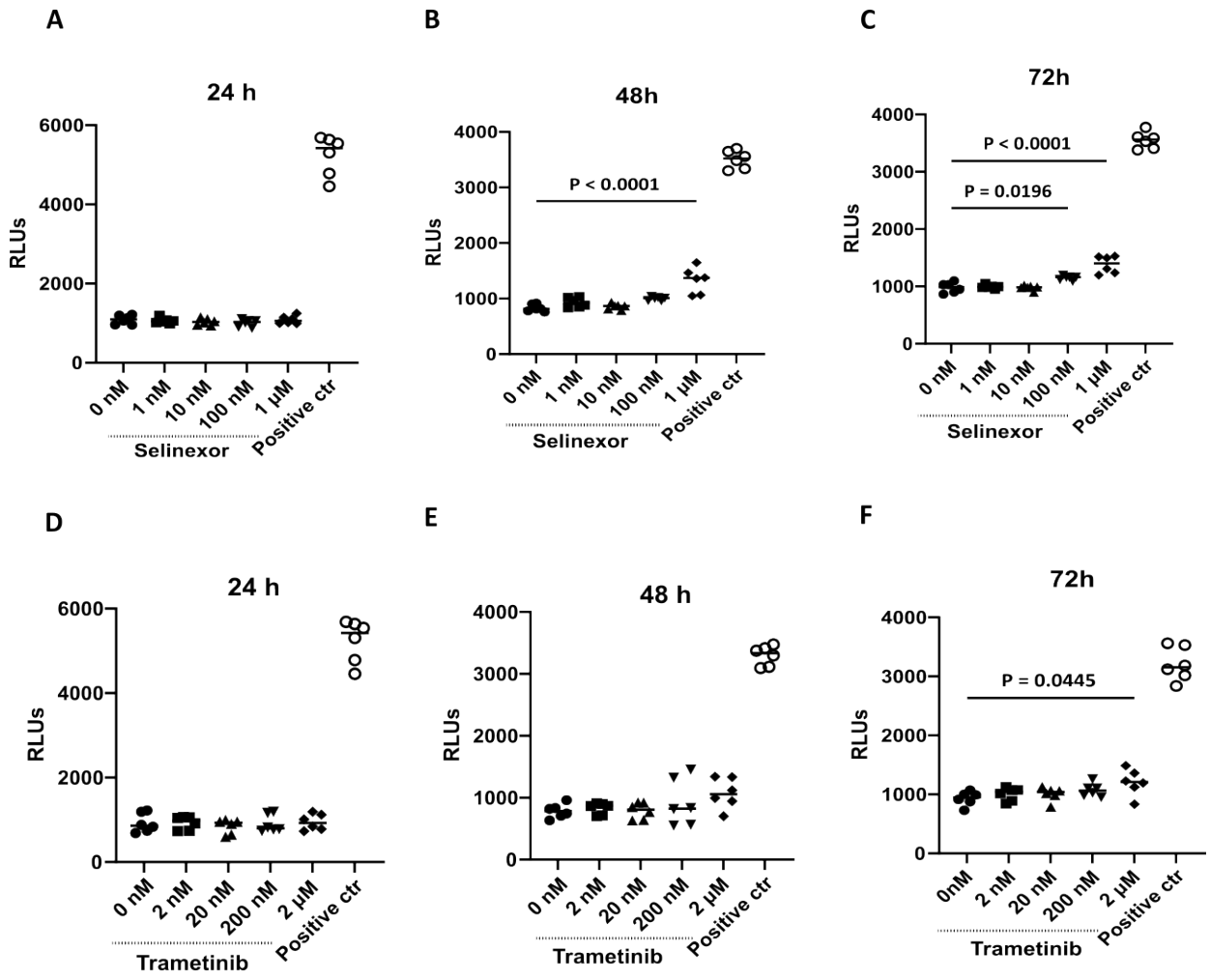

Figure 15: Evaluation of the toxicity of selinexor and trametinib *in vitro* by toxilight assay. **(A-F)** Assessment of cytotoxicity of increasing concentrations of selinexor **(A-C)** and trametinib **(D-F)** after 24 h, 48 h and 72 h in primary cortical cultured cells using the AK detection reagent. The results represent the mean of triplicate wells. Data are represented as single data points and mean ± SEM of three different cultures and were tested by one-way ANOVA.

3.4 Target (XPO1) engagement of selinexor

To demonstrate the functionality of selinexor and its engagement with the drug target, we considered its mechanism of action. selinexor operates by binding to and inhibiting XPO1. This inhibition by selinexor disrupts the export process of several nuclear proteins, promoting their accumulation within the nucleus. Given this mode of action, we hypothesized that selinexor treatment would impede the regular exit of the XPO1 complex from the nucleus (Gandhi et al. 2018). Consequently, this interruption would lead to the accumulation of its targeted proteins within the nucleus, potentially triggering an overall increase in XPO1 expression at both the

gene and protein levels. This response might function as a compensatory mechanism to counterbalance the disrupted nuclear export caused by selinexor. In order to test this hypothesis, we treated the cells with concentrations of 0 nM, 1 nM, 10 nM and 100 nM selinexor for 72 h. Protein and RNA were isolated as described and q-RT-PCR and Western blot was performed. First the total XPO1 gene expression was quantified. Results from 4 different cultures showed a significant increase in XPO1 relative gene expression with 100 nM selinexor compared to 0 nM condition ($\Delta\Delta Ct = 2.6 \pm 0.4$ vs. 1.02 ± 0.06; $P = 0.0132$; ANOVA; $n = 4$; **Figure 16A**). Similar trends as observed in gene expression were also observed for protein expression results. Notably, a substantial increase at the 100 nM selinexor concentration in comparison to 0 nM concentration (XPO1/Lamin B1 band ratio = 4.82 ± 1.34 vs. 1.0 ± 0.0; $P = 0.0258$; ANOVA; $n = 4$; **Figure 16B, C**) supported the compensatory production hypothesis of XPO1. To investigate the impact of XPO1 inhibition on the nuclear accumulation of its target proteins, we focused on p62, an autophagy adaptor known to be among the targets of XPO1. Previous research has demonstrated that XPO1 inhibition results in p62 nuclear accumulation. To verify this hypothesis, we initially employed immunocytochemistry. Cells were subjected to various concentrations of selinexor treatment for 72 hours, fixed, and subsequently stained for MAP2 and p62 (SQSTM1). Remarkably, p62 signal accumulation was observed with higher concentrations of selinexor **(Figure 16D)**. Further insight into these effects was gained by conducting subcellular fractionations to separately assess the protein levels of both XPO1 and p62 in the nucleus and cytoplasm. Western blotting was performed for XPO1 and p62 in distinct nuclear and cytoplasmic fractions across three different cultures. The purity of the fractions was assessed by employing nuclear marker Lamin B1 and cytoplasmic marker pyruvate dehydrogenase (PDH). These designated markers also served as housekeeping proteins for the purpose of normalization. An increase in XPO1 protein expression after treatment with 10 nM and 100 nM selinexor was observed in cytoplasmic fractions in comparison to vehicle-treated cells (XPO1/Lamin B1 band ratio for 10 nM selinexor = 2.2 ± 0.06 vs. 1.0 ± 0.0; $P = 0.0001$; ANOVA; $n = 4$; **Figure 16E, F**) and (XPO1/Lamin B1 band ratio for 100 nM selinexor = 2.3 ± 0.21 vs. 1.0 ± 0.0; $P < 0.0001$; ANOVA; $n = 4$; **Figure 16E, F**). An increase in XPO1 protein expression corresponding to higher selinexor concentrations (10 nM and 100 nM) was also observed in nuclear fractions compared to vehicle-treated condition (XPO1/Lamin B1 band ratio for 10 nM selinexor = 2.6 ± 0.11 vs = 1.0 ± 0.29; $P = 0.0187$; ANOVA; $n= 4$; Figure 16H, I) and (XPO1/Lamin B1 band ratio for 100 nM: 2.9 ± 0.24 vs. 1.0 ± 0.29; $P = 0.0060$; ANOVA; $n = 4$; **Figure 16H, I**). These results are potentially elucidating the rise in total protein levels. As anticipated, augmented p62 protein levels were evident in nuclear fractions with increasing

selinexor concentration **(Figure 16H, J)**. Interestingly, this effect was restricted in cytoplasmic fractions and was particularly prominent with 100 nM selinexor, indicating a possible compensatory cellular response **(Figure 16E, G)**. It is worth noting that although these outcomes lacked statistical significance - possibly due to the limited sample size - they might be substantiated through replication in a larger number of cultures. Such experiments fell out of the scope of this work due to time limitations but will be pursued in the future. Overall, these findings collectively underscore the disruption of the normal XPO1 nuclear transport in response to selinexor.

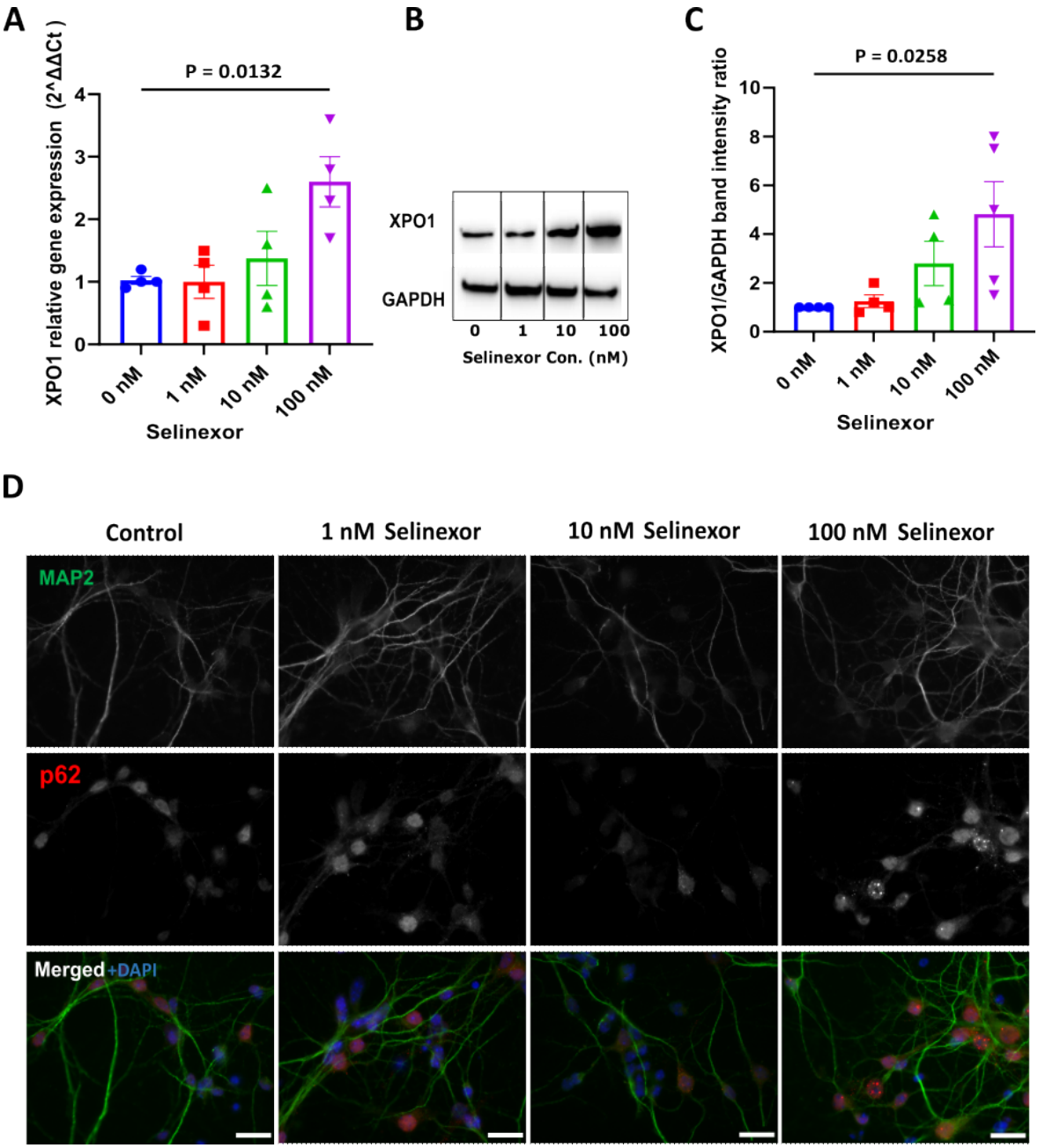

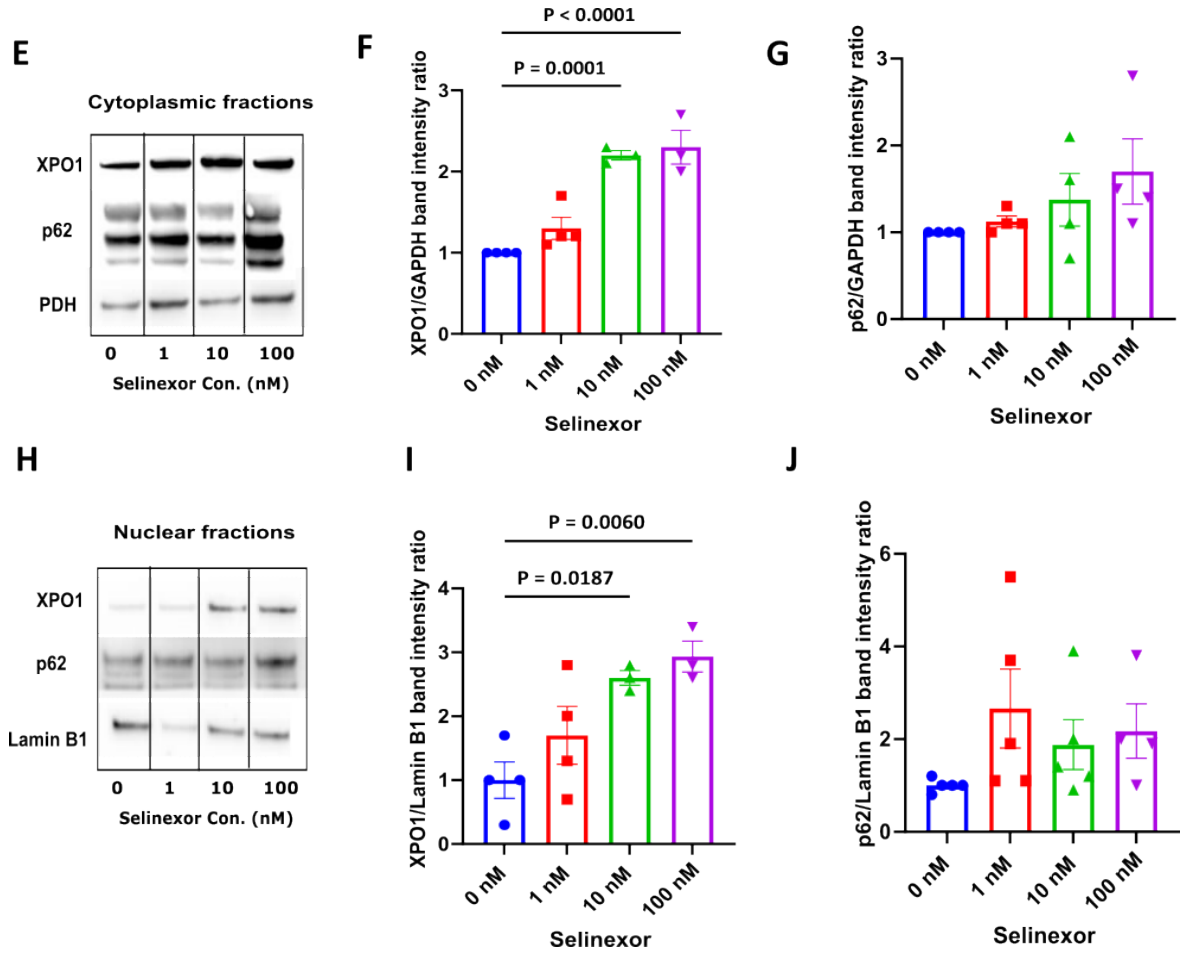

Figure 16: Selinexor effects on XPO1 RNA and protein expression and p62 nuclear accumulation. (A) Bar graphs representing XPO1 relative gene expression after treatment with different concentrations of selinexor for 72 h. **(B, C)** Bar graphs representing effects of selinexor treatment on XPO1 total protein level after 72 h. **(D)** Fluorescence image shows p62 signal intensity after treatment with different concentrations of selinexor after 72 h. **(E-J)** WB analysis of XPO1 and p62 protein levels after treatment with different concentrations of selinexor in cytoplasmic fractions **(E-G)** and in nuclear fractions **(H-J)**. Scale bar: 20 µm for all the images. Data are represented as single data points and mean ± SEM of four different cultures and were tested by one-way ANOVA.

3.4.1 Selinexor reduces cell death in glutamate-intoxicated cells

To explore the neuroprotective potential of selinexor, cells were treated at DIV4 with different concentrations of selinexor (0 nM, 1 nM, 10 nM, 100 nM) for a 72-hour period. To induce excitotoxicity, 5 mM glutamate was introduced for 6 hours at DIV7 in half of the wells in culture plates. Subsequently, the cells were fixed and stained with MAP2 and cleaved caspase-3 and random imaging was conducted. The neuroprotective effects of selinexor were assessed

by quantifying cell death (counting cleaved caspase 3 positive cells) and measuring neurite length. Selinexor alone did not display any discernible impact on cell death or the average length of neurites across any of the tested concentrations in non-stressed cells. Interestingly, in glutamate-treated cells, selinexor at 1 nM and 10 nM demonstrated a notable reduction in cleaved caspase 3 positive cells when compared to vehicle-treated cells (cleaved caspase 3 relative signal intensity for 1 nM selinexor = 1.54 ± 0.15 vs. 2.5 ± 0.1; $P < 0.0001$; ANOVA; n = 5; **Figure 17 A, B**) and (cleaved caspase 3 relative signal intensity for 10 nM selinexor = 1.5 ± 0.12 vs. 2.5 ± 0.1; $P < 0.0001$; ANOVA; n = 5; **Figure 17A, B**). Neurite outgrowth, on the other hand, did not exhibit significant alterations upon exposure to selinexor **(Figure 17A, C)**. These results indicate beneficial effect of selinexor on reducing cell death in excitotoxicity-induced cells.

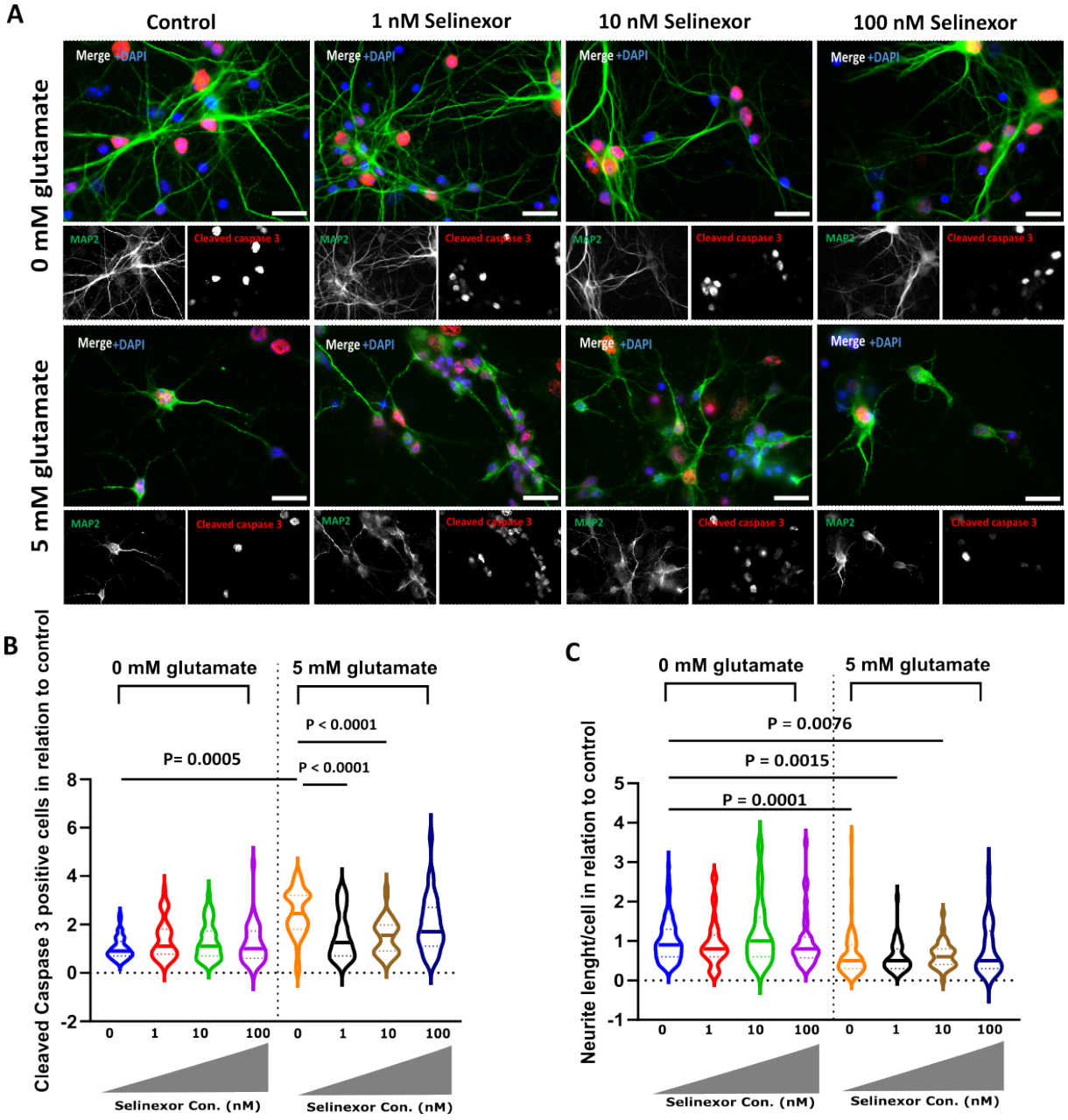

Figure 17: Evaluation of the neuroprotective effects of XPO1 inhibition by selinexor in the glutamate excitotoxicity model. (A, B) Effects of different concentrations of selinexor on apoptosis in glutamate and vehicle-treated cells analyzed by immunostaining. Scale bar: 20 µm for all the images. **(C)** Violin plots showing the effects of different concentrations of selinexor on neurite outgrowth for glutamate- or vehicle-treated cultures. Data are represented as the mean ± SEM of five different cultures and were tested by one-way ANOVA.

3.4.2 Quantification of selinexor effects on XPO1 protein expression and nuclear localization in the glutamate excitotoxicity model

We have demonstrated that glutamate excitotoxicity induces an elevation in the total protein levels of XPO1 and prompts the nuclear accumulation of XPO1. To explore the potential counteractive effects of selinexor on this phenomenon, primary cortical cultures were cultured for four days and subsequently treated with varying concentrations of selinexor. At DIV7, half of the wells were subjected to glutamate excitotoxicity (5 mM for 6 hours). To assess the impact of drug treatment and toxicity on XPO1 localization, cells were fixed and subjected to staining for MAP2 and XPO1. Random microscopy was conducted across three different cultures. The nuclear fluorescence intensity of XPO1 was quantified in 10 images of each condition. Our findings revealed no notable variations in XPO1 nuclear intensity across different selinexor concentrations, both in cells with and without glutamate treatment **(Figure 18A, B)**. To investigate the overall XPO1 protein expression in response to selinexor treatment in stress-induced cells, protein isolation was performed post-drug treatment and intoxication, followed by Western blot analysis. In vehicle-treated cells, selinexor displayed an increased total XPO1 protein expression, consistent with previous observations. This phenomenon was posited as a potential compensatory mechanism to address the trapped XPO1 in the nucleus. In cells subjected to glutamate excitotoxicity induction, selinexor treatment did not exert a significant change in XPO1 protein expression compared to cells without drug treatment. Although a slight increase was observed with higher selinexor concentrations, this effect was notably lower than what was observed in vehicle-treated cells **(Figure 18C-E)**.

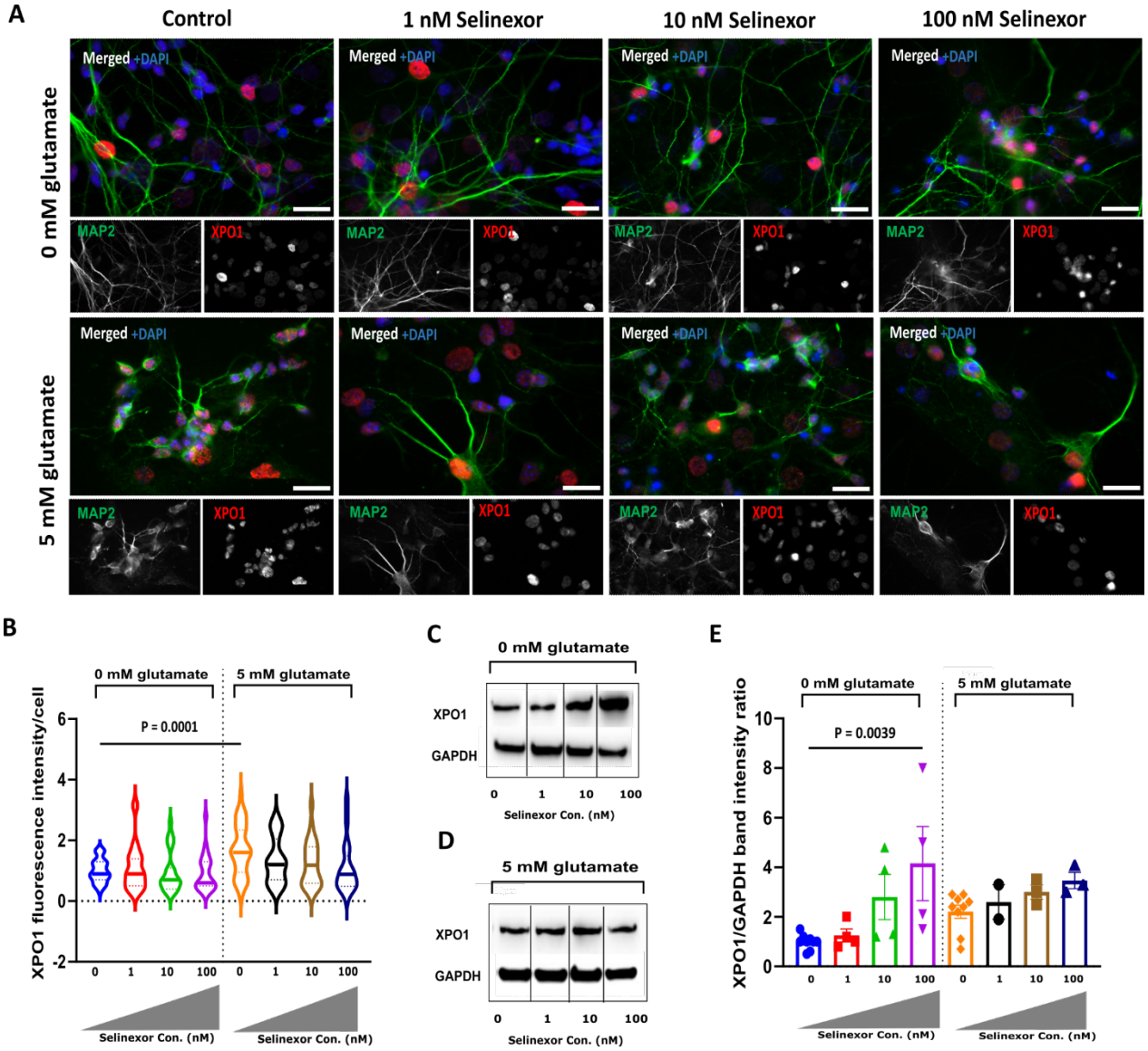

Figure 18: Evaluation of the selinexor effects of XPO1 protein expression and nuclear localization in glutamate excitotoxicity model. (A, B) Effects of different concentrations of selinexor on XPO1 nuclear intensity in glutamate and non-glutamate-treated cells analyzed by immunostaining. Scale bar: 20 µm for all the images. Data are presented as mean ± SEM of three different cultures and were tested using one-way ANOVA. **(C-E)** Western blot analysis and quantification of selinexor effects on XPO1 with and without glutamate treatment. Data are represented as single data points (in bar plots) and mean ± SEM of five different cultures and were tested by one-way ANOVA.

3.4.3 Selinexor did not affect stress granule formation but reduced apoptosis in the stress granule model

As previously demonstrated, 10 mM sodium arsenite treatment induced stress granule formation, increased cell death and reduced average neurite length without affecting XPO1

nuclear localization. Given that selinexor treatment increased XPO1 expression, we aimed to investigate whether this alteration would influence stress granule formation, cell survival, and average neurite length. To investigate the potential neuroprotective effects of selinexor on stress granules model, cortical cultures were subjected to various concentrations (0 nM, 1 nM, 10 nM, 100 nM) of the drug at DIV4 for 72 hours. 10 mM SA was applied on DIV7 for 3 hours. Following treatment, the cultures were fixed and subsequently stained for MAP2, cleaved caspase 3, and the stress granule marker G3BP1. Random images were captured and quantitative analysis of cell death, neurite length and G3BP1 fluorescence intensity were performed. Treatment with selinexor showed no change in G3BP1 intensity in both SA and vehicle-treated cells **(Figure 19A, C)** and had no effect on average neurite length **(Figure 19 B, E)**. However, at concentrations of 1 nM and 10 nM, selinexor significantly reduced the number of cleaved caspase 3-positive cells under SA-treated conditions compared to cultures treated with 0 nM selinexor (cleaved caspase 3 relative signal intensity for 1 nM selinexor vs. 0 nM selinexor = 1.12 ± 0.09; vs. 1.57 ± 0.1; P = 0.0231; ANOVA; n = 4; **Figure B, D**) and (cleaved caspase 3 relative signal intensity for 10 nM vs. 0 nM selinexor = 0.95 ± 0.07 vs. 1.57 ± 0.1; P = 0.0001; ANOVA; n = 4; **Figure 19 B, D**). Therefore, selinexor may have a positive effect on neuronal survival without directly affecting the stress granule pathway.

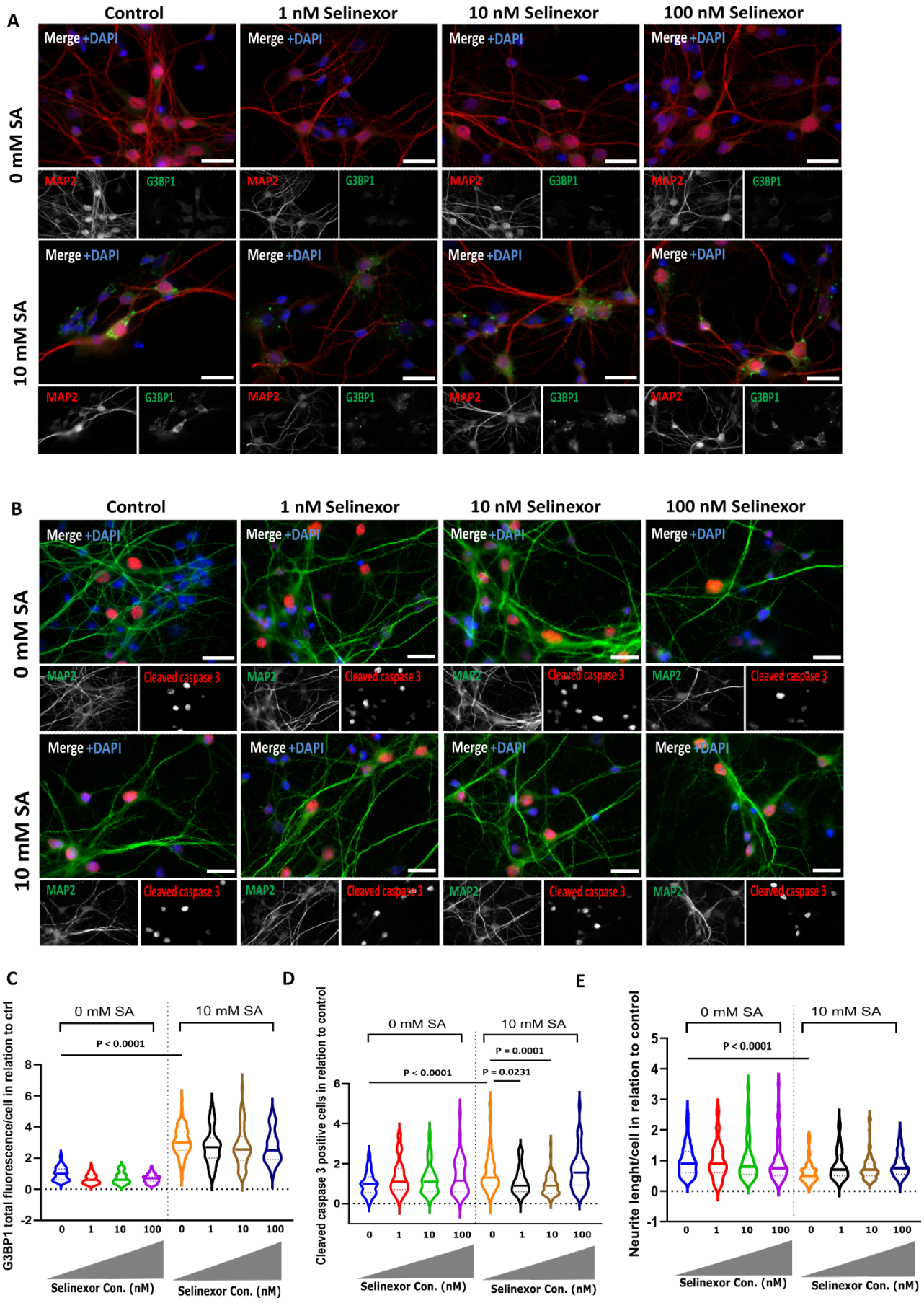

Figure 19: Evaluation of the neuroprotective effects of XPO1 inhibition by selinexor in the stress granule model. (A) Effects of different concentrations of selinexor on G3BP1 signal

intensity in SA and non-SA-treated cells analyzed by immunostaining. Scale bar: 20 µm for all the images. **(B)** Effects of different concentrations of selinexor on cell survival in SA and non-SA-treated cells analyzed by immunostaining. **(C-E)** Quantification plots showing the effects of different concentrations of selinexor on G3BP1 signal intensity **(C)**, on cell death **(D)** and on average neurite length **(E)** in SA or vehicle-treated cells. Data are represented as the mean ± SEM of five independent cultures and were tested by one-way ANOVA.

3.5 Trametinib reduces ERK1/2 phosphorylation and induces MEK2 phosphorylation

To establish the engagement of trametinib with its drug target MEK2, we reviewed the drug's mechanism of action and focused on the broader context of the MEK2-associated pathway. Notably, MEK2 plays a pivotal role in the RAS-RAF-MEK-ERK Pathway, where its phosphorylation is essential for direct modulation of ERK1/2. Given this, we decided to examine the expression levels of MEK2 and its downstream targets subsequent to treatment with varying concentrations of trametinib. Our understanding is that trametinib binds to the activation loop of MEK, disrupting the RAF-dependent phosphorylation of MEK. As a consequence, we anticipated a reduction in p-MEK and p-ERK levels. To validate these effects and the functionality of trametinib, we treated cells at DIV4 with the 2 nM, 20 nM and 200 nM trametinib or DMSO. Post 72 hours, protein isolation was performed, followed by Western blot analysis. We quantified the total protein expression of p-ERK1/2, ERK1/2, p-MEK, and MEK2 in four different cultures. As expected, our findings confirmed a significant reduction in phospho-ERK1/2 protein expression with increasing trametinib concentration, , i.e., 20 nM trametinib compared to 0 nM trametinib (p-ERK1/2/ ERK1/2 band ratio for 20 nM trametinib vs. 0 nM trametinib = 0.25 ± 0.06 vs. 0.6 ± 0.04: P = 0.0051; ANOVA; n = 4; **Figure A, B**) and (p-ERK1/2/ ERK1/2 band ratio for 200 nM trametinib vs. 0 nM trametinib = 0.17 ± 0.05 vs. 0.6 ± 0.04; P = 0.0012; ANOVA; n = 4; **Figure 20A, B**). Notably, the total expression of ERK1/2 and MEK2 exhibited no significant difference compared with vehicle-treated cells **(Figure 20A, C, E)**. Furthermore, 200 nM concentrations of trametinib significantly increased p-MEK2 levels in comparison to vehicle-treated cells (p-MEK2/MEK2 band ratio = 1.0 ± 0.2 vs. 0.27 ± 0.05; P = 0.0119; ANOVA; n = 4; **Figure 20A, D**). Considering the physiological context, ERK activation is subject to negative feedback regulation by DUSPs at various levels both downstream and upstream of MEK. Trametinib essentially disrupts this feedback mechanism, thereby inducing MEK phosphorylation which could explain increased phosphorylation of MEK2. In summary, our results underscore that the inhibition of MEK2 by

trametinib directly hinders ERK1/2 phosphorylation, yet triggering phosphorylation of MEK itself.

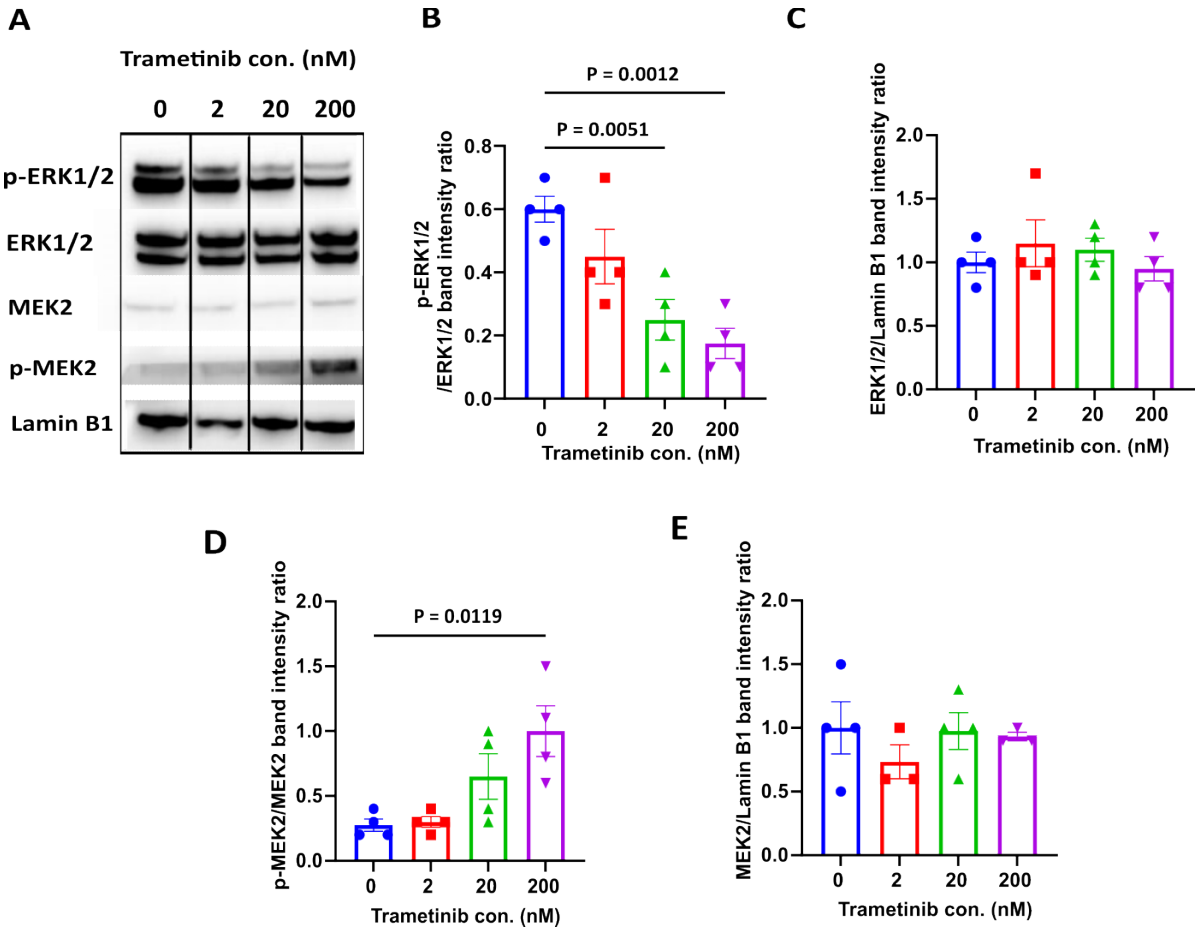

Figure 20: Evaluation of the trametinib and MEK2 interaction. (A-E) WB analysis of p-ERK1/2, ERK1/2, p-MEK2 and MEK2 after treatment with different concentrations of trametinib for 72 h. Bar graphs representing effects of trametinib treatment on p-ERK1/2 **(B)**, ERK1/2 **(C)**, p-MEK2 **(D)** and MEK2 **(E)** total protein level after 72 h. Data are represented as single data points and mean ± SEM of four independent cultures and were tested by one-way ANOVA.

3.5.1 Glutamate-induced excitotoxicity increases p-ERK1/2 and trametinib restores ERK phosphorylation

It is well documented that increased levels of extracellular glutamate trigger the phosphorylation and activation of MAPK signaling pathways. This heightened influx of calcium ions leads to an elevation in ERK phosphorylation **(Figure 21A)**. In our study, we were able to replicate these effects and confirm that glutamate excitotoxicity alone does not alter MEK2 protein expression but can enhance the phosphorylation of ERK1/2. Trametinib, on the other hand, works by binding to the MEK2 activation loop, thereby inhibiting ERK1/2 phosphorylation **(Figure 21B)**. To corroborate these effects in cells subjected to glutamate excitotoxicity, we treated cells at DIV4 with varying trametinib concentrations (0 nM, 2 nM, 20 nM, and 200 nM) for 72 h. Subsequently, glutamate was applied at DIV7 for 6 h, followed by cell lysis and protein isolation. Western blot analysis was performed to investigate total protein expression of p-ERK1/2, p-MEK, ERK1/2 and MEK2 in at least three distinct cultures, both with and without glutamate intoxication. The total protein expression of MEK2 and ERK1/2 remained largely unchanged with trametinib treatment in both stressed and non-stressed cells **(Figure 21 C, E, F, H)**. As previously observed, glutamate excitotoxicity significantly heightened phospho-ERK1/2 levels, which was completely restored by higher concentrations of trametinib application (p-ERK1/2/ ERK1/2 band ratio for 20 nM trametinib = 0.5 ± 0.06 vs. 1.43 ± 0.39; P = 0.0103; for 200 nM = 0.40 ± 0.15 vs. 1.43 ± 0.39; P = 0.0042; ANOVA; n = 3; **Figure 21G, H**). Interestingly, while the application of excitotoxicity induction did not alter p-MEK protein levels, an increase was observed with a concentration of 200 nM trametinib compared to vehicle-treated cells in stress-induced cultures (p-MEK2/ MEK2 band ratio = 3.2 ± 0.8 vs. 1.13 ± 0.14; P = 0.0005; ANOVA; n = 3; **Figure 21G, H**). Additionally, there was a slight, albeit non-significant, increase in MEK2 phosphorylation in vehicle-treated cultures following treatment with higher concentrations of trametinib. Observed response is in line with the negative feedback mechanism in reaction to increased ERK1/2 phosphorylation.

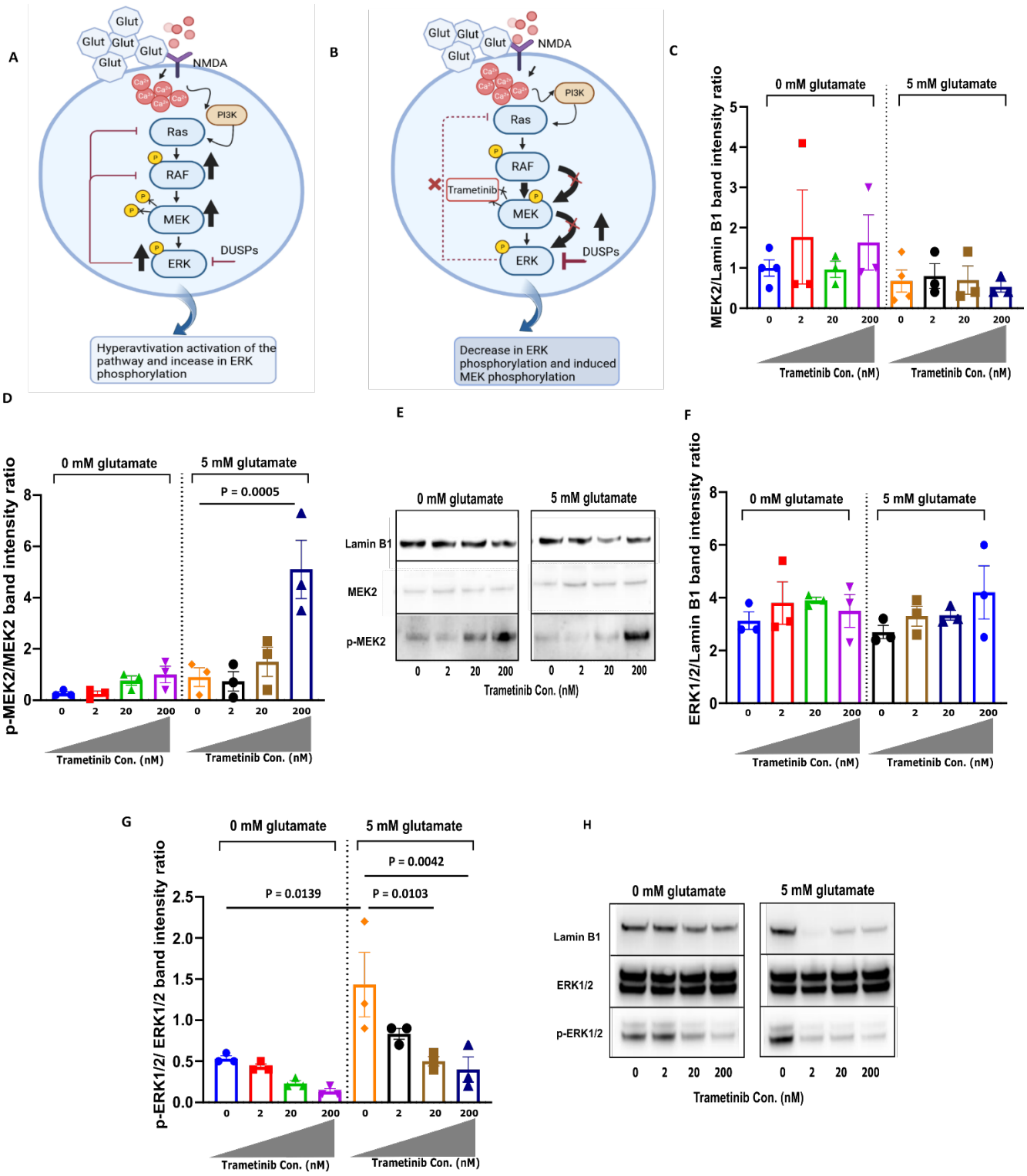

Figure 21: Trametinib effects on MEK2, ERK1/2 protein expression and their phosphorylation in the glutamate excitotoxicity model. (A) Schematic representation of the excitotoxicity effects on RAS-RAF-MEK-ERK pathway. **(B)** Schematic representation of trametinib mechanism of action in RAS-RAF-MEK-ERK pathway in an excitotoxicity situation. **(C-H)** Western blot analysis and quantification of MEK2 **(C, E)**, p-MEK **(D, E)**, ERK1/2 **(F, H)** and p-ERK1/2 **(G, H)**, after treatment with different concentration of trametinib

for 72 h in glutamate and vehicle-treated cells. Data are represented as single data points and mean ± SEM of three independent cultures and were tested by one-way ANOVA.

3.5.2 Trametinib reduces apoptosis and attenuates neurite degeneration in glutamate-intoxicated cells

To explore the potential neuroprotective effects of trametinib within a glutamate excitotoxicity model, we treated cortical cultures with varying concentrations of the drug (0 nM, 2 nM, 20 nM, 200 nM) for a 72-hour period. Subsequently, the cells were subjected to a 6-hour treatment with 5 mM glutamate, after which they were fixed and stained for MAP2 and cleaved caspase-3. Random imaging across five different cultures was conducted and cell death and neurite outgrowth were quantified. As previously demonstrated, excitotoxicity induced by glutamate results in neuronal apoptosis, along with the degeneration of axons and dendrites. Notably, concentrations of 20 nM and 200 nM trametinib showed a significant reduction in apoptosis compared to vehicle condition (cleaved caspase 3 relative signal intensity for 20 nM trametinib: 1.77 ± 0.12 vs. 2.4 ± 0.13; $P = 0.0027$; for 200 nM; 1.89 ± 0.12 vs. 2.4 ± 0.13; $P = 0.0237$; ANOVA; n = 5; **Figure 22A, B**). Furthermore, a significant increase in average neurite length was also observed with same concentrations of trametinib in comparison to vehicle-treated cultures (for 20 nM = 1.35 µm ± 0.18 vs. 0.65 µm ± 0.06; $P < 0.0001$; for 200 nM = 1.18 µm ± 0.18 vs. 0.65 µm ± 0.06173; $P = 0.0003$; ANOVA; n = 5; **Figure 22A, C**). Our data suggests that trametinib functions by attenuating MEK2 activity and reducing ERK1/2 phosphorylation. This orchestrated mechanism leads to decreased cell death and enhancing neurite regeneration, under excitotoxic stress.

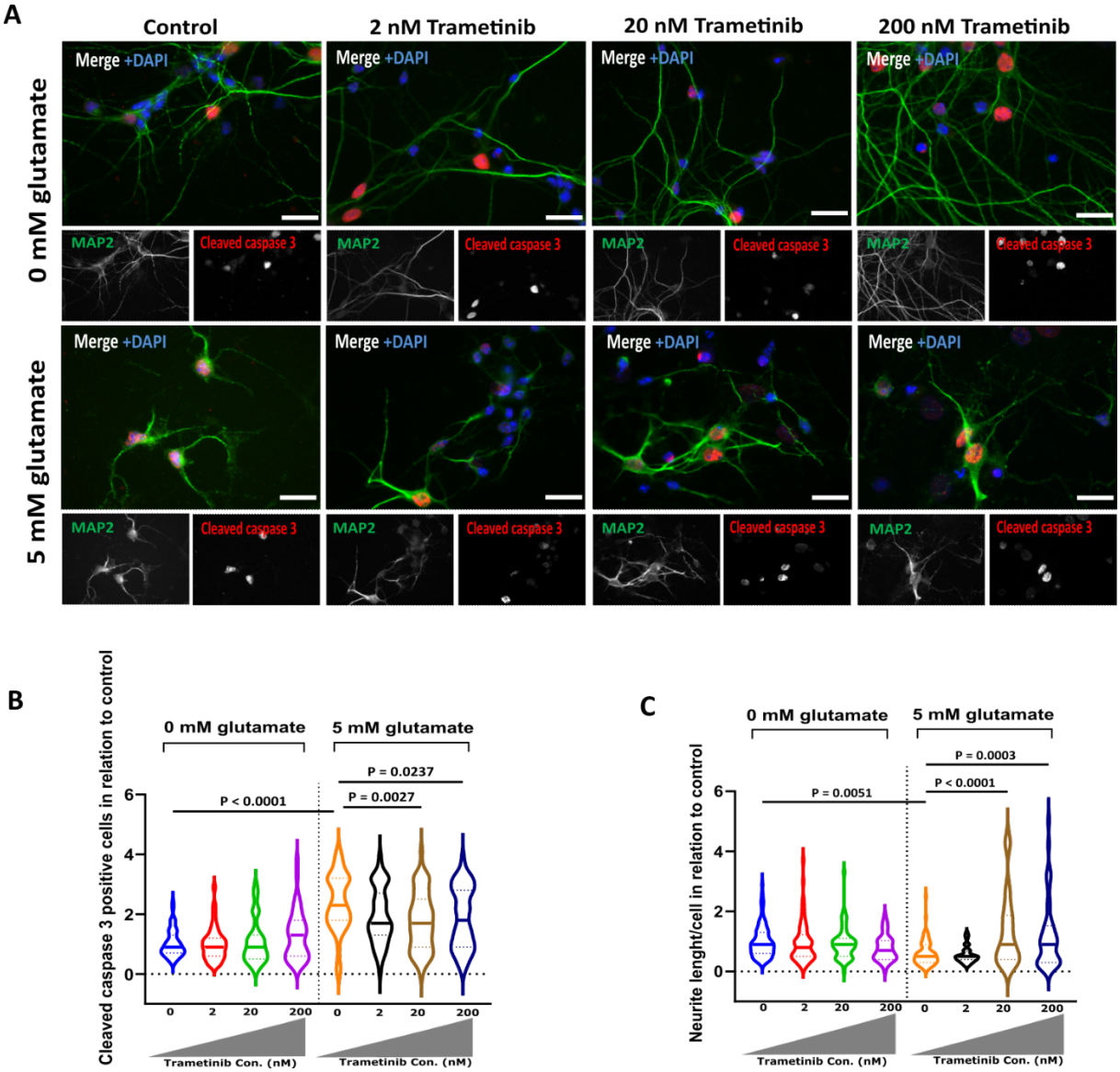

Figure 22: Evaluation of the neuroprotective effects of MEK2 inhibition by trametinib in the glutamate excitotoxicity model. (A) Effects of different concentrations of trametinib on apoptosis and neurite outgrowth in glutamate (5 mM)- and vehicle-treated cells analyzed by immunostaining. Scale bar: 20 µm for all the images. **(B, C)** Quantification plots showing the effects of treatment with trametinib on cell survival **(B)** and neurite outgrowth **(C)** for glutamate- or vehicle-treated cells. Data are represented as the mean ± SEM of five independent cultures and were tested by one-way ANOVA.

3.5.3 Trametinib restores sodium arsenite-induced ERK1/2 phosphorylation and induces MEK2 phosphorylation

Our findings indicate that - similar to glutamate excitotoxicity - sodium arsenite treatment does not induce changes in MEK2 protein expression, yet it elevates ERK1/2 phosphorylation. Arsenite is recognized for its ability to induce chromosomal damage and activate the ERK1/2

signaling pathway. To determine whether trametinib could counteract observed effects, we treated the cortical cultures at DIV4 with 0 nM, 2 nM, 20 nM, and 200 nM trametinib for a 72-hour period. At DIV7, cells were exposed to 10 mM SA for 3 hours, subsequently lysed, and protein was isolated. We investigated total protein expression of p-ERK1/2, ERK1/2, p-MEK, and MEK2 across at least three distinct cultures by WB, both with and without SA exposure. The total protein expression of MEK2 and ERK1/2 remained unchanged with trametinib treatment in both stressed and non-stressed cells, a result consistent with the previous data **(Figure 23A, C, D, F)**. Application of 20 nM trametinib and 200 nM trametinib effectively reduced the phosphorylation of ERK1/2 in comparison to vehicle condition (p-ERK1/2/ ERK1/2 band ratio for 20 nM trametinib = 0.63 ± 0.19 vs. 1.53 ± 0.23; P = 0.0058; for 200 nM trametinib = 0.5 ± 0.15 vs. 1.53 ± 0.23; P = 0.0016; ANOVA; n = 3; **Figure 23E, F**). Interestingly, p-MEK protein levels remained unaffected upon sodium arsenite application; however, its levels increased with 200 nM trametinib concentration compared to vehicle-treated cells (p-MEK2/MEK2 band ratio = 2.27 ± 0.5 vs. 0.77 ± 0.18; P = 0.0086; ANOVA; n = 3; **Figure 23B, C**) in stress-induced cultures. A slight but not significant increase in MEK2 phosphorylation was also observed in vehicle-treated cultures after treatment with higher concentrations of trametinib **(Figure 23B, C)**. This response might be attributed to a previously described feedback loop also observed in glutamate-intoxicated cells.

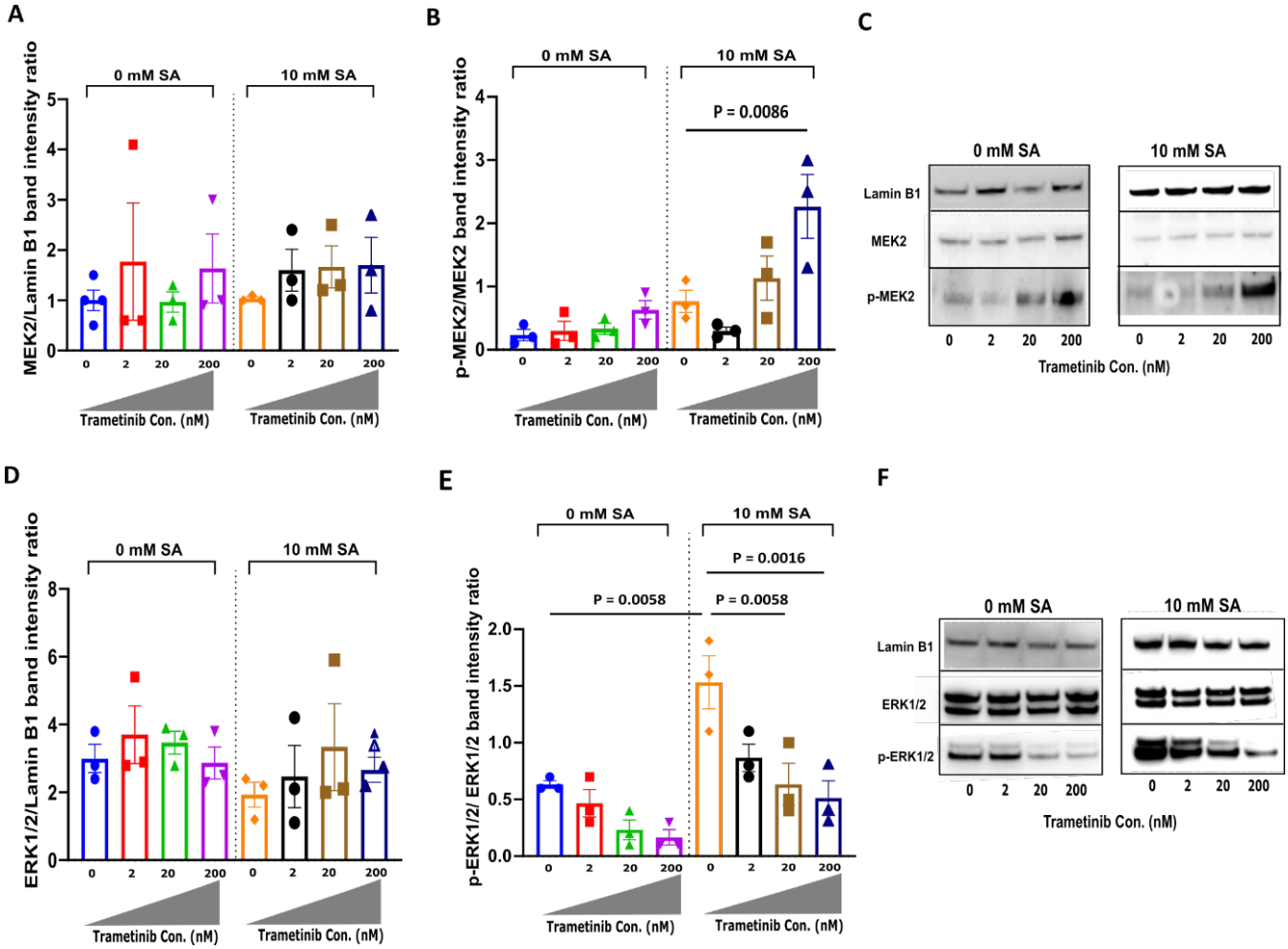

Figure 23: Trametinib effects on MEK2, ERK1/2 protein expression and their phosphorylation in the SA-intoxication model. (A-F) Western blot analysis and quantification of MEK2 **(A, C)**, p-MEK2 **(B, C)**, ERK1/2 **(D, F)** and p-ERK 1/2 **(E, F)** after treatment with different concentrations of trametinib for 72 h in SA and vehicle-treated cells. Data are represented as single data points and mean ± SEM of three independent cultures and were tested by one-way ANOVA.

3.5.4 Trametinib significantly increases the average neurite length in SA-treated cells

In order to validate the potential neuroprotective effects of trametinib in SA-treated cells, cortical cultures were subjected to various concentrations (0 nM, 2 nM, 20 nM, 200 nM) of the drug at DIV4 for a duration of 72 hours. SG-induction was accomplished by treating the cultures with 10 mM sodium arsenite on DIV7 for 3 hours. Following treatment, the cultures were fixed and stained for MAP2, cleaved caspase 3, and G3BP1. Random images were captured and cell death, neurite outgrowth, and G3BP1 fluorescence intensity were analyzed. No notable changes were detected in G3BP1 intensity with different concentrations of trametinib both in arsenite-

and vehicle-treated cells **(Figure 24A, C)**. Nonetheless, small but significant reduction in the number of cleaved caspase 3 positive cells was noted following 2 nM trametinib treatment compared to vehicle-treated cultures (cleaved caspase 3 relative signal intensity = 1.12 ± 0.06 vs. 1.43 ± 0.09; P = 0.0348; ANOVA; n = 4; **Figure 24B, D**). Interestingly, all three trametinib concentrations resulted in significant increase in the average neurite length in arsenite-treated cells compared to vehicle-treated cells (for 2 nM = 0.86 µm ± 0.05 vs. 0.55 µm ± 0.04; P = 0.0145 ; for 20 nM = 1.07 µm ± 0.07 vs. 0.55 µm ± 0.04; P < 0.0001; for 200 nM = 0.88 µm ± 0.05 vs. 0.55 µm ± 0.04; P = 0.0047; ANOVA; n = 4; **Figure 24B, E**) although they did not manifest the same effect in non-stressed cells. Our findings highlight the potential impact of trametinib on neurite outgrowth under conditions of arsenite-induced stress.

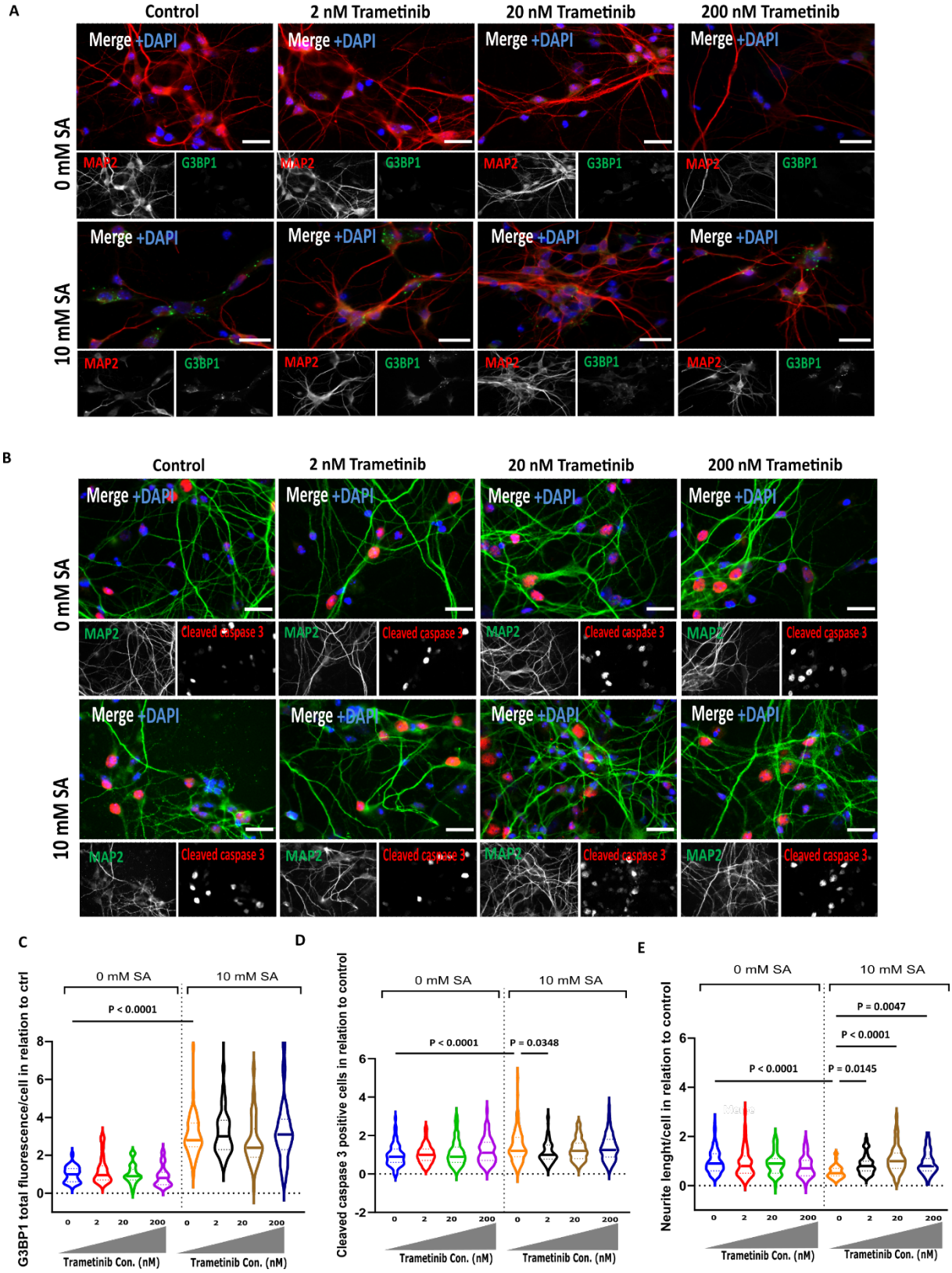

Figure 24: Evaluation of the neuroprotective effects of MEK2 inhibition by trametinib in the SA-intoxication model. (A, C) Effects of different concentrations of trametinib on G3BP1 signal intensity in SA and non-SA-treated cells analyzed by immunostaining. Scale bar: 20 µm for all the images. **(B)** Effects of different concentrations of trametinib on cell survival in SA and non-SA-treated cells analyzed by immunostaining. **(D, E)** Quantification plots showing the

effects of different concentrations of trametinib on cell death **(D)** and on neurite length **(E)** for SA-treated cells and vehicle-treated cells. independent cultures. Data are represented as the mean ± SEM of five independent cultures and were tested by one-way ANOVA.

3.6 Schematic summary of the results

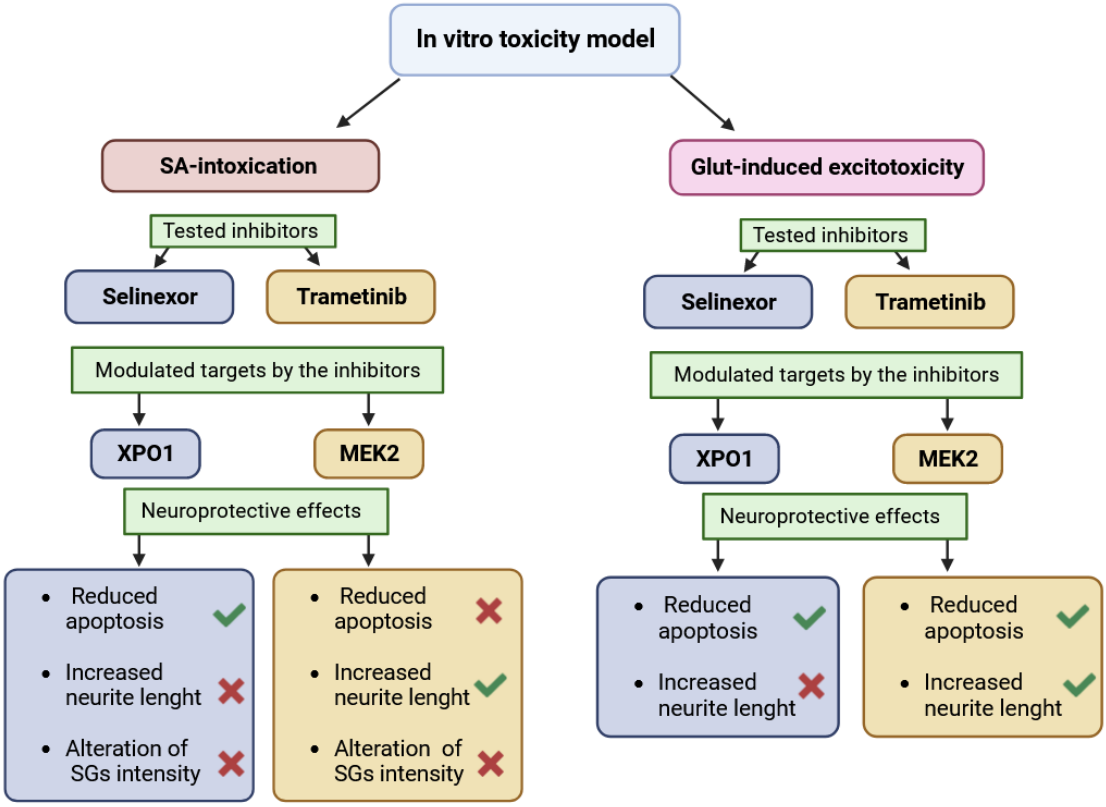

Figure 25: Summary of the main findings. Graphical abstract demonstrates which neuroprotective effects were observed by applying the inhibitors and modulating the targets in SA-intoxication and glutamate-induced excitotoxicity models.

4 Discussion

4.1 Multi-omic profiling approaches revealed the MAPK signaling and the nucleocytoplasmic transport pathways as important pharmacological targets in ALS

In this research, we undertook a comprehensive examination of ALS in the PFC using both individual and combined analyses of various omics datasets. Our aim was to gain a thorough understanding of the molecular framework in this brain region, which is impacted only in later stages by TDP-43 pathology. Furthermore, by focusing on the PFC, we aimed to uncover potential early disease mechanisms that may not anymore be detected in tissue that is affected for a longer time. Interestingly, our integrative analyses drove our focus toward the MAPK. It appeared as one of the most deregulated pathways in WGCNA analyses for animal models. Functional enrichment showed a strong representation of the MAPK signaling pathway particularly in the human samples. As a result, the MAPK pathway was proposed as an auspicious therapeutic target across all human ALS subgroups. MEK2 plays a crucial role in various aspects of neuronal biology, including neuronal differentiation, microtubule assembly, and overall neuronal survival. As a key constituent of the MAPK signaling pathway, it emerges as a compelling candidate for targeted intervention and pathway modulation. Furthermore, our proteomic analyses revealed dysregulation of MEK2 in both the C9orf72 model (males and females) and the SOD1 model (females). Involvement of members from the MAPK superfamily in ALS pathology has been previously discussed. For instance, the Ser/Thr kinase, also known as MAPK/MAK/MRK (MOK) kinase, has been shown to be linked to compromised microglial function and the inflammation-related challenges associated with ALS pathophysiology (Pérez-Cabello et al. 2023). MAPK signaling overactivity, including abnormal ERK1/2 phosphorylation, have been documented in ALS patients and ALS mouse models (Ayala et al. 2011). In our glutamate toxicity model, we also observed an increase in the phosphorylation of ERK1/2. This mirrored the abnormal activation of the pathway, which was effectively attenuated by the MEK2-inhibitor trametinib.

Apart from MEK2, our comprehensive multi-omic analysis underscored the significance of XPO1 as a promising molecular target for drug intervention. In both male and female SOD1 animal models, XPO1 emerged as one of the most differentially expressed proteins, displaying significant upregulation. This trend was consistent with the corresponding increase in gene expression levels within the same model. The perturbation of XPO1 was similarly evident in

other models, including TDP-43 females, FUS males, and the C9orf72 animals, thus highlighting its widespread involvement across various molecular contexts. The functional enrichment analysis also indicated that nucleocytoplasmic transport plays a significant role in human samples. The consistent deregulation of XPO1 across multiple molecular layers in distinct models underscores its pivotal role in the underlying mechanisms of ALS. All together this cumulative evidence renders XPO1 and MEK2 compelling and intriguing candidates for potential pharmacological intervention.

4.2 Exportin 1-inhibition has neuroprotective effects in the glutamate excitotoxicity model

Excitotoxic mechanisms and their role in driving the development of neurodegenerative diseases are gaining widespread recognition, but there is still a need to better understand their contribution to neurodegeneration in ALS (Dong, Wang, and Qin 2009). We chose the glutamate excitotoxicity model in order to validate our targets. Despite the fact that previous studies typically revealed toxicity effects at micromolar glutamate levels, we observed cell death only at millimolar concentrations. The heightened tolerance of cortical neurons to lower glutamate levels and shorter exposure periods could potentially be attributed to the supportive role of astrocytes. Astrocytes can protect cortical neurons against acute damage induced by glutamate (L.-N. Zhang et al. 2019). Our results showed that a 72-h treatment with selinexor significantly reduced apoptosis in glutamate-intoxicated cells. This demonstrates neuroprotective effects of XPO1-inhibition that could potentially also be translated for ALS. It has been shown that neurodegeneration and axonal damage in ALS are associated with mis-localization of nuclear molecules such as TDP-43 to the cytoplasm as a result of nucleoporin dysfunction (Aizawa et al. 2019). It is also known that excitotoxicity induces the movement of specific RBPs associated with ALS, such as TDP-43 and FUS, from the nucleus to the cytoplasm in neurons. FUS's translocation depends on calcium and is accompanied by significant alterations in nucleocytoplasmic transport. Furthermore, FUS plays a critical role in increasing the levels of GRIA2, an AMPA-type glutamate receptor subunit, when neurons are exposed to glutamate-induced stress. As a result, retention of these molecules within the nuclear compartment appears to be protective against such damage (Tischbein et al. 2019). These findings establish important connections between important factors involved in neurodegenerative diseases, including excitotoxicity, disease-related RBPs, and nucleocytoplasmic transport. In 2015 Haines et al., demonstrated that excitotoxic levels of glutamate could induce the nuclear egress of FUS and TDP-43, into the cytoplasm of neurons

and targeting nuclear exportin was an effective approach to reduce axonal damage (Haines et al. 2015) This hypothesis suggests that inhibiting or modulating the activity of specific exportins could potentially be a therapeutic strategy for neurodegenerative conditions. By preventing the abnormal export of nuclear molecules, it may be possible to preserve their normal function within the nucleus and promote neuronal health. In the next steps this could be validated in our models by showing the accumulation of RBPs such as TDP-43 in nuclear fractions after treatment with selinexor.

On the other hand, the neuroprotective effects of XPO1-inhibition which we observed in our results could be explained by other important processes in which XPO1 is involved. XPO1 is also known to play a pivotal role in regulating cellular proteostasis. As a key nuclear export receptor, XPO1 is primarily responsible for transporting a wide array of critical cargo molecules, such as protein kinases, pre-ribosomal subunits, translation factors, cytoskeletal proteins, and transcription factors from the nucleus to the cytoplasm (Kumar et al. 2022) (Thakar et al. 2013). It has been shown that excitotoxic stimulation with glutamate can reduce the proteasome activity, and lead to an accumulation of ubiquitinated proteins (Caldeira et al. 2013). Polyubiquitinated substrate transporter (POST)/DeSI1 contains a nuclear NES signal. It interacts with UBIN and XPO1 to move UBIN and its polyubiquitinated protein cargo out of the nucleus and into the cytosol. This UBIN-POST mechanism serves as a pathway designed to effectively remove polyubiquitinated proteins from the nuclear environment, which could play a role in maintaining nuclear protein balance (Hirayama et al. 2018). In our excitotoxicity model we observed that there is an increase in XPO1 protein expression and nuclear localization as a result of excitotoxicity. The observed effects could also stem from a disruption in the proteostasis machinery, which requires validation. In this scenario, the inhibition of XPO1 through selinexor may regulate the transport of ubiquitinated proteins, potentially leading to neuroprotection.

It is known that the autophagy process plays a pivotal role in safeguarding against and mitigating pathological threats that could trigger neurodegeneration. Consequently, mutations in genes responsible for autophagy components disrupt this process resulting in compromised autophagy and ultimately contributing to neurodegenerative disorders like ALS (Chua et al. 2022). XPO1 has been identified as a modulator, participating in the transport of various autophagy-related factors, such as transcription factors, kinases, and adaptor proteins such as p62, from the nucleus to the cytoplasm. These exported factors, in turn, engage in orchestrating autophagy induction, autophagosome formation, and lysosomal fusion. It has been shown that

XPO1-inhibition could enhance autophagy and induce p62 nuclear retention (Meng and Gao 2021) which we confirmed with our results. A pivotal orchestrator of autophagy and lysosomal function genes, the transcription factor EB (TFEB), has gained attention as a promising target for pharmacological intervention. It has been shown that obstructing the nuclear XPO1 through RNA interference or SINE compounds results in the accumulation of TFEB within the nucleus. This, in turn, amplifies autophagy as a safeguard against cellular aging. This could shift the focus of the application of SINE compounds in cancer treatments to the potential advantages of these compounds in neurodegenerative conditions and the aging process (Kumar et al. 2022).

4.3 Exportin 1-inhibition has neuroprotective effects in the SA-toxicity model

Research on SGs in the context of ALS has attracted significant attention due to their involvement in the degeneration of motor and cortical neurons. To assess our targets within this model, we induced the formation of SGs in our cortical neurons. Notably, as previously indicated, cortical neurons exhibited heightened resistance in generating SGs in comparison to astrocytes. The effects were observed only under high concentration of SA and a longer incubation time. Our results revealed improvement in cell survival by applying selinexor in stress granule-induced cells. Disruptions in nucleocytoplasmic transport have been recognized as a central factor in ALS and FTD triggered by the GGGGCC hexanucleotide repeat expansion in *C9ORF72* as well as other neurodegenerative disorders characterized by protein aggregation, suggesting a common mechanism through which protein stress interferes with this transport process (Freibaum et al. 2015), (Jovičić et al. 2015). It has been demonstrated that cellular stress leads to the mislocalization of crucial nucleocytoplasmic transport components such as RNA/protein complexes in stress granules that play a significant role in ALS progression. It was shown that inhibition of stress granule formation alleviates both nucleocytoplasmic transport impairments and neurodegeneration in C9ORF72-related ALS/FTD. These findings establish a connection between stress granule assembly and nucleocytoplasmic transport (Kang Zhang et al. 2019). On the other hand, a recent study showed that stress granules have the potential to capture a notable portion of nucleocytoplasmic transport client proteins within the cytoplasm. However, in that study, they showed that even though the arsenite treatment significantly disturbed nucleocytoplasmic transport, the rate of nuclear import remained unchanged over time when they inhibited the SGs formation. Therefore, there is no indication that stress granules directly hinder nuclear import by sequestering nuclear import factors (Vanneste et al. 2022). We also observed that XPO1 total gene and protein expression as well

as its nuclear intensity was not changed by sodium arsenite, which was sufficient to induce the formation of stress granules. Our validation results also showed that inhibition of XPO1 with selinexor did not significantly reduce the stress granule signal intensity which confirms the independence of nucleocytoplasmic process from SGs assembly. As it was shown in the study of Vanneste et al, arsenite treatment increased XPO1-mediated export or decreased importin-β1-mediated import (Vanneste et al. 2022). Therefore, neuroprotective effects of selinexor could be the consequence of inhibiting the export of ALS-related protein aggregates to the cytoplasm, which needs to be further confirmed by Western blot in our model in the future.

4.4 MEK2-inhibition has neuroprotective effects in the glutamate excitotoxicity model

The role of glutamate excitotoxicity in neurodegeneration and cell death in the context of neurodegenerative diseases, such as ALS, has been demonstrated (Shaw and Ince 1997). We confirmed that glutamate excitotoxicity negatively impacts cell survival and neurite length in cortical neurons. It is known that the MAPK pathway has an important role in the regulation of essential cellular functions. The exact involvement of this pathway in neurodegeneration is not clear but there have been studies showing the role of MAPK/ERK pathway in neurodegenerative diseases mostly through the inflammatory response and glial cell functions (Ransohoff 2016). It has also been shown that glutamate can induce the activation of MAPK pathways by promoting ERK1/2 phosphorylation (Ortuño-Sahagún et al. 2014). Even though ERK activation is important in cell survival and proliferation, delayed or persistent activation of it can also be associated with neuronal damage (Stanciu et al. 2000). After glutamate treatment in primary cortical cultures, we observed significant upregulation of p-ERK1/2. This aberrant phosphorylation of ERK1/2, could be restored with 20 nM and 200 nM of trametinib. Similar results were obtained by Xu et al. 2016 using T-006, a promising anti-Alzheimer compound. In this publication, they demonstrated that inhibition of the MAPK/ERK pathway with T-006 improves cell survival under glutamate-induced toxicity, but increase in neurite length was shown only in unstressed conditions (Daping Xu et al. 2016). We observed that trametinib does not impact cells in unstressed conditions. However, under excitotoxicity, trametinib had an impact on cell survival and also significantly increased neurite length in surviving cells. It is known that RAF-1/MEK/ERK 1/2 signaling cascade has an important role in the regulation of neurite outgrowth through the phosphorylation of ERK1/2 (Liao et al. 2012). However, this effect seems to be dependent on the duration and/or strength of the ERK signal (Hausott and Klimaschewski 2019). Thus, an aberrantly increased phosphorylation or long-

lasting activation of ERK could result in negative effects, which could be the case in our toxicity model. The effects of trametinib, achieved through the inhibition of ERK1/2 phosphorylation, may explain the reduction in apoptosis and the increase of neurite length in surviving cells in a stress-induced model. However, since the activation of this pathway is a result of the phosphorylation cascade and involvement of many different players, investigating other up- and down-stream components is necessary for a better understanding of the mechanism behind it (Stanciu et al. 2000).

4.5 MEK2 inhibition has neuroprotective effects in the SA-toxicity model

Our data showed that sodium arsenite treatment resulted in cell death and also increased p-ERK. It has been shown that arsenic compounds lead to activation of the MAPK pathways (p38, JNK, and ERK1/2). This modulation in turn activates the caspase pathway, ultimately culminating in apoptosis (Juan et al. 2022). Increased phosphorylation of ERK in response to arsenite was also shown in CL3 cells. Li et al, showed in their study that arsenite-activated ERK could be blocked by two MEK1/2 inhibitors, PD98059 and U0126 (Li, Lin, and Yang 2006). We also demonstrated that the elevated p-ERK levels were restored upon trametinib application. This restoration was associated with a slight reduction in the number of cells positive for cleaved caspase 3 and a notable increase in neurite length, showcasing overall neuroprotective effects. Our findings indicated that trametinib treatment had no discernible impact on the intensity of stress granules. The role of the MAPK signaling pathway in stress granule formation has been previously established. However, previous studies unveil the novel involvement of PI3K and MAPK/p38, which enhances the stress granule formation. These kinases utilize the mTORC1 pathway, a master regulator of metabolism, to facilitate the assembly of stress granules (Heberle et al. 2019). It's important to note that trametinib serves as a MEK1/2 inhibitor, primarily influencing downstream components of the MEK pathway without direct effects on upstream kinases. Consequently, we do not anticipate significant alterations in stress granule formation as a direct outcome of trametinib treatment. Nevertheless, given that the activation of MAPK signaling pathway involves a complex phosphorylation cascade with numerous contributing factors as well as feedback responses, it is important to explore additional upstream and downstream components to gain a more comprehensive insight in the underlying mechanism.

4.6 Selinexor and trametinib as potential drugs for the treatment of ALS

We have observed neuroprotective effects of selinexor in our *in vitro* models of ALS. However, the exact mechanism of action behind this observation remains unclear and requires closer investigation to substantiate the hypothesis regarding its precise mode of action. Nevertheless, these findings also lend support to the potential of targeting the nucleocytoplasmic pathway as a candidate for ALS therapy. Selinexor, has primarily been investigated in cancer studies and in the context of neurodegenerative diseases due to its mechanism of action. Despite its examination in relation to nucleocytoplasmic transport in ALS pathology, conclusive evidence of its functional neuroprotective effects remains elusive (Vanneste and Van Den Bosch 2021). Understanding this link is crucial for effective therapeutic targeting of nucleocytoplasmic transport and harmful protein aggregates. Clinical trials have inadequately addressed nucleocytoplasmic transport, despite its widespread dysfunction in ALS (Tzeplaeff et al. 2023). To our knowledge, the only clinical trial investigating nucleocytoplasmic transport in ALS was conducted by Biogen. This trial involved BIIB100, a nuclear-export inhibitor targeting XPO1 which was terminated in June 2021 without a clear explanation at the phase I trial stage (NCT03945279). Nonetheless, this does not diminish the potential importance of targeting this process for ALS therapy, particularly in the exploration of other underlying aspects of ALS etiology.

We noted an elevated level of phosphorylated ERK1/2 in our both toxicity models. Furthermore, in the SOD1 mouse model, we observed an increase in p-MEK2 level, replicating the abnormal activation of MAPK pathway. Importantly, this aberrant activation was effectively reversed by the MEK2 inhibitor trametinib (Caldi Gomes et al. 2023). Trametinib has gained attention as a candidate for drug repurposing in the realm of neurodegenerative diseases. Currently, a phase I/II clinical trial (clinicaltrials.gov identifier: NCT04326283) is underway to assess the safety, tolerability, and effectiveness of trametinib in ALS patients. No previous published result demonstrates efficacy of trametinib, neither *in vivo* nor *in vitro*. Our multi-omic data support the importance of separately evaluating male and female patients (Caldi Gomes et al. 2023). It provides a unique insight into the molecular mechanisms of trametinib using an *in vitro* model that mimics ALS pathology. Our work distinguishes itself by separating the data by sex, revealing specific effects in females (Caldi Gomes et al. 2023). This underscores the importance of considering sex as a variable, especially since ALS predominantly affects males. In general, positive results in the validation of both molecular targets and their inhibitors could advocate the translation of these to more clinical trials and

paves the way for considering selinexor and trametinib as promising candidates for potential ALS treatment.

5 Concluding remarks

The experiments conducted in this project highlighted the advantages of using high-throughput omics techniques and leveraging of comprehensive datasets for the exploration of molecular pathomechanisms of neurodegenerative disorders such as ALS. Our multi-omic profiling approaches revealed multiple disease-relevant pathways and molecular therapeutic candidates in ALS derived from the analysis of human prefrontal cortex tissue of ALS patients and different transgenic ALS mouse models. XPO1 and MEK2 were identified as being deregulated and functionally enriched in various models, underscoring the significance of the MAPK signaling pathway and nucleocytoplasmic transport in the pathomechanism of ALS. These crucial targets were further corroborated through validation in stress-induced *in vitro* models. The pharmacological compounds selinexor and trametinib targeting XPO1 and MEK2, respectively, demonstrated neuroprotective effects in primary cell cultures subjected to stress. We manipulated the expression of XPO-1 and MEK2 using small molecule inhibitors, selinexor and trametinib. Our findings revealed that after a 72-hour treatment with trametinib at concentrations of 20 nM and 200 nM, there was a complete restoration of elevated phospho-ERK1/2 protein levels, a direct target of MEK2. This treatment also led to a significant reduction in apoptosis and an increase in the average neurite length in cells exposed to glutamate toxicity. Increase in neurite length was also observed with all 3 concentrations of trametinib in SA-treated cultures without a direct effect on SGs intensity. This observation underscores MEK2 and the MAPK pathway as potential candidates to be targeted for halting neurite degeneration. Conversely, when cells were exposed to selinexor at concentrations of 1 nM and 10 nM, a significant reduction in cell death was observed in both stress-induced models. However, it did not induce a substantial effect on neurite length. This could draw attention to the potential role of XPO1 and nucleocytoplasmic transport in regulation of apoptosis, this time within the context of neurodegenerative diseases. Overall, these findings suggest the potential of these compounds as promising novel therapeutic approaches for treating ALS.

6 Summary

In the context of MAXOMOD project, we conducted a comprehensive analysis involving multiple omics data sets from the prefrontal cortex of 51 sporadic ALS patients and 50 control subjects, along with four transgenic mouse models representing C9orf72-, SOD1-, TDP-43-, and FUS-ALS, aiming to elucidate early and gender-specific disease mechanisms in ALS. Our investigation revealed multiple deregulated molecular targets and pathways. XPO1 and MAP2K2 (MEK2) were selected to be validated *in vitro*. XPO1 is a major regulator of nuclear RNA export and MEK2 has important roles in cell survival. To validate these molecular targets, we established primary cortical cultures from P0 C57/Bl6 mice. To assess the role of XPO1 and MEK2 on neuronal survival we used *in vitro* toxicity models mimicking known disease pathways in ALS, such as glutamate excitotoxicity and arsenite-induced stress granule formation. We modulated the expression of XPO1 and MEK2 with pharmacological small molecule inhibitors (selinexor and trametinib). Toxicity and functionality of the inhibitors were investigated by Western blot, while neuroprotective effects of target inhibition were investigated by immunocytochemistry (cleaved caspase 3) and analysis of neurite outgrowth using image J. Our results demonstrated that 72 h treatment with 20 nM and 200 nM trametinib, completely restored elevated phospho-ERK1/2 protein which is a direct target of MEK2 and significantly reduced apoptosis and increased average neurite length in glutamate-intoxicated cells. 1 nM and 10 nM selinexor on the other hand, significantly reduced cell death in both stress-induced models but didn't affect average neurite length. Our findings suggest that XPO1 and MEK2 could be auspicious drug targets to be further explored for the treatment of ALS.

7 References

Aizawa, Hitoshi, Takenari Yamashita, Haruhisa Kato, Takashi Kimura, and Shin Kwak. 2019. “Impaired Nucleoporins Are Present in Sporadic Amyotrophic Lateral Sclerosis Motor Neurons That Exhibit Mislocalization of the 43-KDa TAR DNA-Binding Protein.” *Journal of Clinical Neurology (Seoul, Korea)* 15 (1): 62–67. https://doi.org/10.3988/jcn.2019.15.1.62.

Archbold, Hilary C., Kasey L. Jackson, Ayush Arora, Kaitlin Weskamp, Elizabeth M.-H. Tank, Xingli Li, Roberto Miguez, et al. 2018. “TDP43 Nuclear Export and Neurodegeneration in Models of Amyotrophic Lateral Sclerosis and Frontotemporal Dementia.” *Scientific Reports* 8 (March): 4606. https://doi.org/10.1038/s41598-018-22858-w.

Aronica, Eleonora, Frank Baas, Anand Iyer, Anneloor L. M. A. ten Asbroek, Giovanna Morello, and Sebastiano Cavallaro. 2015. “Molecular Classification of Amyotrophic Lateral Sclerosis by Unsupervised Clustering of Gene Expression in Motor Cortex.” *Neurobiology of Disease* 74 (February): 359–76. https://doi.org/10.1016/j.nbd.2014.12.002.

Ayala, Victòria, Ana Belén Granado-Serrano, Daniel Cacabelos, Alba Naudí, Ekaterina V. Ilieva, Jordi Boada, Víctor Caraballo-Miralles, et al. 2011. “Cell Stress Induces TDP-43 Pathological Changes Associated with ERK1/2 Dysfunction: Implications in ALS.” *Acta Neuropathologica* 122 (3): 259–70. https://doi.org/10.1007/s00401-011-0850-y.

Azizian, Nancy G., and Yulin Li. 2020. “XPO1-Dependent Nuclear Export as a Target for Cancer Therapy.” *Journal of Hematology & Oncology* 13 (June): 61. https://doi.org/10.1186/s13045-020-00903-4.

Bang, Yung-Jue, Jin Hwa Kwon, Shin Hyeok Kang, Jong Woo Kim, and Yun Chung Yang. 1998. “Increased MAPK Activity and MKP-1 Overexpression in Human Gastric Adenocarcinoma.” *Biochemical and Biophysical Research Communications* 250 (1): 43–47. https://doi.org/10.1006/bbrc.1998.9256.

Barschke, Peggy, Patrick Oeckl, Petra Steinacker, Albert Ludolph, and Markus Otto. 2017. “Proteomic Studies in the Discovery of Cerebrospinal Fluid Biomarkers for Amyotrophic Lateral Sclerosis.” *Expert Review of Proteomics* 14 (9): 769–77. https://doi.org/10.1080/14789450.2017.1365602.

Beers, David R., Jenny S. Henkel, Weihua Zhao, Jinghong Wang, and Stanley H. Appel. 2008. “CD4+ T Cells Support Glial Neuroprotection, Slow Disease Progression, and Modify Glial Morphology in an Animal Model of Inherited ALS.” *Proceedings of the National Academy of Sciences of the United States of America* 105 (40): 15558–63. https://doi.org/10.1073/pnas.0807419105.

Bettencourt, Conceição, and Henry Houlden. 2015. “Exome Sequencing Uncovers Hidden Pathways in Familial and Sporadic ALS.” *Nature Neuroscience* 18 (5): 611–13. https://doi.org/10.1038/nn.4012.

Blair, Hannah A. 2023. “Tofersen: First Approval.” *Drugs* 83 (11): 1039–43. https://doi.org/10.1007/s40265-023-01904-6.

Blasco, H., F. Patin, B. Madji Hounoum, P. H. Gordon, P. Vourc’h, C. R. Andres, and P. Corcia. 2016. “Metabolomics in Amyotrophic Lateral Sclerosis: How Far Can It Take Us?” *European Journal of Neurology* 23 (3): 447–54. https://doi.org/10.1111/ene.12956.

Bozzoni, Virginia, Orietta Pansarasa, Luca Diamanti, Guido Nosari, Cristina Cereda, and Mauro Ceroni. 2016. “Amyotrophic Lateral Sclerosis and Environmental Factors.” *Functional Neurology* 31 (1): 7–19. https://doi.org/10.11138/FNeur/2016.31.1.007.

Brettschneider, Johannes, Kelly Del Tredici, Jon B. Toledo, John L. Robinson, David J. Irwin, Murray Grossman, EunRan Suh, et al. 2013. “Stages of PTDP-43 Pathology in Amyotrophic Lateral Sclerosis.” *Annals of Neurology* 74 (1): 20–38. https://doi.org/10.1002/ana.23937.

Butovsky, Oleg, Shafiuddin Siddiqui, Galina Gabriely, Amanda J. Lanser, Ben Dake, Gopal Murugaiyan, Camille E. Doykan, et al. 2012. “Modulating Inflammatory Monocytes with a Unique MicroRNA Gene Signature Ameliorates Murine ALS.” *The Journal of Clinical Investigation* 122 (9): 3063–87. https://doi.org/10.1172/JCI62636.

Caballero-Hernandez, Diana, Miguel G. Toscano, Marta Cejudo-Guillen, Maria L. Garcia-Martin, Soledad Lopez, Jaime M. Franco, Francisco J. Quintana, Cintia Roodveldt, and David Pozo. 2016. “The ‘Omics’ of Amyotrophic Lateral Sclerosis.” *Trends in Molecular Medicine* 22 (1): 53–67. https://doi.org/10.1016/j.molmed.2015.11.001.

Cady, Janet, Peggy Allred, Taha Bali, Alan Pestronk, Alison Goate, Timothy M. Miller, Rob Mitra, John Ravits, Matthew B. Harms, and Robert H. Baloh. 2015. “ALS Onset Is Influenced by the Burden of Rare Variants in Known ALS Genes.” *Annals of Neurology* 77 (1): 100–113. https://doi.org/10.1002/ana.24306.

Caldeira, Margarida V., Michele Curcio, Graciano Leal, Ivan L. Salazar, Miranda Mele, Ana Rita A. Santos, Carlos V. Melo, Paulo Pereira, Lorella M. T. Canzoniero, and Carlos B. Duarte. 2013. “Excitotoxic Stimulation Downregulates the Ubiquitin–Proteasome System through Activation of NMDA Receptors in Cultured Hippocampal Neurons.” *Biochimica et Biophysica Acta (BBA) - Molecular Basis of Disease* 1832 (1): 263–74. https://doi.org/10.1016/j.bbadis.2012.10.009.

Caldi Gomes, Lucas, Sonja Hänzelmann, Sergio Oller, Mojan Parvaz, Fabian Hausmann, Robin Khatri, Melanie Ebbing, et al. 2023. *Multiomic ALS Signatures Highlight Sex Differences and Molecular Subclusters and Identify the MAPK Pathway as Therapeutic Target*. https://doi.org/10.1101/2023.08.14.553180.

Camacho-Soto, Alejandra, Susan Searles Nielsen, Irene M. Faust, Robert C. Bucelli, Timothy M. Miller, and Brad A. Racette. 2022. “Incidence of Amyotrophic Lateral Sclerosis in Older Adults.” *Muscle & Nerve* 66 (3): 289–96. https://doi.org/10.1002/mus.27652.

Campos-Melo, Danae, Zachary C. E. Hawley, Cristian A. Droppelmann, and Michael J. Strong. 2021. “The Integral Role of RNA in Stress Granule Formation and Function.” *Frontiers in Cell and Developmental Biology* 9 (May): 621779. https://doi.org/10.3389/fcell.2021.621779.

Carrì, Maria Teresa, Cristiana Valle, Francesca Bozzo, and Mauro Cozzolino. 2015. “Oxidative Stress and Mitochondrial Damage: Importance in Non-SOD1 ALS.” *Frontiers in Cellular Neuroscience* 9 (February): 41. https://doi.org/10.3389/fncel.2015.00041.

Catanese, Alberto, Sandeep Rajkumar, Daniel Sommer, Pegah Masrori, Nicole Hersmus, Philip Van Damme, Simon Witzel, et al. 2023. “Multiomics and Machine-Learning Identify Novel Transcriptional and Mutational Signatures in Amyotrophic Lateral Sclerosis.” *Brain* 146 (9): 3770–82. https://doi.org/10.1093/brain/awad075.

Chen, Michael, Supriya Ramesha, Laura Weinstock, Tianwen Gao, Linyang Ping, Hailian Xiao, Eric Dammer, et al. 2019. *Microglial ERK Activation Is a Critical Regulator of Pro-Inflammatory Immune Responses in Alzheimer’s Disease*. https://doi.org/10.1101/798215.

Chen, Tong, Bradley J. Turner, Philip M. Beart, Lucy Sheehan-Hennessy, Chinasom Elekwachi, and Hakan Muyderman. 2018. “Glutathione Monoethyl Ester Prevents TDP-43 Pathology in Motor

Neuronal NSC-34 Cells." *Neurochemistry International* 112 (January): 278–87. https://doi.org/10.1016/j.neuint.2017.08.009.

Chua, Jason P., Hortense De Calbiac, Edor Kabashi, and Sami J. Barmada. n.d. "Autophagy and ALS: Mechanistic Insights and Therapeutic Implications." *Autophagy* 18 (2): 254–82. https://doi.org/10.1080/15548627.2021.1926656.

Cirulli, Elizabeth T., Brittany N. Lasseigne, Slavé Petrovski, Peter C. Sapp, Patrick A. Dion, Claire S. Leblond, Julien Couthouis, et al. 2015. "Exome Sequencing in Amyotrophic Lateral Sclerosis Identifies Risk Genes and Pathways." *Science (New York, N.Y.)* 347 (6229): 1436–41. https://doi.org/10.1126/science.aaa3650.

Ciura, Sorana, Serena Lattante, Isabelle Le Ber, Morwena Latouche, Hervé Tostivint, Alexis Brice, and Edor Kabashi. 2013. "Loss of Function of C9orf72 Causes Motor Deficits in a Zebrafish Model of Amyotrophic Lateral Sclerosis." *Annals of Neurology* 74 (2): 180–87. https://doi.org/10.1002/ana.23946.

Collins, Mahlon A., Jiyan An, Brian L. Hood, Thomas P. Conrads, and Robert P. Bowser. 2015. "Label-Free LC-MS/MS Proteomic Analysis of Cerebrospinal Fluid Identifies Protein/Pathway Alterations and Candidate Biomarkers for Amyotrophic Lateral Sclerosis." *Journal of Proteome Research* 14 (11): 4486–4501. https://doi.org/10.1021/acs.jproteome.5b00804.

Commissioner, Office of the. 2020. "FDA Approves New Treatment for Refractory Multiple Myeloma." FDA. FDA. March 24, 2020. https://www.fda.gov/news-events/press-announcements/fda-approves-new-treatment-refractory-multiple-myeloma.

Costa, Júlia, Marta Gromicho, Ana Pronto-Laborinho, Conceição Almeida, Ricardo A. Gomes, Ana C. L. Guerreiro, Abel Oliva, Susana Pinto, and Mamede de Carvalho. 2021. "Cerebrospinal Fluid Chitinases as Biomarkers for Amyotrophic Lateral Sclerosis." *Diagnostics* 11 (7): 1210. https://doi.org/10.3390/diagnostics11071210.

De Felice, Bruna, Anna Annunziata, Giuseppe Fiorentino, Marco Borra, Elio Biffali, Cinzia Coppola, Roberto Cotrufo, et al. 2014. "MiR-338-3p Is over-Expressed in Blood, CFS, Serum and Spinal Cord from Sporadic Amyotrophic Lateral Sclerosis Patients." *Neurogenetics* 15 (4): 243–53. https://doi.org/10.1007/s10048-014-0420-2.

Deng, Han-Xiang, Hong Zhai, Eileen H. Bigio, Jianhua Yan, Faisal Fecto, Kaouther Ajroud, Manjari Mishra, et al. 2010. "FUS-Immunoreactive Inclusions Are a Common Feature in Sporadic and Non-SOD1 Familial Amyotrophic Lateral Sclerosis." *Annals of Neurology* 67 (6): 739–48. https://doi.org/10.1002/ana.22051.

Dong, Xiao-xia, Yan Wang, and Zheng-hong Qin. 2009. "Molecular Mechanisms of Excitotoxicity and Their Relevance to Pathogenesis of Neurodegenerative Diseases." *Acta Pharmacologica Sinica* 30 (4): 379. https://doi.org/10.1038/aps.2009.24.

Dudman, Jessica, and Xin Qi. 2020. "Stress Granule Dysregulation in Amyotrophic Lateral Sclerosis." *Frontiers in Cellular Neuroscience* 14 (November): 598517. https://doi.org/10.3389/fncel.2020.598517.

Durham, H. D., J. Roy, L. Dong, and D. A. Figlewicz. 1997. "Aggregation of Mutant Cu/Zn Superoxide Dismutase Proteins in a Culture Model of ALS." *Journal of Neuropathology and Experimental Neurology* 56 (5): 523–30. https://doi.org/10.1097/00005072-199705000-00008.

Ederle, Helena, Christina Funk, Claudia Abou-Ajram, Saskia Hutten, Eva B. E. Funk, Ralph H. Kehlenbach, Susanne M. Bailer, and Dorothee Dormann. 2018. “Nuclear Egress of TDP-43 and FUS Occurs Independently of Exportin-1/CRM1.” *Scientific Reports* 8 (May): 7084. https://doi.org/10.1038/s41598-018-25007-5.

Eshima, Jarrett, Samantha A. O’Connor, Ethan Marschall, Robert Bowser, Christopher L. Plaisier, and Barbara S. Smith. 2023. “Molecular Subtypes of ALS Are Associated with Differences in Patient Prognosis.” *Nature Communications* 14 (January): 95. https://doi.org/10.1038/s41467-022-35494-w.

Etchin, Julia, Takaomi Sanda, Marc R. Mansour, Alex Kentsis, Joan Montero, Bonnie T. Le, Amanda L. Christie, et al. 2013. “KPT-330 Inhibitor of CRM1 (XPO1)-Mediated Nuclear Export Has Selective Anti-Leukaemic Activity in Preclinical Models of T-ALL and AML.” *British Journal of Haematology* 161 (1): 117–27. https://doi.org/10.1111/bjh.12231.

Fang, Jing Yuan, and Bruce C Richardson. 2005. “The MAPK Signalling Pathways and Colorectal Cancer.” *The Lancet Oncology* 6 (5): 322–27. https://doi.org/10.1016/S1470-2045(05)70168-6.

Fels, Jasmine A., Jalia Dash, Kent Leslie, Giovanni Manfredi, and Hibiki Kawamata. 2022. “Effects of PB-TURSO on the Transcriptional and Metabolic Landscape of Sporadic ALS Fibroblasts.” *Annals of Clinical and Translational Neurology* 9 (10): 1551–64. https://doi.org/10.1002/acn3.51648.

Fischer, Utz, Clemens Englbrecht, and Ashwin Chari. 2011. “Biogenesis of Spliceosomal Small Nuclear Ribonucleoproteins.” *Wiley Interdisciplinary Reviews. RNA* 2 (5): 718–31. https://doi.org/10.1002/wrna.87.

Freibaum, Brian D., Yubing Lu, Rodrigo Lopez-Gonzalez, Nam Chul Kim, Sandra Almeida, Kyung-Ha Lee, Nisha Badders, et al. 2015. “GGGGCC Repeat Expansion in C9ORF72 Compromises Nucleocytoplasmic Transport.” *Nature* 525 (7567): 129–33. https://doi.org/10.1038/nature14974.

Freischmidt, Axel, Kathrin Müller, Lisa Zondler, Patrick Weydt, Alexander E. Volk, Anže Lošdorfer Božič, Michael Walter, et al. 2014. “Serum MicroRNAs in Patients with Genetic Amyotrophic Lateral Sclerosis and Pre-Manifest Mutation Carriers.” *Brain* 137 (11): 2938–50. https://doi.org/10.1093/brain/awu249.

Frémin, Christophe, and Sylvain Meloche. 2010. “From Basic Research to Clinical Development of MEK1/2 Inhibitors for Cancer Therapy.” *Journal of Hematology & Oncology* 3 (February): 8. https://doi.org/10.1186/1756-8722-3-8.

Gandhi, Ujjawal H., William Senapedis, Erkan Baloglu, Thaddeus J. Unger, Ajai Chari, Dan Vogl, and Robert F. Cornell. 2018. “Clinical Implications of Targeting XPO1-Mediated Nuclear Export in Multiple Myeloma.” *Clinical Lymphoma, Myeloma and Leukemia* 18 (5): 335–45. https://doi.org/10.1016/j.clml.2018.03.003.

Geser, Felix, Maria Martinez-Lage, John Robinson, Kunihiro Uryu, Manuela Neumann, Nicholas J. Brandmeir, Sharon X. Xie, et al. 2009. “Clinical and Pathological Continuum of Multisystem TDP-43 Proteinopathies.” *Archives of Neurology* 66 (2): 180–89. https://doi.org/10.1001/archneurol.2008.558.

Gilmartin, Aidan G., Maureen R. Bleam, Arthur Groy, Katherine G. Moss, Elisabeth A. Minthorn, Swarupa G. Kulkarni, Cynthia M. Rominger, et al. 2011a. “GSK1120212 (JTP-74057) Is an Inhibitor of MEK Activity and Activation with Favorable Pharmacokinetic Properties for Sustained In Vivo Pathway Inhibition.” *Clinical Cancer Research* 17 (5): 989–1000. https://doi.org/10.1158/1078-0432.CCR-10-2200.

———. 2011b. “GSK1120212 (JTP-74057) Is an Inhibitor of MEK Activity and Activation with Favorable Pharmacokinetic Properties for Sustained In Vivo Pathway Inhibition.” *Clinical Cancer Research* 17 (5): 989–1000. https://doi.org/10.1158/1078-0432.CCR-10-2200.

Gordon, David, Ruxandra Dafinca, Jakub Scaber, Javier Alegre-Abarrategui, Lucy Farrimond, Connor Scott, Daniel Biggs, et al. 2019. “Single-Copy Expression of an Amyotrophic Lateral Sclerosis-Linked TDP-43 Mutation (M337V) in BAC Transgenic Mice Leads to Altered Stress Granule Dynamics and Progressive Motor Dysfunction.” *Neurobiology of Disease* 121 (January): 148–62. https://doi.org/10.1016/j.nbd.2018.09.024.

Goutman, Stephen A., Kai Guo, Masha G. Savelieff, Adam Patterson, Stacey A. Sakowski, Hani Habra, Alla Karnovsky, Junguk Hur, and Eva L. Feldman. 2022. “Metabolomics Identifies Shared Lipid Pathways in Independent Amyotrophic Lateral Sclerosis Cohorts.” *Brain: A Journal of Neurology* 145 (12): 4425–39. https://doi.org/10.1093/brain/awac025.

Gurney, M. E. 1997. “Transgenic Animal Models of Familial Amyotrophic Lateral Sclerosis.” *Journal of Neurology* 244 Suppl 2 (May): S15-20. https://doi.org/10.1007/BF03160575.

Gurney, M. E., H. Pu, A. Y. Chiu, M. C. Dal Canto, C. Y. Polchow, D. D. Alexander, J. Caliendo, A. Hentati, Y. W. Kwon, and H. X. Deng. 1994. “Motor Neuron Degeneration in Mice That Express a Human Cu,Zn Superoxide Dismutase Mutation.” *Science (New York, N.Y.)* 264 (5166): 1772–75. https://doi.org/10.1126/science.8209258.

Haeusler, Aaron R., Christopher J. Donnelly, Goran Periz, Eric A.J. Simko, Patrick G. Shaw, Min-Sik Kim, Nicholas J. Maragakis, et al. 2014. “C9orf72 Nucleotide Repeat Structures Initiate Molecular Cascades of Disease.” *Nature* 507 (7491): 195–200. https://doi.org/10.1038/nature13124.

Haines, Jeffery D., Olivier Herbin, Belén de la Hera, Oscar G. Vidaurre, Gregory A. Moy, Qingxiang Sun, Ho Yee Joyce Fung, et al. 2015. “Selective Inhibitors of Nuclear Export Avert Progression in Preclinical Models of Inflammatory Demyelination.” *Nature Neuroscience* 18 (4): 511–20. https://doi.org/10.1038/nn.3953.

Hardiman, Orla, Leonard H. van den Berg, and Matthew C. Kiernan. 2011. “Clinical Diagnosis and Management of Amyotrophic Lateral Sclerosis.” *Nature Reviews. Neurology* 7 (11): 639–49. https://doi.org/10.1038/nrneurol.2011.153.

Hardiman, Orla, and Leonard H Van Den Berg. 2017. “Edaravone: A New Treatment for ALS on the Horizon?” *The Lancet Neurology* 16 (7): 490–91. https://doi.org/10.1016/S1474-4422(17)30163-1.

Harraz, Maged M., Jennifer J. Marden, Weihong Zhou, Yulong Zhang, Aislinn Williams, Victor S. Sharov, Kathryn Nelson, et al. 2008. “SOD1 Mutations Disrupt Redox-Sensitive Rac Regulation of NADPH Oxidase in a Familial ALS Model.” *The Journal of Clinical Investigation* 118 (2): 659–70. https://doi.org/10.1172/JCI34060.

Hausott, Barbara, and Lars Klimaschewski. 2019. “Promotion of Peripheral Nerve Regeneration by Stimulation of the Extracellular Signal-Regulated Kinase (ERK) Pathway.” *Anatomical Record (Hoboken, N.j. : 2007)* 302 (8): 1261–67. https://doi.org/10.1002/ar.24126.

Heberle, Alexander Martin, Patricia Razquin Navas, Miriam Langelaar-Makkinje, Katharina Kasack, Ahmed Sadik, Erik Faessler, Udo Hahn, et al. 2019. “The PI3K and MAPK/P38 Pathways Control Stress Granule Assembly in a Hierarchical Manner.” *Life Science Alliance* 2 (2): e201800257. https://doi.org/10.26508/lsa.201800257.

Hirayama, Shoshiro, Munechika Sugihara, Daisuke Morito, Shun-ichiro Iemura, Tohru Natsume, Shigeo Murata, and Kazuhiro Nagata. 2018. “Nuclear Export of Ubiquitinated Proteins via the UBIN-POST System.” *Proceedings of the National Academy of Sciences of the United States of America* 115 (18): E4199–4208. https://doi.org/10.1073/pnas.1711017115.

Ince, P. G., J. Tomkins, J. Y. Slade, N. M. Thatcher, and P. J. Shaw. 1998. “Amyotrophic Lateral Sclerosis Associated with Genetic Abnormalities in the Gene Encoding Cu/Zn Superoxide Dismutase: Molecular Pathology of Five New Cases, and Comparison with Previous Reports and 73 Sporadic Cases of ALS.” *Journal of Neuropathology and Experimental Neurology* 57 (10): 895–904. https://doi.org/10.1097/00005072-199810000-00002.

Ishizawa, Jo, Kensuke Kojima, Numsen Hail, Yoko Tabe, and Michael Andreeff. 2015. “Expression, Function, and Targeting of the Nuclear Exporter Chromosome Region Maintenance 1 (CRM1) Protein.” *Pharmacology & Therapeutics* 153 (September): 25–35. https://doi.org/10.1016/j.pharmthera.2015.06.001.

Ito, Daisuke, and Norihiro Suzuki. 2011. “Conjoint Pathologic Cascades Mediated by ALS/FTLD-U Linked RNA-Binding Proteins TDP-43 and FUS.” *Neurology* 77 (17): 1636–43. https://doi.org/10.1212/WNL.0b013e3182343365.

Jovičić, Ana, Jerome Mertens, Steven Boeynaems, Elke Bogaert, Noori Chai, Shizuka B. Yamada, Joseph W. Paul, et al. 2015. “Modifiers of C9orf72 DPR Toxicity Implicate Nucleocytoplasmic Transport Impairments in C9FTD/ALS.” *Nature Neuroscience* 18 (9): 1226–29. https://doi.org/10.1038/nn.4085.

Juan, Wei-Sheng, Yi-Fen Mu, Chia-Yih Wang, Edmund-Cheung So, Yi-Ping Lee, Sheng-Che Lin, and Bu-Miin Huang. 2022. “Arsenic Compounds Activate MAPK and Inhibit Akt Pathways to Induce Apoptosis in MA-10 Mouse Leydig Tumor Cells.” *Cancer Medicine* 12 (3): 3260–75. https://doi.org/10.1002/cam4.5068.

Karch, Celeste M., Mercedes Prudencio, Duane D. Winkler, P. John Hart, and David R. Borchelt. 2009. “Role of Mutant SOD1 Disulfide Oxidation and Aggregation in the Pathogenesis of Familial ALS.” *Proceedings of the National Academy of Sciences of the United States of America* 106 (19): 7774–79. https://doi.org/10.1073/pnas.0902505106.

Kawahara, Yukio, Kyoko Ito, Hui Sun, Hitoshi Aizawa, Ichiro Kanazawa, and Shin Kwak. 2004. “Glutamate Receptors: RNA Editing and Death of Motor Neurons.” *Nature* 427 (6977): 801. https://doi.org/10.1038/427801a.

Kenna, Kevin P, Perry T C van Doormaal, Annelot M Dekker, Nicola Ticozzi, Brendan J Kenna, Frank P Diekstra, Wouter van Rheenen, et al. 2016. “NEK1 Variants Confer Susceptibility to Amyotrophic Lateral Sclerosis.” *Nature Genetics* 48 (9): 1037–42. https://doi.org/10.1038/ng.3626.

Kennel, P., F. Revah, G. A. Bohme, R. Bejuit, P. Gallix, J. M. Stutzmann, A. Imperato, and J. Pratt. 2000. “Riluzole Prolongs Survival and Delays Muscle Strength Deterioration in Mice with Progressive Motor Neuronopathy (Pmn).” *Journal of the Neurological Sciences* 180 (1–2): 55–61. https://doi.org/10.1016/s0022-510x(00)00423-8.

Khalfallah, Yousra, Rachel Kuta, Camille Grasmuck, Alexandre Prat, Heather D. Durham, and Christine Vande Velde. 2018. “TDP-43 Regulation of Stress Granule Dynamics in Neurodegenerative Disease-Relevant Cell Types.” *Scientific Reports* 8 (May): 7551. https://doi.org/10.1038/s41598-018-25767-0.

Khalil, Bilal, Deepak Chhangani, Melissa C. Wren, Courtney L. Smith, Jannifer H. Lee, Xingli Li, Christian Puttinger, et al. 2022. “Nuclear Import Receptors Are Recruited by FG-Nucleoporins to

Rescue Hallmarks of TDP-43 Proteinopathy." *Molecular Neurodegeneration* 17 (1): 80. https://doi.org/10.1186/s13024-022-00585-1.

Kumar, Anita V., Taewook Kang, Tara G. Thakurta, Celeste Ng, Aric N. Rogers, Martin R. Larsen, and Louis R. Lapierre. 2022. "Exportin 1 Modulates Life Span by Regulating Nucleolar Dynamics via the Autophagy Protein LGG-1/GABARAP." *Science Advances* 8 (13): eabj1604. https://doi.org/10.1126/sciadv.abj1604.

LaClair, Katherine D., Qihui Zhou, Meike Michaelsen, Benedikt Wefers, Monika S. Brill, Aleksandar Janjic, Birgit Rathkolb, et al. 2020. "Congenic Expression of Poly-GA but Not Poly-PR in Mice Triggers Selective Neuron Loss and Interferon Responses Found in C9orf72 ALS." *Acta Neuropathologica* 140 (2): 121–42. https://doi.org/10.1007/s00401-020-02176-0.

Laszlo, Zsofia I., Nicole Hindley, Anna Sanchez Avila, Rachel A. Kline, Samantha L. Eaton, Douglas J. Lamont, Colin Smith, Tara L. Spires-Jones, Thomas M. Wishart, and Christopher M. Henstridge. 2022. "Synaptic Proteomics Reveal Distinct Molecular Signatures of Cognitive Change and C9ORF72 Repeat Expansion in the Human ALS Cortex." *Acta Neuropathologica Communications* 10 (1): 156. https://doi.org/10.1186/s40478-022-01455-z.

Lattante, Serena, Amelia Conte, Marcella Zollino, Marco Luigetti, Alessandra Del Grande, Giuseppe Marangi, Angela Romano, et al. 2012. "Contribution of Major Amyotrophic Lateral Sclerosis Genes to the Etiology of Sporadic Disease." *Neurology* 79 (1): 66–72. https://doi.org/10.1212/WNL.0b013e31825dceca.

Leblond, Claire S., Hannah M. Kaneb, Patrick A. Dion, and Guy A. Rouleau. 2014. "Dissection of Genetic Factors Associated with Amyotrophic Lateral Sclerosis." *Experimental Neurology*, Special Issue: ALS genetics and pathogenesis, 262 (December): 91–101. https://doi.org/10.1016/j.expneurol.2014.04.013.

Li, Ju-Pi, Jin-Ching Lin, and Jia-Ling Yang. 2006. "ERK Activation in Arsenite-Treated G1-Enriched CL3 Cells Contributes to Survival, DNA Repair Inhibition, and Micronucleus Formation." *Toxicological Sciences* 89 (1): 164–72. https://doi.org/10.1093/toxsci/kfj004.

Liao, Kuo-Kai, Ming-Jiuan Wu, Pei-Yi Chen, Szu-Wei Huang, Shu-Jun Chiu, Chi-Tang Ho, and Jui-Hung Yen. 2012. "Curcuminoids Promote Neurite Outgrowth in PC12 Cells through MAPK/ERK- and PKC-Dependent Pathways." *Journal of Agricultural and Food Chemistry* 60 (1): 433–43. https://doi.org/10.1021/jf203290r.

Lin, Chien-Liang Glenn, Lynn A. Bristol, Lin Jin, Margaret Dykes-Hoberg, Thomas Crawford, Lora Clawson, and Jeffrey D. Rothstein. 1998. "Aberrant RNA Processing in a Neurodegenerative Disease: The Cause for Absent EAAT2, a Glutamate Transporter, in Amyotrophic Lateral Sclerosis." *Neuron* 20 (3): 589–602. https://doi.org/10.1016/S0896-6273(00)80997-6.

Lu, Ching-Hua, Corrie Macdonald-Wallis, Elizabeth Gray, Neil Pearce, Axel Petzold, Niklas Norgren, Gavin Giovannoni, et al. 2015. "Neurofilament Light Chain." *Neurology* 84 (22): 2247–57. https://doi.org/10.1212/WNL.0000000000001642.

Luna, Noemí de, Álvaro Carbayo, Oriol Dols-Icardo, Janina Turon-Sans, David Reyes-Leiva, Ignacio Illan-Gala, Ivonne Jericó, et al. 2022. "Neuroinflammation-Related Proteins NOD2 and Spp1 Are Abnormally Upregulated in Amyotrophic Lateral Sclerosis." *Neurology® Neuroimmunology & Neuroinflammation* 10 (2): e200072. https://doi.org/10.1212/NXI.0000000000200072.

Maragakis, Nicholas J., Margaret Dykes-Hoberg, and Jeffrey D. Rothstein. 2004. “Altered Expression of the Glutamate Transporter EAAT2b in Neurological Disease.” *Annals of Neurology* 55 (4): 469–77. https://doi.org/10.1002/ana.20003.

Marin, Benoît, Farid Boumédiene, Giancarlo Logroscino, Philippe Couratier, Marie-Claude Babron, Anne Louise Leutenegger, Massimilano Copetti, Pierre-Marie Preux, and Ettore Beghi. 2017. “Variation in Worldwide Incidence of Amyotrophic Lateral Sclerosis: A Meta-Analysis.” *International Journal of Epidemiology* 46 (1): 57–74. https://doi.org/10.1093/ije/dyw061.

Marino, Carmen, Manuela Grimaldi, Eduardo Maria Sommella, Tania Ciaglia, Angelo Santoro, Michela Buonocore, Emanuela Salviati, et al. 2022. “The Metabolomic Profile in Amyotrophic Lateral Sclerosis Changes According to the Progression of the Disease: An Exploratory Study.” *Metabolites* 12 (9): 837. https://doi.org/10.3390/metabo12090837.

Meng, Wen, and Shou-Jiang Gao. 2021. “Targeting XPO1 Enhances Innate Immune Response and Inhibits KSHV Lytic Replication during Primary Infection by Nuclear Stabilization of the P62 Autophagy Adaptor Protein.” *Cell Death & Disease* 12 (1): 29. https://doi.org/10.1038/s41419-020-03303-1.

Miller, Robert G, J D Mitchell, and Dan H Moore. 2012. “Riluzole for Amyotrophic Lateral Sclerosis (ALS)/Motor Neuron Disease (MND).” *The Cochrane Database of Systematic Reviews* 2012 (3): CD001447. https://doi.org/10.1002/14651858.CD001447.pub3.

Mitchell, Jacqueline C., Philip McGoldrick, Caroline Vance, Tibor Hortobagyi, Jemeen Sreedharan, Boris Rogelj, Elizabeth L. Tudor, et al. 2013. “Overexpression of Human Wild-Type FUS Causes Progressive Motor Neuron Degeneration in an Age- and Dose-Dependent Fashion.” *Acta Neuropathologica* 125 (2): 273. https://doi.org/10.1007/s00401-012-1043-z.

Mitropoulos, Konstantinos, Theodora Katsila, George P. Patrinos, and Georgios Pampalakis. 2018. “Multi-Omics for Biomarker Discovery and Target Validation in Biofluids for Amyotrophic Lateral Sclerosis Diagnosis.” *Omics: A Journal of Integrative Biology* 22 (1): 52–64. https://doi.org/10.1089/omi.2017.0183.

Monahan, Zachary, Frank Shewmaker, and Udai Bhan Pandey. 2016. “Stress Granules at the Intersection of Autophagy and ALS.” *Brain Research* 1649 (Pt B): 189–200. https://doi.org/10.1016/j.brainres.2016.05.022.

Mori, Kohji, Shih-Ming Weng, Thomas Arzberger, Stephanie May, Kristin Rentzsch, Elisabeth Kremmer, Bettina Schmid, et al. 2013. “The C9orf72 GGGGCC Repeat Is Translated into Aggregating Dipeptide-Repeat Proteins in FTLD/ALS.” *Science (New York, N.Y.)* 339 (6125): 1335–38. https://doi.org/10.1126/science.1232927.

Nishimura, Agnes L., Vera Zupunski, Claire Troakes, Claudia Kathe, Pietro Fratta, Michael Howell, Jean-Marc Gallo, Tibor Hortobágyi, Christopher E. Shaw, and Boris Rogelj. 2010. “Nuclear Import Impairment Causes Cytoplasmic Trans-Activation Response DNA-Binding Protein Accumulation and Is Associated with Frontotemporal Lobar Degeneration.” *Brain: A Journal of Neurology* 133 (Pt 6): 1763–71. https://doi.org/10.1093/brain/awq111.

Nowak, Grażyna, Ginger L. Clifton, Malinda L. Godwin, and Diana Bakajsova. 2006. “Activation of ERK1/2 Pathway Mediates Oxidant-Induced Decreases in Mitochondrial Function in Renal Cells.” *American Journal of Physiology. Renal Physiology* 291 (4): F840–55. https://doi.org/10.1152/ajprenal.00219.2005.

Obayashi, Konen, Kimiko Sato, Rie Shimazaki, Tomoko Ishikawa, Katsumasa Goto, Hidetsugu Ueyama, Teruaki Mori, Yukio Ando, and Toshihide Kumamoto. 2008. “Salivary Chromogranin A: Useful and

Quantitative Biochemical Marker of Affective State in Patients with Amyotrophic Lateral Sclerosis." *Internal Medicine (Tokyo, Japan)* 47 (21): 1875–79. https://doi.org/10.2169/internalmedicine.47.1278.

O'Rourke, J. G., L. Bogdanik, A. Yáñez, D. Lall, A. J. Wolf, A.K.M.G. Muhammad, R. Ho, et al. 2016. "C9orf72 Is Required for Proper Macrophage and Microglial Function in Mice." *Science (New York, N.Y.)* 351 (6279): 1324–29. https://doi.org/10.1126/science.aaf1064.

Ortuño-Sahagún, Daniel, Raúl Montes González, Ester Verdaguer, Verónica Chaparro Huerta, Blanca M. Torres-Mendoza, Lourdes Lemus, Martha Catalina Rivera-Cervantes, A. Camins, and C. Beas Zárate. 2014. "Glutamate Excitotoxicity Activates the MAPK/ERK Signaling Pathway and Induces the Survival of Rat Hippocampal Neurons In Vivo." *Journal of Molecular Neuroscience* 52 (3): 366–77. https://doi.org/10.1007/s12031-013-0157-7.

Pehar, Mariana, Benjamin A. Harlan, Kelby M. Killoy, and Marcelo R. Vargas. 2017. "Role and Therapeutic Potential of Astrocytes in Amyotrophic Lateral Sclerosis." *Current Pharmaceutical Design* 23 (33): 5010–21. https://doi.org/10.2174/1381612823666170622095802.

Pérez-Cabello, Jesús A., Lucía Silvera-Carrasco, Jaime M. Franco, Vivian Capilla-González, Alexandros Armaos, María Gómez-Lima, Raquel García-García, et al. 2023. "MAPK/MAK/MRK Overlapping Kinase (MOK) Controls Microglial Inflammatory/Type-I IFN Responses via Brd4 and Is Involved in ALS." *Proceedings of the National Academy of Sciences* 120 (28): e2302143120. https://doi.org/10.1073/pnas.2302143120.

Perlson, Eran, Goo-Bo Jeong, Jenny L. Ross, Ram Dixit, Karen E. Wallace, Robert G. Kalb, and Erika L. F. Holzbaur. 2009. "A Switch in Retrograde Signaling from Survival to Stress in Rapid-Onset Neurodegeneration." *The Journal of Neuroscience* 29 (31): 9903–17. https://doi.org/10.1523/JNEUROSCI.0813-09.2009.

Peters, Owen M., Mehdi Ghasemi, and Robert H. Brown. 2015. "Emerging Mechanisms of Molecular Pathology in ALS." *The Journal of Clinical Investigation* 125 (6): 2548. https://doi.org/10.1172/JCI82693.

Philips, T, and JD Rothstein. 2014. "Glial Cells in Amyotrophic Lateral Sclerosis." *Experimental Neurology* 262PB (December): 111–20. https://doi.org/10.1016/j.expneurol.2014.05.015.

Philips, Thomas, and Wim Robberecht. 2011. "Neuroinflammation in Amyotrophic Lateral Sclerosis: Role of Glial Activation in Motor Neuron Disease." *The Lancet. Neurology* 10 (3): 253–63. https://doi.org/10.1016/S1474-4422(11)70015-1.

Polymenidou, Magdalini, and Don W. Cleveland. 2011. "The Seeds of Neurodegeneration: Prion-like Spreading in ALS." *Cell* 147 (3): 498–508. https://doi.org/10.1016/j.cell.2011.10.011.

Pratilas, Christine A., Barry S. Taylor, Qing Ye, Agnes Viale, Chris Sander, David B. Solit, and Neal Rosen. 2009. "V600EBRAF Is Associated with Disabled Feedback Inhibition of RAF–MEK Signaling and Elevated Transcriptional Output of the Pathway." *Proceedings of the National Academy of Sciences of the United States of America* 106 (11): 4519–24. https://doi.org/10.1073/pnas.0900780106.

Rabin, Stuart J., Jae Mun 'Hugo' Kim, Michael Baughn, Ryan T. Libby, Young Joo Kim, Yuxin Fan, Randell T. Libby, Albert La Spada, Brad Stone, and John Ravits. 2010. "Sporadic ALS Has Compartment-Specific Aberrant Exon Splicing and Altered Cell–Matrix Adhesion Biology." *Human Molecular Genetics* 19 (2): 313–28. https://doi.org/10.1093/hmg/ddp498.

Ranganathan, Srikanth, Eric Williams, Philip Ganchev, Vanathi Gopalakrishnan, David Lacomis, Leo Urbinelli, Kristyn Newhall, Merit E. Cudkowicz, Robert H. Brown, and Robert Bowser. 2005. "Proteomic Profiling of Cerebrospinal Fluid Identifies Biomarkers for Amyotrophic Lateral Sclerosis." *Journal of Neurochemistry* 95 (5): 1461–71. https://doi.org/10.1111/j.1471-4159.2005.03478.x.

Ransohoff, Richard M. 2016. "How Neuroinflammation Contributes to Neurodegeneration." *Science (New York, N.Y.)* 353 (6301): 777–83. https://doi.org/10.1126/science.aag2590.

Reaume, A. G., J. L. Elliott, E. K. Hoffman, N. W. Kowall, R. J. Ferrante, D. F. Siwek, H. M. Wilcox, et al. 1996. "Motor Neurons in Cu/Zn Superoxide Dismutase-Deficient Mice Develop Normally but Exhibit Enhanced Cell Death after Axonal Injury." *Nature Genetics* 13 (1): 43–47. https://doi.org/10.1038/ng0596-43.

Rheenen, Wouter van, Aleksey Shatunov, Annelot M Dekker, Russell L McLaughlin, Frank P Diekstra, Sara L Pulit, Rick A A van der Spek, et al. 2016. "Genome-Wide Association Analyses Identify New Risk Variants and the Genetic Architecture of Amyotrophic Lateral Sclerosis." *Nature Genetics* 48 (9): 1043–48. https://doi.org/10.1038/ng.3622.

Riviere, M., V. Meininger, P. Zeisser, and T. Munsat. 1998. "An Analysis of Extended Survival in Patients with Amyotrophic Lateral Sclerosis Treated with Riluzole." *Archives of Neurology* 55 (4): 526–28. https://doi.org/10.1001/archneur.55.4.526.

Rossi, Simona, Valentina Rompietti, Ylenia Antonucci, Daniela Giovannini, Chiara Scopa, Silvia Scaricamazza, Raffaella Scardigli, et al. 2020. "UsnRNP Trafficking Is Regulated by Stress Granules and Compromised by Mutant ALS Proteins." *Neurobiology of Disease* 138 (May): 104792. https://doi.org/10.1016/j.nbd.2020.104792.

Rothstein, Jeffrey D., Guochuan Tsai, Ralph W. Kuncl, Lora Clawson, David R. Cornblath, Daniel B. Drachman, Alan Pestronk, Barbara L. Stauch, and Joseph T. Coyle. 1990. "Abnormal Excitatory Amino Acid Metabolism in Amyotrophic Lateral Sclerosis." *Annals of Neurology* 28 (1): 18–25. https://doi.org/10.1002/ana.410280106.

Rowland, Lewis P. 2001. "How Amyotrophic Lateral Sclerosis Got Its Name: The Clinical-Pathologic Genius of Jean-Martin Charcot." *Archives of Neurology* 58 (3): 512–15. https://doi.org/10.1001/archneur.58.3.512.

Saberi, Shahram, Jennifer E. Stauffer, Derek J. Schulte, and John Ravits. 2015. "'Neuropathology of Amyotrophic Lateral Sclerosis and Its Variants.'" *Neurologic Clinics* 33 (4): 855–76. https://doi.org/10.1016/j.ncl.2015.07.012.

Sahu, Rakesh, Shubham Upadhayay, and Sidharth Mehan. 2021. "Inhibition of Extracellular Regulated Kinase (ERK)-1/2 Signaling Pathway in the Prevention of ALS: Target Inhibitors and Influences on Neurological Dysfunctions." *European Journal of Cell Biology* 100 (7): 151179. https://doi.org/10.1016/j.ejcb.2021.151179.

Samir, Parimal, Sannula Kesavardhana, Deanna M. Patmore, Sebastien Gingras, R. K. Subbarao Malireddi, Rajendra Karki, Clifford S. Guy, et al. 2019. "DDX3X Acts as a Live-or-Die Checkpoint in Stressed Cells by Regulating NLRP3 Inflammasome." *Nature* 573 (7775): 590–94. https://doi.org/10.1038/s41586-019-1551-2.

Satarker, Sairaj, Sree Lalitha Bojja, Prasada Chowdari Gurram, Jayesh Mudgal, Devinder Arora, and Madhavan Nampoothiri. 2022. "Astrocytic Glutamatergic Transmission and Its Implications in Neurodegenerative Disorders." *Cells* 11 (7): 1139. https://doi.org/10.3390/cells11071139.

Scholl, Florence A., Phillip A. Dumesic, Deborah I. Barragan, Kazutoshi Harada, Vickram Bissonauth, Jean Charron, and Paul A. Khavari. 2007. “Mek1/2 MAPK Kinases Are Essential for Mammalian Development, Homeostasis, and Raf-Induced Hyperplasia.” *Developmental Cell* 12 (4): 615–29. https://doi.org/10.1016/j.devcel.2007.03.009.

Shaw, P. J., and P. G. Ince. 1997. “Glutamate, Excitotoxicity and Amyotrophic Lateral Sclerosis.” *Journal of Neurology* 244 (2): S3–14. https://doi.org/10.1007/BF03160574.

Shepheard, Stephanie R., Joanne Wuu, Michell Cardoso, Luke Wiklendt, Phil G. Dinning, Tim Chataway, David Schultz, Michael Benatar, and Mary-Louise Rogers. 2017. “Urinary P75ECD.” *Neurology* 88 (12): 1137–43. https://doi.org/10.1212/WNL.0000000000003741.

Silvestrini, Melissa J., Joseph R. Johnson, Anita V. Kumar, Tara G. Thakurta, Karine Blais, Zachary A. Neill, Sarah W. Marion, Victoria St Amand, Robert A. Reenan, and Louis R. Lapierre. 2018. “Nuclear Export Inhibition Enhances HLH-30/TFEB Activity, Autophagy, and Lifespan.” *Cell Reports* 23 (7): 1915–21. https://doi.org/10.1016/j.celrep.2018.04.063.

Smith, Richard A., Timothy M. Miller, Koji Yamanaka, Brett P. Monia, Thomas P. Condon, Gene Hung, Christian S. Lobsiger, et al. 2006. “Antisense Oligonucleotide Therapy for Neurodegenerative Disease.” *The Journal of Clinical Investigation* 116 (8): 2290–96. https://doi.org/10.1172/JCI25424.

Song, Yanlin, Zhenfei Bi, Yu Liu, Furong Qin, Yuquan Wei, and Xiawei Wei. 2023. “Targeting RAS–RAF–MEK–ERK Signaling Pathway in Human Cancer: Current Status in Clinical Trials.” *Genes & Diseases* 10 (1): 76–88. https://doi.org/10.1016/j.gendis.2022.05.006.

Stanciu, Madalina, Ying Wang, Ruth Kentor, Nancy Burke, Simon Watkins, Geraldine Kress, Ian Reynolds, et al. 2000. “Persistent Activation of ERK Contributes to Glutamate-Induced Oxidative Toxicity in a Neuronal Cell Line and Primary Cortical Neuron Cultures *.” *Journal of Biological Chemistry* 275 (16): 12200–206. https://doi.org/10.1074/jbc.275.16.12200.

Thakar, Ketan, Samir Karaca, Sarah A. Port, Henning Urlaub, and Ralph H. Kehlenbach. 2013. “Identification of CRM1-Dependent Nuclear Export Cargos Using Quantitative Mass Spectrometry.” *Molecular & Cellular Proteomics : MCP* 12 (3): 664–78. https://doi.org/10.1074/mcp.M112.024877.

Tischbein, Maeve, Desiree M. Baron, Yen-Chen Lin, Katherine V. Gall, John E. Landers, Claudia Fallini, and Daryl A. Bosco. 2019. “The RNA-Binding Protein FUS/TLS Undergoes Calcium-Mediated Nuclear Egress during Excitotoxic Stress and Is Required for GRIA2 MRNA Processing.” *The Journal of Biological Chemistry* 294 (26): 10194–210. https://doi.org/10.1074/jbc.RA118.005933.

Turner, Joel G., Jana Dawson, and Daniel M. Sullivan. 2012. “Nuclear Export of Proteins and Drug Resistance in Cancer.” *Biochemical Pharmacology* 83 (8): 1021–32. https://doi.org/10.1016/j.bcp.2011.12.016.

Turner, Martin R, Orla Hardiman, Michael Benatar, Benjamin R Brooks, Adriano Chio, Mamede De Carvalho, Paul G Ince, et al. 2013. “Controversies and Priorities in Amyotrophic Lateral Sclerosis.” *The Lancet Neurology* 12 (3): 310–22. https://doi.org/10.1016/S1474-4422(13)70036-X.

Turner, Martin R, and Michael Swash. 2015. “The Expanding Syndrome of Amyotrophic Lateral Sclerosis: A Clinical and Molecular Odyssey.” *Journal of Neurology, Neurosurgery, and Psychiatry* 86 (6): 667–73. https://doi.org/10.1136/jnnp-2014-308946.

Tzeplaeff, Laura, Sibylle Wilfling, Maria Viktoria Requardt, and Meret Herdick. 2023. “Current State and Future Directions in the Therapy of ALS.” *Cells* 12 (11): 1523. https://doi.org/10.3390/cells12111523.

Vanneste, Joni, and Ludo Van Den Bosch. 2021. “The Role of Nucleocytoplasmic Transport Defects in Amyotrophic Lateral Sclerosis.” *International Journal of Molecular Sciences* 22 (22): 12175. https://doi.org/10.3390/ijms222212175.

Vanneste, Joni, Thomas Vercruysse, Steven Boeynaems, Philip Van Damme, Dirk Daelemans, and Ludo Van Den Bosch. 2022. “Cellular Stress Induces Nucleocytoplasmic Transport Deficits Independent of Stress Granules.” *Biomedicines* 10 (5): 1057. https://doi.org/10.3390/biomedicines10051057.

Verma, Ashok, and Rup Tandan. 2013. “RNA Quality Control and Protein Aggregates in Amyotrophic Lateral Sclerosis: A Review.” *Muscle & Nerve* 47 (3): 330–38. https://doi.org/10.1002/mus.23673.

Widmann, Christian, Spencer Gibson, Matthew B. Jarpe, and Gary L. Johnson. 1999. “Mitogen-Activated Protein Kinase: Conservation of a Three-Kinase Module From Yeast to Human.” *Physiological Reviews* 79 (1): 143–80. https://doi.org/10.1152/physrev.1999.79.1.143.

Wobst, Heike J., Korrie L. Mack, Dean G. Brown, Nicholas J. Brandon, and James Shorter. 2020. “The Clinical Trial Landscape in Amyotrophic Lateral Sclerosis – Past, Present and Future.” *Medicinal Research Reviews* 40 (4): 1352–84. https://doi.org/10.1002/med.21661.

Wolozin, Benjamin. 2012. “Regulated Protein Aggregation: Stress Granules and Neurodegeneration.” *Molecular Neurodegeneration* 7 (November): 56. https://doi.org/10.1186/1750-1326-7-56.

Worms, P. M. 2001. “The Epidemiology of Motor Neuron Diseases: A Review of Recent Studies.” *Journal of the Neurological Sciences* 191 (1–2): 3–9. https://doi.org/10.1016/s0022-510x(01)00630-x.

Writing Group and Edaravone (MCI-186) ALS 19 Study Group. 2017. “Safety and Efficacy of Edaravone in Well Defined Patients with Amyotrophic Lateral Sclerosis: A Randomised, Double-Blind, Placebo-Controlled Trial.” *The Lancet. Neurology* 16 (7): 505–12. https://doi.org/10.1016/S1474-4422(17)30115-1.

Xu, Daping, Haiyun Chen, Shinghung Mak, Shengquan Hu, Karl W. K. Tsim, Yuanjia Hu, Yewei Sun, et al. 2016. “Neuroprotection against Glutamate-Induced Excitotoxicity and Induction of Neurite Outgrowth by T-006, a Novel Multifunctional Derivative of Tetramethylpyrazine in Neuronal Cell Models.” *Neurochemistry International* 99 (October): 194–205. https://doi.org/10.1016/j.neuint.2016.07.006.

Xu, Darui, Nick V. Grishin, and Yuh Min Chook. 2012. “NESdb: A Database of NES-Containing CRM1 Cargoes.” *Molecular Biology of the Cell* 23 (18): 3673–76. https://doi.org/10.1091/mbc.E12-01-0045.

Yamaguchi, Takayuki, Reina Kakefuda, Nobuyuki Tajima, Yoshihiro Sowa, and Toshiyuki Sakai. 2011. “Antitumor Activities of JTP-74057 (GSK1120212), a Novel MEK1/2 Inhibitor, on Colorectal Cancer Cell Lines in Vitro and in Vivo.” *International Journal of Oncology* 39 (1): 23–31. https://doi.org/10.3892/ijo.2011.1015.

Yoon, Seunghee, and Rony Seger. 2006. “The Extracellular Signal-Regulated Kinase: Multiple Substrates Regulate Diverse Cellular Functions.” *Growth Factors* 24 (1): 21–44. https://doi.org/10.1080/02699050500284218.

Zhang, Kang, Qing Liu, Dongchao Shen, Hongfei Tai, Shuangwu Liu, Zhili Wang, Jiayu Shi, et al. 2019. “Mutation Analysis of KIF5A in Chinese Amyotrophic Lateral Sclerosis Patients.” *Neurobiology of Aging* 73 (January): 229.e1-229.e4. https://doi.org/10.1016/j.neurobiolaging.2018.08.006.

Zhang, Ke, Christopher J. Donnelly, Aaron R. Haeusler, Jonathan C. Grima, James B. Machamer, Peter Steinwald, Elizabeth L. Daley, et al. 2015. “The C9ORF72 Repeat Expansion Disrupts Nucleocytoplasmic Transport.” *Nature* 525 (7567): 56–61. https://doi.org/10.1038/nature14973.

Zhang, Li-Nan, Qi Wang, Xiao-Hui Xian, Jie Qi, Li-Zhe Liu, and Wen-Bin Li. 2019. “Astrocytes Enhance the Tolerance of Rat Cortical Neurons to Glutamate Excitotoxicity.” *Molecular Medicine Reports* 19 (3): 1521–28. https://doi.org/10.3892/mmr.2018.9799.

Zhang, Wei, and Hui Tu Liu. 2002. “MAPK Signal Pathways in the Regulation of Cell Proliferation in Mammalian Cells.” *Cell Research* 12 (1): 9–18. https://doi.org/10.1038/sj.cr.7290105.

Zhang, YueMei, and Bhagu R Bhavnani. 2005. “Glutamate-Induced Apoptosis in Primary Cortical Neurons Is Inhibited by Equine Estrogens via down-Regulation of Caspase-3 and Prevention of Mitochondrial Cytochrome c Release.” *BMC Neuroscience* 6 (February): 13. https://doi.org/10.1186/1471-2202-6-13.

Zhao, Weihua, David R. Beers, Kristopher G. Hooten, Douglas H. Sieglaff, Aijun Zhang, Shanker Kalyana-Sundaram, Christopher M. Traini, et al. 2017. “Characterization of Gene Expression Phenotype in Amyotrophic Lateral Sclerosis Monocytes.” *JAMA Neurology* 74 (6): 677–85. https://doi.org/10.1001/jamaneurol.2017.0357.

Zou, Zhang-Yu, Zhi-Rui Zhou, Chun-Hui Che, Chang-Yun Liu, Rao-Li He, and Hua-Pin Huang. 2017. “Genetic Epidemiology of Amyotrophic Lateral Sclerosis: A Systematic Review and Meta-Analysis.” *Journal of Neurology, Neurosurgery & Psychiatry* 88 (7): 540–49. https://doi.org/10.1136/jnnp-2016-315018.

8 Acknowledgment

I want to express my heartfelt gratitude to Prof. Paul Lingor for his constant support, exceptional supervision, and invaluable guidance throughout my PhD journey. Being a member of the Lingor group has been a rewarding experience that has significantly contributed to both my professional and personal growth. During moments of success or challenges, Prof. Lingor provided me with not only academic but also emotional support. I would also like to thank the members of my Thesis committee, Prof. Wurst and my mentor Dr. Michael Menden for their support and their constructive feedbacks during my project.

I would like to extend my sincere gratitude to the entire MAXOMOD team, whose incredible efforts have played a pivotal role in shaping this remarkable project into what it is today. I also want to express my thanks to the members of the Lingor Group for their help and support.

I offer special appreciation to my direct supervisor and dear friend, Dr. Lucas Caldi Gomes. His mentorship, patience, and unwavering support, especially during challenging times, have been invaluable. I couldn't have completed this journey without his support.

I'd also like to acknowledge Dr. Laura Tzeplaeff, a postdoc who joined our group later on. Her assistance and insights in the final stages of my PhD, both academically and emotionally, along with her wealth of experience, were extremely valuable.

My gratitude extends to the entire Neurology Lab at Klinikum Recht der Isar, including all the technicians and scientists in Prof. Hemmers's group. Their contributions have created a supportive and conducive environment for scientific research. I want to thank all my friends and colleagues who have become like family to me, while being far from home for all the unforgettable moments and for always being there for me.

I would like to express my deepest appreciation to my family, my parents, my brother, and my sister-in-law. Even though I've been away from them, their unwavering support has always been there for me, no matter the challenges I've faced. Lastly, I want to extend my heartfelt gratitude to my husband, Payam. I am profoundly grateful that you joined me on this journey. Your constant support, encouragement, strength, determination, patience, and tireless efforts have made you an incredible and wonderful person in my life. Your belief in me gave me the courage to complete this challenging journey, and I am forever grateful for everything you've done for me.

9 List of abbreviations

AK: Adenylate kinase

AKDR: AK detection reagent

ALS: Amyotrophic lateral sclerosis

AMPA: α-amino-3-hydroxy-5-methyl-4-isoxazolepropionic acid

ANG: Angiogenin

ANOVA: Analysis of variance

ATXN2: Ataxin-2

C21ORF2: Chromosome 21 open reading frame 2

C9ORF72: Chromosome 9 open reading frame 72

CHIT1: Chitotriosidase

CHI3L1: Chitinase-3-like protein 1

CNS: Central nervous system

CRM1: Chromosome maintenance protein 1

CSF: Cerebrospinal fluid

DDX3X: DEAD-Box Helicase 3 X-Linked

DIV: Day in vitro

DPRs: Dipeptide repeat proteins

DUSPs: Dual specificity phosphatases

EAAT2: Excitatory amino acid transporter 2

ERK: Extracellular signal-regulated kinase

FDA: Food and Drug Administration

FTD: Frontotemporal dementia

FUS: Fused in sarcoma

G3BP1: GTPase-activating protein-binding protein 1

Glut: Glutamate

HBSS: Hanks' Balanced Salt Solution

HRE: Hexanucleotide repeat expansion

ICC: Immunocytochemistry

iPSC: Induced pluripotent stem cells

ISR: Integrated stress response

JNK: Jun N-terminal kinase

LC3: Microtubule-associated protein 1A/1B-light chain 3

MAP2K2: Mitogen-activated protein kinase kinase 2

MAPK: Mitogen-activated protein kinase

MAXOMOD: Multiomic analysis of axono-synaptic degeneration in motoneuron disease

MEK2: Mitogen-activated protein kinase kinase 2

MND: Motor neuron disease

NEK1: NIMA related kinase 1

NES: Nuclear export signal

Nf: Neurofilaments

NLRP3: NLR family pyrin domain containing 3

NMDA: N-methyl-D-aspartate

NOD2: Nucleotide-binding oligomerization domain-containing protein 2

NPC: Nuclear pore complex

OPTN: Optineurin

PBS: Phosphate buffered saline

PDH: pyruvate dehydrogenase

PFC: Prefrontal cortex

PI3K: Phosphoinositide 3-kinases

PSN: Penicillin-Streptomycin-Neomycin

RAN: Repeat-associated non-ATG

RBPs: RNA-binding proteins

ROS: Reactive oxygen species

RT: Room temperature

RTKs: Tyrosine kinase receptors

SA: Sodium arsenite

SETX: Senataxin

SG: Stress granule

SINE: Selective inhibitors of nuclear export

SOD1: Superoxide dismutase 1

SQSTM1: Sequestosome 1

TBK1: TANK-binding kinase 1

TDP-43: TAR DNA-binding protein 43

Trk: Tropomyosin receptor kinase

UsnRNPs: U-rich small nuclear ribonucleoproteins

WGCNA: Weighted gene co-expression network analysis

XPO1: Exportin 1